DIGITAL ACCESS TO SCHOLARSHIP AT HARVARD
DASH.HARVARD.EDU

HARVARD LIBRARY
Office for Scholarly Communication

Microbial colonization and dissolution of mercury sulfide minerals

Citation
Vazquez Rodriguez, Adiari Iraida. 2014. Microbial colonization and dissolution of mercury sulfide minerals. Doctoral dissertation, Harvard University.

Permanent link
http://nrs.harvard.edu/urn-3:HUL.InstRepos:13070080

Terms of Use
This article was downloaded from Harvard University's DASH repository, and is made available under the terms and conditions applicable to Other Posted Material, as set forth at http://nrs.harvard.edu/urn-3:HUL.InstRepos:dash.current.terms-of-use#LAA

Share Your Story

The Harvard community has made this article openly available.
Please share how this access benefits you. Submit a story .

Accessibility

MICROBIAL COLONIZATION AND DISSOLUTION OF MERCURY SULFIDE MINERALS

A dissertation presented

by

Adiari Iraida Vázquez Rodríguez

to

The School of Engineering and Applied Sciences

in partial fulfillment of the requirements

for the degree of

Doctor of Philosophy

in the subject of

Environmental Science and Engineering

Harvard University

Cambridge, Massachusetts

August 2014

© 2014 Adiari I. Vázquez Rodríguez
All rights reserved

Dissertation advisor: Colleen Hansel Adiari Iraida Vázquez Rodríguez

MICROBIAL COLONIZATION AND DISSOLUTION OF MERCURY SULFIDE MINERALS

ABSTRACT

Mercury (Hg) is a toxic heavy metal that poses significant human and environmental health risks. Mineral-associated Hg is the largest reservoir of Hg in the environment where it can account for nearly 60% of the global Hg mass inventory. A large fraction of this pool is comprised of mercury sulfide (HgS) minerals, including metacinnabar (beta-HgS). HgS minerals have long been considered insignificant sources of Hg to aqueous or atmospheric pools in all but severely acidic environments due to their low solubility and slow abiotic dissolution kinetics. Little previous work has been conducted investigating the bacterial colonization of HgS minerals and the potential role of these mineral-associated communities in impacting the mobility of mineral-hosted Hg. To address this gap in knowledge, the studies within this dissertation employed a combination of field- and laboratory-based methods. Using culture-independent techniques, this work revealed that sulfur-oxidizing bacteria can extensively colonize metacinnabar within aerobic, near neutral pH, creek sediments, suggesting a potential role for chemolithotrophic bacteria in metacinnabar weathering. Within laboratory incubations, the dominant bacterial colonizer (*Thiobacillus thioparus*), induced extensive release and volatilization of metacinnabar-hosted Hg. These findings expose a new pathway for metacinnabar dissolution and point to mineral-hosted Hg as an underappreciated source of elemental Hg that may contribute to global atmospheric Hg budgets. In addition, this work

elucidates the importance of thiosulfate, a major intermediate sulfur species in the environment, in stimulating metacinnabar dissolution. Therefore, the work within this dissertation shows that authigenic HgS minerals are not merely a sink for Hg within non-acidic natural environments and instead are a source of dissolved and gaseous Hg. This work provides critical information for predicting the transport of Hg in the environment and for developing appropriate management and remediation strategies for Hg-contaminated systems.

TABLE OF CONTENTS

CHAPTER 3 - MERCURY SULFIDE MINERALS AS A SOURCE OF MERCURY TO THE ATMOSPHERE

CHAPTER 4 - DISSOLUTION AND VOLATILIZATION OF METACINNABAR-HOSTED MERCURY IN *THIOBACILLUS THIOPARUS* CULTURES

LIST OF FIGURES

Chapter 1

Chapter 2

Chapter 3

Chapter 4

Appendix B - Chapter 3 Supplement

Appendix C - Chapter 4 Supplement

LIST OF TABLES

ACKNOWLEDGEMENTS

I am sincerely grateful to the many amazing people who contributed to the work within this dissertation, and to those near and far from the university who contributed on a professional and personal level to my success as a graduate student.

I would like to thank my advisor Colleen Hansel for believing in me and taking me into her group six years ago. Thank you for entrusting me with the scientific freedom to pursue the questions that interested me most, while providing the guidance and support to answer them. I have nothing but gratitude for the many hours you have dedicated to discussing and improving the body of work that has gone into this dissertation. Thank you for offering me not only your mentorship, but also your friendship.

I would also like to thank my committee, Carl Lamborg, David Johnston, and Steven Wofsy, for taking the time to learn about my research and provide insightful feedback. A special thank you to my collaborators Tong Zhang, Carl Lamborg, Cara Santelli, Chris Kim, Sam Webb, and Scott Brooks for your commitment and support throughout this project.

A big thank you to the former and current members of the Hansel group family at Harvard and WHOI for their encouragement and help. Whether you were asking or answering insightful science questions, teaching me the ropes during my first beam run, letting me borrow your tools and equipment, assisting me with IC fill ups and repairs, or keeping me company on long nights in the lab, I always felt your encouragement. My graduate experience would not have been the same without your scientific insight and your camaraderie.

I am grateful to the entire team of the Shine group at the Harvard School of Public Health for opening their doors to me. Thank you for sharing your workspace and warmly adopting me

into your lab. Nick and Zhao, thank you for taking the time to help me with DMA troubleshooting. Jim, thank you for your support in my pursuit of research and graduate school. Your mentorship and friendship have had a great impact in shaping me as a scientist.

Carl, thank you for making your facilities at WHOI available to me. Your easygoing approach and guidance always helped to put things in perspective. Gretchen, thank you for your assistance at the WHOI mercury lab. Tong, I am grateful that you took the time to train me on the Tekran, among other things. Your support was invaluable to the completion of this project.

I am also grateful to the financial sponsors of this work: the National Science Foundation Graduate Research Fellowship and the Harvard Graduate Prize Fellowship.

To my friends near and far, whose phone calls, skype dates, and dinner dates never failed to make me smile: thank you for your love and encouragement.

Finally I would like to thank my family. Gracias a todos mis familiares, mis padres, hermanos, sobrinos y abuelos presentes y no presentes, porque de una manera u otra han sido parte de esta disertación. A mis tres hermanos, gracias por el cariño y la fuerza que siempre me han brindado, saben lo mucho que los aprecio. A papi y a mami, todo lo que he logrado ha sido gracias al fomento y sacrificio de ustedes. Mami, gracias por tu apoyo, tu cariño, tu compasión, por ser mi partidaria y por escucharme siempre pacientemente. Papi, gracias por haber sido el primero en motivarme hacia el mundo científico, por tu aliento constante, por tu energía y tu cariño. Ricardo, mi compañero, tu solidaridad en este esfuerzo mutuo ha sido invalorable. Bien sabes que este trabajo ha sido posible gracias a tu paciencia inquebrantable y tu apoyo constante. Lo logramos.

To everyone who has made this work possible, please accept my most genuine gratitude.

CHAPTER 1

ELUCIDATING THE POTENTIAL FOR A MICROBIAL ROLE IN MERCURY SULFIDE MINERAL DISSOLUTION

Justification

Mercury (Hg), a highly toxic metal that interferes with human neurological development, is found in excessively high levels in approximately half a million children in the United States [1-3]. The major dietary source of Hg is consumption of marine and freshwater fish, as a result of Hg bioaccumulation and biomagnification in natural waters [4]. Hg discharged into natural waters is largely not accumulated in fish, but rather trapped in sediments [5]. In anaerobic sediments, Hg is principally precipitated as Hg sulfides (HgS (s)), thought to be highly immobile and therefore not represent a high risk to ecosystems and human health [6]. However, over time these sediments can also release soluble Hg. Though much progress has been made in elucidating the biological and chemical transformations of dissolved Hg in natural waters, the factors inducing mobilization of Hg from the solid to the dissolved phase are to a great extent unknown. An enhanced understanding of the mobilization of entrained Hg from HgS(s) within sediments to aqueous environments can be used to mitigate human exposure to this toxic metal.

Hydrologically fluctuating environments, such as the hyporheic zone, can account for a significant release of entrained metals [7]. In the hyporheic zone, both oxidative and reductive conditions may arise within a small spatial scale; the steep redox gradients produced along with the high concentration of labile organic matter, often give rise to substantial biological growth and activity that may support microbially mediated Hg speciation changes, leading to HgS(s) dissolution and transport of Hg into both surface and groundwater [8-10]. Transformations of solid-phase Hg in such aerobic/anaerobic transition zones are not well-understood [6].

Microbial communities in this zone may play an important, though as yet understudied, role in the mobilization of HgS(s) by inducing a number of physical and chemical transformations of the mineral. Previous research on HgS(s) dissolution and mobilization was

often conducted with abiotic conditions not likely to be found in natural environments, making it difficult to assess the extent to which studied processes are environmentally significant. Recent studies indicate that the presence of a microbial consortium derived from mine tailings can substantially enhance HgS(s) solubility [11]. This profound microbial effect on the solubility of HgS(s), suggests that the mobilization of Hg from solid-phases in the presence of relevant organisms under various conditions needs to be determined. Further research needs to be conducted under environmentally significant biotic conditions in order to assess the extent to which legacy HgS(s) minerals are dissolved in natural environments. Understanding the processes affecting Hg mobilization and resulting chemical speciation is imperative to understanding the fate of Hg in the environment and mitigating transformations that will pose a greater threat to human health. Due to its potentially pivotal role in contaminant transport, microbially induced HgS(s) dissolution in the hyporheic zone warrants further research.

The following chapter summarizes the state of knowledge of microbially mediated Hg transformations and environmental HgS(s) dissolution. Emphasis is placed on the potential for bacteria and, in some cases fungi, to induce chemical changes that may affect HgS(s) dissolution in the hyporheic zone as microorganisms colonizing HgS(s) surfaces are potential key players in mobilizing Hg from this highly insoluble mineral. This hypothesis is based on the capacity of bacteria and fungi to live in Hg-contaminated environments, the wide array of physical and chemical transformations that these organisms can exert on Hg and S, and the ability of the dynamic and diverse microenvironments in the hyporheic zone to enhance metal mobility.

The chapters that follow (**Chapters 2, 3, 4**) will elucidate the role that bacteria play in controlling the mobility of HgS(s)-hosted Hg in the hyporheic zone and aerobic neutral freshwater environments.

Background

General Hg Chemistry

Though Hg inputs into the environment result from both anthropogenic and natural discharges, anthropogenic inputs account for the majority of global Hg inputs to the environment [5, 12, 13]. Anthropogenic sources to land and aquatic systems include existing and former industries, landfills, sludge application processes, the use of Hg-contaminated fertilizers, and atmospheric deposition [14, 15]. Though there have been advances in the control of emissions of Hg pollution in the US, these advances are tempered by the existence of legacy Hg residing in sediments, soils, and water systems [16].

Sediments are the major reservoir of Hg in aquatic systems. Inorganic Hg discharged into aquatic systems is mostly incorporated into soils and sediments, owing to its large association constant with sulfide and to the metal's high affinity for organic matter [4, 17]. Therefore, soils and sediments can initially serve as an efficient sink for Hg. However, over time, they can also be a source of Hg species to the water column [4]. The solubility of the solid phases and chemical form of resulting aqueous species affects their retention, mobility, and bioavailability in the soil environment thereby governing their distribution in the soil profile and displacement to other reservoirs such as groundwater or surface water [13, 18]. As such, understanding the processes affecting Hg mobilization and resulting chemical speciation is imperative to understanding the fate of Hg in the environment and mitigating transformations that will pose a greater threat to human and ecosystem health.

The chemical speciation of Hg depends in part on its oxidation state. Hg exists in three oxidation states: Hg(0) (elemental mercury), Hg(I) (mercurous mercury), and Hg(II) (mercuric

mercury) depending on redox conditions [19]. Hg(0) has a low aqueous solubility (60 µg/L water at 25°C) and high volatility (Henry's coefficient of 0.3) [4]. A negligibly small fraction of Hg may be present as Hg(I) in natural waters as it quickly dismutates to Hg(0) and Hg(II) [20], and hence will not be included in this discussion. Hg(II) generally forms various complexes with Cl^- and OH^- ions, hence its chemical form also depends on pH and salinity [13]. In many soils and sediments, Hg is predominantly found as Hg(II) sulfides (HgS(s)), such as cinnabar and its polymorph metacinnabar, owing to these minerals' low solubility [4]. Hg(II) can also be found in organic forms, namely as methyl Hg (MeHg), which has the chemical formula $CH_3Hg(II)X$, where X is a ligand, typically Cl^- and OH^- [4]. Dimethyl Hg, $(CH_3)_2Hg(II)$, has been found in seawater, but has not been observed in common freshwater environments [16]. Unlike the inorganic forms, MeHg has the potential to bioaccumulate in living organisms and biomagnify through the food chain.

Hg Transformations

Both biotic and abiotic processes can affect the cycling of Hg in soils and water [4]. A substantial number of known abiotic Hg transformations are photo-induced, however these photochemical processes are not expected to play a role in the hyporheic zone due to low light penetration. As such, the following sections will highlight the wide range of chemical transformations that microbes can exert on Hg species that can be reasonably expected to occur in hyporheic zone sediments, while also noting potentially significant abiotic processes (***Figure 1.1***). These shifts in Hg speciation can shift equilibrium concentrations, and therefore have the potential to impact HgS(s) dissolution.

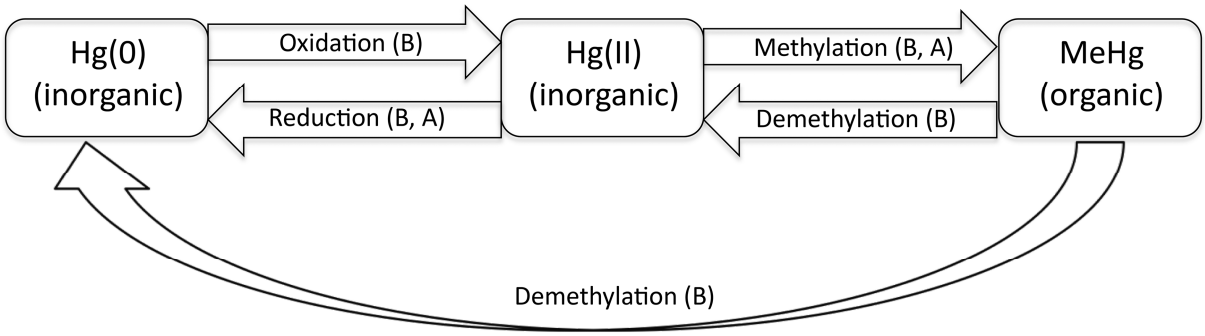

Figure 1.1. Transformations of mercury (Hg). "A" represents a transformation expected to occur through an abiotic mechanism in the hyporheic zone, and "B" represents a transformation that can be microbially mediated (biotic).

Hg(II) Reduction.

In general, reduction of Hg(II) to Hg(0) represents a sink for Hg from water and soil/sediment systems, as Hg(0)'s low solubility and high vapor pressure result in its transport back to the atmosphere. Both abiotic processes and biotic processes mediated by bacteria and fungi contribute to Hg reduction. In general, it is thought that reduction is chiefly biotic in Hg polluted waters (> 50 pM Hg) [20]. In these high Hg conditions, bacteria have developed resistance mechanisms against toxic Hg.

Hg(II) is toxic to bacteria as it mimics reactive oxygen species in its interactions with cellular constituents; this has led bacteria to evolve a specialized system to deal with Hg toxicity [4]. Environments contaminated with high concentrations of Hg(II) induce the activity of the bacterial mercury resistance (*mer*) operon [4]. The *mer* operon is broadly distributed in bacteria [4], and is widespread in Hg-contaminated environments as a result of horizontal gene transfer and natural selection for resistance [21]. Hg(II) is transported into the cell by the MerT transmembrane protein. Once inside the cell, MerA, the mercuric reductase, uses NAD(P)H as a reductant to reduce Hg(II) to Hg(0) [4]. The resulting Hg(0) does not need a transport system to excrete it out of the cell as it easily diffuses out through the cell membrane.

Fungi, using extracellular metabolites, have also been implicated in Hg reduction. More specifically the yeasts *Cryptococcus sp.*, *Candida albicans*, and *Sacchraromyces cerevisiae*, have been found capable of reducing Hg, creating Hg(0) presumably as a detoxification mechanism [22, 23]. Coincidently, yeast species have been reported to become the dominating species in some polluted environments [23, 24], which could broaden the significance of fungal Hg(II) reduction in contaminated environments. Despite this, little is known about fungal Hg(II) reduction, and this is an area that warrants further research.

At natural Hg concentrations in the low picomolar range, reduction seems to be a chiefly abiotic photochemical process rather than a biotically-mediated process [20]. However, we do not expect photochemical processes to play a role in the hyporheic zone due to low light penetration. It should be noted that Hg(II) can also be reduced abiotically in the dark, by fulvic and humic acid-associated free radicals [4]. Hg reduction by humic acids has been found to be highest in O_2-free systems, in the absence of Cl^-, at pH 4.5 during lab experiments. It is thought that the presence of Cl^- inhibits reduction as it complexes and stabilizes Hg(II) thereby preventing its reduction [25]. The exact mechanism has not been fully elaborated, but it may need to be taken into account to close the Hg cycle in light-limited systems [25].

Hg(0) Oxidation.

Until recently, it was thought that the oxidation of Hg(0) to Hg(II) in natural waters was a negligible process [20]. As a result, relatively little is known about the mechanisms of Hg(0) oxidation in soils and natural waters, particularly when compared to the body of knowledge on Hg(II) reduction in natural waters [4]. Should this process be significant, it may be critical to MeHg production by increasing available Hg(II), a substrate for methylation. It may also be

critical to HgS(s) dissolution/precipitation processes by shifting the equilibrium and inhibiting dissolution and/or enhancing precipitation.

Thus far, abiotic Hg(0) oxidation has only been found to occur in seawater [4], [20], [26]. Biotic oxidation of Hg(0), on the other hand, is not limited to seawater environments. Plants and mammals have been shown to have Hg(0)-oxidizing capabilities using the catalase[1] enzyme and possibly other peroxidases[2]. H_2O_2 is the oxidant in this two-electron transfer [27]. In 1998 it was first established that bacteria can also contribute to the oxidative phase of the global Hg cycle, through a study demonstrating that the hydroperoxidase-catalase, KatG, of *Escherichia coli* can oxidize Hg(0) to Hg(II) [28]. Wild type strains of common aerobic soil bacteria *Bacillus* and *Streptomyces spp.* have also been shown to exhibit high levels of Hg(0)-oxidizing activity (approximately 1 uM in 3 hrs) [28]. The degree to which these bacterial oxidative reactions contribute to the global Hg cycle has not been explicitly assessed. Some [28] argue that the fast pace of the process in the laboratory suggests that the contribution might be considerable. However, others [4] note that although these oxidation rates are fast they are still considerably slower than reduction of Hg(II) to Hg(0) effected by bacteria carrying the *mer* operon. More recent results suggest that the ability to oxidize Hg(0) to Hg(II) is widespread among diverse anaerobic bacteria, and microbial oxidation of Hg(0) may play an important role in the redox transformation of mercury contaminants in subsurface environments [29, 30]. Further assessment

[1] A catalase is a common enzyme found in nearly all aerobic living organisms, where it functions to catalyze the decomposition of hydrogen peroxide to water and oxygen.

[2] A peroxidase is an enzyme that catalyzes the oxidation of a number of substrates with the concomitant reduction of hydrogen peroxide.

of the prevalence of Hg oxidation in soils/natural freshwaters and an enhanced mechanistic understanding are needed to shed light on this pathway.

Hg(II) Methylation.

Hg methylation produces organic, bioavailable MeHg from Hg(II). MeHg threatens public health due to its high toxicity and potential for bioaccumulation [3]. Bioaccumulation and biomagnification in the food chain can lead to Hg concentrations in fish that are more than 6 orders of magnitude greater than those in the surrounding water [16]. The majority of Hg in the environment is in inorganic forms, and both biotic and abiotic processes can lead to its methylation [4].

Hg methylation appears to be a predominantly biotic process. Although abiotic mechanisms of methylation by fulvic and humic acids, carboxylic acids and alkylated tin compounds exist, their environmental significance has not been established [4]. Sulfate-reducing bacteria (SRB) have been largely implicated as the principal methylators [31] in natural anaerobic environments, with soluble, neutral HgS(aq) as the substrate for methylation [32] and methylcorrinoids acetyl CoA or serine C3 as the intracellular source of the methyl group [4, 32-34]. Recent research shows that strains of anaerobic iron-reducing bacteria (IRB) *Geobacter* and *Desulfuromonas spp.* are also able to methylate Hg [35-37]. A two-gene cluster, *hgcA* and *hgcB*, has been identified to be necessary for methylation in *Desulfovibrio desulfuricans* ND132 and *Geobacter sulfurreducens* PCA, and is present in confirmed methylators but absent in nonmethylators [38]. Further, the presence of homologs of this gene cluster in the genomes of microorganisms distributed across 52 bacteria and methanogenic archaea suggests these

organisms might also be capable of methylation, and the ability to methylate might be more broadly distributed than previously thought [38]. In the environment, the production of MeHg by methylating bacteria is influenced by a number of factors including concentrations of inorganic Hg, organic matter, sulfate, and sulfide, factors which affect the activity of the methylating organisms and/or the availability Hg for methylation [16].

Hg methylation can also be catalyzed by several fungi, where this mechanism may serve a detoxifying role. The mycelia of *Aspergillus niger* and *Scopulariopsis brevicaulis* as well as the cells of yeast *Saccharomyces cerevisiae* have been shown to produce MeHg aerobically in lab cultures [39]. Unlike bacterial methylation, fungal methylation processes occur within aerobic environments. Future research should focus on identifying these processes in nature, as fungal methylation has the potential to change the methylation step of the global Hg cycle, which has traditionally been thought to prevail only in anaerobic environments.

MeHg Demethylation.

MeHg accumulation is natural systems in the net result of methylation, accumulation, and demethylation. MeHg can be demethylated biotically through either 1) reductive demethylation or 2) oxidative demethylation. Reductive demethylation is mediated by the *mer* system. MeHg that diffuses into the cell is first demethylated by protein MerB, releasing CH_4, and Hg(II) is subsequently reduced by the mercuric reductase MerA, producing Hg(0) [4]. This reductive process results in the creation of Hg(0), and therefore in a potential removal of Hg from sediments or the water column through vaporization. Oxidative demethylation, on the other hand, is mediated by anaerobic bacteria through an, as yet, undefined mechanism yielding CO_2, a small amount of CH_4, and an unidentified Hg(II) moiety [4]. In contrast to reductive

demethylation, this oxidative process likely produces Hg(II), which is in turn a substrate for methylation, potentially creating a methylation/demethylation cycle [40].

There is a wide range of chemical transformations, including reduction, oxidation, methylation and demethylation that microorganisms such as bacteria and fungi can exert on Hg species. These changes affect the speciation of Hg, and can therefore influence HgS(s) dissolution in the hyporheic zone. Though some work has looked at the ability of microorganisms to conduct these changes directly on the solid phase [32], this is a largely understudied area of research. Microorganisms may interact with the solid phase through aqueous intermediates or they may interact directly with the surface. Regardless of the nature of the interaction, microbially mediated chemical changes will affect Hg speciation and will ultimately influence Hg mobility.

Solid-Phase Hg

Speciation.

The solid speciation of Hg is an important factor in determining the biotic and abiotic processes that might impact the dissolution of the phase, and gauging the mobility of Hg. In many soils and sediments Hg is predominantly found as the HgS(s) minerals, cinnabar and metacinnabar, as a result of Hg's extreme chalcophilic nature. Cinnabar is the red, hexagonal, α-form of HgS(s) and is the major Hg-bearing mineral in nature [41], while metacinnabar is the black, cubic, β-form polymorph of cinnabar [42, 43]. Cinnabar is the primary ore of Hg, while metacinnabar can form authigenically as a result of precipitation in Hg-contaminated soils and floodplains or upon heating of cinnabar at high temperatures [41, 42, 44, 45]. HgS(s) minerals

are generally considered to be unreactive and stable [6]. HgS(s) phases are extremely insoluble: the $\log K_{so}$ of cinnabar is -39.8, while metacinnabar is slightly more soluble with a $\log K_{so}$ = -38.5 [46].

In addition to mineral Hg, Hg can also be associated with the solid phase as an adsorbate. Iron and aluminum (hydr)oxides, clays, and particulate organic matter are effective substrates for Hg sorption. Hg(II) adsorbs predominantly though an inner-sphere mode on goethite (FeOOH) and bayerite ($Al(OH)_3$) over the pH range of natural waters [47, 48]. Hg(II) sorption on γ-alumina (γ-Al_2O_3) occurs through inner-sphere and likely also through outer-sphere complexation [47, 48]. Hg(II) also adsorbs onto clays (e.g. kaolinite) mainly as inner-sphere but also through outer-sphere complexes [49]. Finally, Hg also has a high affinity for organic matter in soils, largely as a result of Hg's affinity for sulfur-containing functional groups in organic molecules [17].

Although solid associated Hg may be found in the mineral or adsorbed phase, the Hg solid phase tends to be dominated by HgS(s) minerals in anthropogenic Hg-contaminated environments as well as in mine waste environments [45, 50-53].

HgS(s) Dissolution

Sediments represent the largest reservoir of Hg in aquatic environments where Hg is largely found as HgS(s) minerals. These sulfides have largely been considered highly immobile [6]. Though the solubility constants ($\log K_{so}$) of cinnabar and metacinnabar are low (-39.8, -38.5 respectively) [46], the mobility and/or solubility if HgS(s) minerals has been shown to be enhanced by a number of factors including the presence of organic matter, organic acids, sulfur, oxygen, and Hg-resistant bacteria.

Dissolved organic matter (DOM) is known to affect the solubility, mobility, and toxicity of many trace metals [54]. Cinnabar can dissolve in the presence of DOM by means of surface complexation under well-agitated conditions [55, 56]. Particularly, the humic fraction of DOM has been shown to enhance the dissolution of cinnabar to different extents by interacting directly with the mineral surface, resulting in aqueous Hg concentrations that are 12 to 13 orders of magnitudes above those calculated in equilibrium with pure water (10^{-8} M vs. 7 x 10^{-20} M) [55, 56]. The ubiquitous presence of humic substances in natural waters makes the organic matter-enhanced solubilization of cinnabar a potentially important source of aqueous Hg in the environment [55].

Organic acids may also promote Hg mobilization. Low molecular weight organic acids (e.g. ascorbic acid and oxalic acid) have been shown to promote the release of particles from aquifer material by dissolving aquifer cementing agents (i.e. iron (oxy)hydroxides), and adsorbing to minerals thereby reducing and potentially reversing their surface charge promoting repulsive forces between adjacent particles [57]. Due to this effect, organic acids have been shown to promote the release of colloidal HgS(s) in mine waste environments where cinnabar and metacinnabar dominate the solid phase [58-60]. Through lab column experiments, oxalic and citric acid, two common organic acids, have been shown to enhance colloidal transport of HgS(s) from Hg mine tailings [58-60]. This effect is enhanced during high seepage velocities which might be expected in an arid mine waste environment as a result of the steep slopes of mine waste disposal sites and seasonally intense rainfall [59], but would be reduced in an environment with more moderate flow rate (such as the hyporheic zone).

Some sulfur species may also promote mobilization. Theoretical investigations have suggested that cinnabar dissolution is more favorable in the presence of HS^- as compared to pure

water [61]. The presence of polysulfides (S_x^{2-}) has also been shown to increase the solubility of cinnabar [62, 63]. In addition, enhanced dissolution of metacinnabar has been observed in the laboratory in the presence of HS^- and Fe(III) through a polysulfide intermediate [6]. The proposed mechanism involves the oxidation of HS^- to S(0) by Fe(III), and the formation of polysulfides which subsequently facilitate metacinnabar dissolution according to the following reactions:

For 10^{-5} M < $[HS^-]$ < 10^{-4} M

$$HgS(s) + HS^- + 2(x - 1)S(0) \rightarrow Hg(S_x)_2^{2-}(aq) + H^+$$

$$HgS(s) + (x - 1)S(0) + H_2O \rightarrow HgS_xOH^-(aq) + H^+ \text{ [6].}$$

For 10^{-3} M < $[HS^-]$ < 10^{-2} M

$$HgS(s) + HS^- + (x - 1)S(0) \rightarrow Hg(S_x)(SH)^-(aq) + H^+ \text{ [62].}$$

Aqueous sulfur species therefore also play a key role in the dissolution of HgS(s) minerals.

Minerals made up of redox active elements may also dissolve through redox reactions. Oxidative dissolution of cinnabar and metacinnabar has been shown under aqueous oxygenated conditions [42]. The sulfide (S^{2-}) in the mineral is oxidized to thiosulfate ($S_2O_3^{2}$) and sulfate (SO_4^{2-}), while Hg(II) is released from the mineral matrix [42]. Interestingly, cinnabar dissolves to a greater extent than metacinnabar under these conditions [42], though the latter is generally considered to be less soluble [46]. This was the first observation of O_2 effects on HgS(s) dissolution, as previous research on cinnabar had shown that O_2 did not induce Hg release [55, 56]. This may be due to the fact that much of the Hg(II) produced through dissolution is

subsequently immobilized through adsorption to the solid itself [42]. Furthermore, the well-oxygenated conditions in the study by Holley et al. [42] may not match up with the conditions of previous experiments and may also not be representative of the natural environment.

Very little is known about the role of microbes in inducing HgS(s) dissolution [64]. However, it is widely recognized that the bacterial oxidation of metal sulfides to soluble metal sulfates and sulfuric acid, is induced by mesoacidophilic chemolithotrophic bacteria [65]. It has been thought that these sulfide-oxidizing bacteria might also be able to oxidize HgS(s). Although much research has been devoted to the bacterial oxidation of iron sulfides and other sulfides, little experimental work has been conducted on the effect of bacteria in promoting HgS(s) dissolution.

Three bacterial species have been most widely studied in promoting sulfur mineral dissolution due to their industrial application to bioleaching: *Acidithiobacillus ferrooxidans*, *A. thiooxidans*, and *Leptospirillum ferrooxidans. A. ferrooxidans* oxidizes reduced sulfur compounds to sulfate and Fe(II) to Fe(III). *A. thiooxidans* is able to oxidize only reduced sulfur compounds, whereas *L. ferrooxidans* can oxidize only Fe(II) [66]. A Hg-resistant strain of *A. ferrooxidans* was found to induce the mobilization of Hg from cinnabar by producing Hg(0) while oxidizing pyrite (FeS) under acidic conditions [64]. The Hg(0) was likely the result of the action of the *mer* operon discussed earlier. This bacterium could not gain energy in the presence of HgS(s) alone, leading to the conclusion that HgS(s) cannot serve as a growth substrate for either Hg-resistant or Hg-sensitive strains of *T. ferrooxidans* [64]. However, this finding does not preclude the existence of other bacteria capable of using the sulfide in cinnabar or metacinnabar as a substrate for growth. Further, researchers have shown that the HgS(s) dissolution constant is increased over 20-orders of magnitude compared to equilibrium values in the presence of mine

tailing-derived microbial cultures in acidic pH conditions (pH 3.25) [11]. However, the mechanisms for this enhanced solubility have not yet been assessed.

The role of heterotrophic bacteria and fungi in the mobilization of HgS(s) has not yet been investigated. However, heterotrophic bacteria and fungi are known to contribute to metal mobilization though the production of organic acids (e.g., lactic acid, oxalic acid, citric acid, gluconic acid) and compounds such as phenol derivatives which dissolve heavy metals by direct displacement of metal ions from the ore matrix by hydrogen ions and by the formation of soluble metal complexes and chelates [66].

Microbial communities including bacteria and fungi, may promote HgS(s) mobility through a number of mechanisms including but not limited to: Hg reduction, Hg methylation, production of extracellular compounds such as organic acids, increasing the concentration of DOM in the environment, and through S^{2-} oxidation by chemolithotrophic bacteria. Despite this potential effect, the majority of Hg mobilization studies are conducted in abiotic conditions. Further research should be conducted on the effect of microbes in inducing HgS(s) dissolution and elucidating the mechanisms involved.

Despite the mineral's low solubility constants, cinnabar and metacinnabar dissolution can be enhanced by a number of factors. Further research needs to be conducted on HgS(s) dissolution and subsequent Hg mobilization under more environmentally significant conditions.

The Hyporheic Zone

The hyporheic zone is an area that may promote HgS(s) mobilization, as this zone is known to account for a significant flux of metals in the environment [67]. The hyporheic zone is the subsurface region of a stream where there is active mixing of shallow groundwater and

surface water [68]. The mixture of surface water flow (termed downwelling flow) and groundwater flow (termed upwelling flow) into this zone makes this a hydrologic transition zone [68]. Downwelling flows generally bring high dissolved oxygen (DO), organic matter (OM) and nutrients into the hyporheic zone, while upwelling flows generally have lower DO and OM, and lower nutrient concentrations [67]. Heterogeneity produced, for example by sediment surface irregularities or local OM deposits, can lead to the creation of anoxic or hypoxic pockets in an aerobic zone [67]. Steep redox gradients along with high OM concentrations, may promote substantial biological activity which may lead to Hg speciation changes, resulting in mobility and transport into surface and groundwater. Work on hyporheic Hg transformations has focused on anaerobic conditions, but the zone's heterogeneity makes aerobic and anaerobic processes possible within close proximity making for a dynamic habitat affected by diverse chemical reactions and communities of microorganism. Despite their potential significance, the transformations of solid-phase Hg in aerobic/anaerobic transition zones such as the hyporheic zone are little understood [6], and relatively little work has been done to elucidate processes that govern HgS(s) dissolution and Hg mobilization in the aerobic/anaerobic hyporheic zone. Due to its potentially pivotal role in contaminant transport, microbially induced Hg mobilization in the hyporheic zone warrants further research.

Dissertation Objectives

The goal of the subsequent chapters in this dissertation are as follows:

Chapter 2: Identify the bacterial community colonizing HgS(s) and other mineral sulfides *in situ* along the hyporheic zone redox gradient of a circumneutral Hg-contaminated freshwater environment.

Chapter 3: Elucidate the role of the abundant metacinnabar colonizer *Thiobacillus thioparus* and its substrate thiosulfate on inducing the release and volatilization of metacinnabar-hosted Hg.

Chapter 4: Probe the effects of mineral synthesis, mineral loading, and thiosulfate concentration on metacinnabar weathering and subsequent Hg volatilization in the presence of *T. thioparus* cultures.

Our results show that metacinnabar, pyrite, and sphalerite surface colonization in the shallow sediments of a circumneutral Hg-contaminated creek was dominated by sulfur-oxidizing bacteria, while in deeper incubations *Geobacter*, a genus comprising obligately anaerobic metal reducing bacteria, was an abundant community member. The bacterial community on cinnabar, on the other hand, was different being comprised predominantly of methylotrophic bacteria, highlighting the importance of mineral structure in bacterial mineral colonization. Further, this work underlines the importance of understanding microbial ecology at mineral surfaces, rather than bulk soil ecology, to elucidate the potential for microbial communities to effect chemical changes on a given mineral. The discovery that sulfur-oxidizing bacteria dominate colonization of metacinnabar surfaces suggests a potential role for chemolithotrophic bacteria in the weathering of secondary HgS.

Subsequently, we show that the abundant and widespread neutrophilic sulfur-oxidizing bacterium *T. thioparus,* which extensively colonizes metacinnabar surfaces within aerobic, circumneutral creek sediments, also induces the release and volatilization of metacinnabar-hosted Hg. *T. thioparus* incubations exhibit mineral dissolution and subsequent Hg volatilization from both natural and synthetic metacinnabar at various mineral loadings and thiosulfate

concentrations. These findings reveal a new pathway for metacinnabar dissolution and point to mineral-hosted Hg as an underappreciated source of elemental Hg that may contribute to atmospheric Hg budgets.

Finally, we show that thiosulfate, a major intermediate sulfur species in environmental systems and strong Hg(II)-complexing ligand, stimulates metacinnabar dissolution. Higher initial thiosulfate concentrations lead to higher concentrations of dissolved Hg, and adding the thiosulfate in small fluxes over time, as is expected to occur in natural environments, has a further enhancing effect on dissolution. Our work underscores the importance of thiosulfate, formed through both oxidative and reductive legs of the sulfur cycle, in enhancing HgS(s) dissolution.

Therefore, this dissertation shows that authigenic HgS minerals are not merely a sink for Hg within non-acidic natural environments and instead are a source of dissolved and gaseous Hg. The work presented within this dissertation provides critical information to predicting the transport of Hg in the environment and develop appropriate management and remediation strategies for Hg-contaminated systems.

Chapter 1 - References Cited

1. ATSDR. *2007 CERCLA Priority List of Hazardous Substances*. 2007 01/10/2008 [cited 2009; Available from: http://www.atsdr.cdc.gov/cercla/07list.html.

2. Nies, D.H., *Microbial heavy-metal resistance.* Applied Microbiology and Biotechnology, 1999. **51**(6): p. 730-750.

3. Swain, E.B., et al., *Socioeconomic consequences of mercury use and pollution.* Ambio, 2007. **36**(1): p. 45-61.

4. Barkay, T., S.M. Miller, and A.O. Summers, *Bacterial mercury resistance from atoms to ecosystems.* FEMS Microbiology Reviews, 2003. **27**(2-3): p. 355-384.

5. Mason, R.P., Fitzgerald, W.F., Hurley, J., Hanson, A.K., Donaghay, P.L., Sieburth, J.M., *Mercury biogeochemical cycling in a stratified estuary.* Limnology and Oceanography, 1993. **38**: p. 1227–1241.

6. Slowey, A.J. and G.E. Brown, *Transformations of mercury, iron, and sulfur during the reductive dissolution of iron oxyhydroxide by sulfide.* Geochimica et Cosmochimica Acta, 2007. **71**(4): p. 877-894.

7. Zachara, J.M., et al., *Geochemical processes controlling migration of tank wastes in Hanford's Vadose Zone.* Vadose Zone Journal, 2007. **6**: p. 985-1003.

8. Bencala, K.E., *Hyporheic zone hydrological processes.* Hydrological Processes, 2000. **140**(15): p. 2797–2798.

9. Harvey, J.W., and B. J.Wagner, *Quantifying hydrologic interactions between streams and their subsurface hyporheic zones, in Streams and Ground Waters*, J.B. Jones, Mulholland, P.J. , Editor. 2000, Academic: San Diego. p. 3-44.

10. Winter, T.C., Harvey, J.W., Franke, O.L., Alley, W.M., *Ground water and surface water: A single resource*, U.G. Survey, Editor. 1998. p. 79.

11. Jew, A.D., et al., *Microbially enhanced dissolution of HgS in an acid mine drainage system in the California Coast Range.* Geobiology, 2014. **12**(1): p. 20-33.

12. Hurley, J.P., et al. *The Madison declaration on mercury pollution*. in *8th International Conference on Mercury as a Global Pollutant, Madison, Wisconsin, USA, 6-11 August 2006.* 2007. Royal Swedish Academy of Sciences.

13. Anderson, A., *Mercury in soils*, in *The biogeochemistry of mercury in the environment*, J.O. Nriagu, Editor. 1973, Elsevier/North Holland Biomedical Press: Ontario. p. 70-112.

14. Petanen, U. and M. Romantschuk, *Use of bioluminescent bacterial sensors as an alternative method for measuring heavy metals in soil extracts.* Analytica Chimica Acta, 2002. **456**(1): p. 55-61.

15. Council, N.R., *Toxicological Effects of Methylmercury*. 2000, Washington, D.C.: National Academy Press.

16. Fitzgerald, W.F. and C.H. Lamborg, *Geochemistry of Mercury in the Environment*, in *Environmental Geochemistry*, B.S. Lollar, Editor. 2003, Elsevier/Pergamon: Amsterdam, Boston.

17. Schuster, E., *The Behavior of Mercury in the Soil with Special Emphasis on Complexation and Adsorption Processes - a Review of the Literature.* Water Air and Soil Pollution, 1991. **56**: p. 667-680.

18. Creswell, J.E., et al., *Factors controlling temporal and spatial distribution of total mercury and methylmercury in hyporheic sediments of the Allequash Creek wetland, northern Wisconsin.* Journal of Geophysical Research-Biogeosciences, 2008. **113**(G00C02).

19. Andren, A.W., Nriagu, J.O., *The global cycle of mercury*, in *The biogeochemistry of mercury in the environment*, J.O. Nriagu, Editor. 1979, Elsevier/North Holland Biomedical Press: Ontario. p. 1-21.

20. Morel, F.M.M., A.M.L. Kraepiel, and M. Amyot, *The chemical cycle and bioaccumulation of mercury.* Annual Review of Ecology and Systematics, 1998. **29**: p. 543-566.

21. Oregaard, G. and S.J. Sorensen, *High diversity of bacterial mercuric reductase genes from surface and sub-surface floodplain soil (Oak Ridge, USA).* ISME Journal, 2007. **1**(5): p. 453-467.

22. Brunker, R.L. and T.L. Bott, *Reduction of Mercury to Elemental State by a Yeast.* Applied Microbiology, 1974. **27**(5): p. 870-873.

23. Yannai, S., I. Berdicevsky, and L. Duek, *Transformations of Inorganic Mercury by Candida-Albicans and Saccharomyces-Cerevisiae.* Applied and Environmental Microbiology, 1991. **57**(1): p. 245-247.

24. Hagler, A.N. and L.C. Mendoncahagler, *Yeasts from Marine and Estuarine Waters with Different Levels of Pollution in the State of Rio-De-Janeiro, Brazil.* Applied and Environmental Microbiology, 1981. **41**(1): p. 173-178.

25. Allard, B. and I. Arsenie, *Abiotic Reduction of Mercury by Humic Substances in Aquatic System - an Important Process for the Mercury Cycle.* Water Air and Soil Pollution, 1991. **56**: p. 457-464.

26. Amyot, M., F.M.M. Morel, and P.A. Ariya, *Dark oxidation of dissolved and liquid elemental mercury in aquatic environments.* Environmental Science & Technology, 2005. **39**(1): p. 110-114.

27. Wigfield, D.C. and S. Tse, *Kinetics and Mechanism of the Oxidation of Mercury by Peroxidase.* Canadian Journal of Chemistry-Revue Canadienne De Chimie, 1985. **63**(11): p. 2940-2944.

28. Smith, T., et al., *Bacterial oxidation of mercury metal vapor, Hg(0).* Applied and Environmental Microbiology, 1998. **64**(4): p. 1328-1332.

29. Colombo, M.J., et al., *Oxidation of Hg(0) to Hg(II) by diverse anaerobic bacteria.* Chemical Geology, 2014. **363**: p. 334-340.

30. Colombo, M.J., et al., *Anaerobic oxidation of Hg(0) and methylmercury formation by Desulfovibrio desulfuricans ND132.* Geochimica et Cosmochimica Acta, 2013. **112**: p. 166-177.

31. Compeau, G.C. and R. Bartha, *Sulfate-Reducing Bacteria - Principal Methylators of Mercury in Anoxic Estuarine Sediment.* Applied and Environmental Microbiology, 1985. **50**(2): p. 498-502.

32. Benoit, J.M., C.C. Gilmour, and R.P. Mason, *The influence of sulfide on solid phase mercury bioavailability for methylation by pure cultures of Desulfobulbus propionicus (1pr3).* Environmental Science & Technology, 2001. **35**(1): p. 127-132.

33. Choi, S.C., T. Chase, and R. Bartha, *Metabolic Pathways Leading to Mercury Methylation in Desulfovibrio Desulfuricans Ls.* Applied and Environmental Microbiology, 1994. **60**(11): p. 4072-4077.

34. Berman, M., T. Chase, and R. Bartha, *Carbon Flow in Mercury Biomethylation by Desulfovibrio Desulfuricans.* Applied and Environmental Microbiology, 1990. **56**(1): p. 298-300.

35. Fleming, E.J., et al., *Mercury methylation from unexpected sources: Molybdate-inhibited freshwater sediments and an iron-reducing bacterium.* Applied and Environmental Microbiology, 2006. **72**(1): p. 457-464.

36. Kerin, E.J., et al., *Mercury methylation by dissimilatory iron-reducing bacteria.* Applied and Environmental Microbiology, 2006. **72**(12): p. 7919-7921.

37. Warner, K.A., E.E. Roden, and J.C. Bonzongo, *Microbial mercury transformation in anoxic freshwater sediments under iron-reducing and other electron-accepting conditions.* Environmental Science & Technology, 2003. **37**(10): p. 2159-2165.

38. Parks, J.M., et al., *The genetic basis for bacterial mercury methylation.* Science, 2013. **339**(6125): p. 1332-5.

39. Vonk, J.W. and Sijpeste.Ak, *Studies on Methylation of Mercuric Chloride by Pure Cultures of Bacteria and Fungi.* Antonie Van Leeuwenhoek Journal of Microbiology, 1973. **39**(3): p. 505-513.

40. Schaefer, J.K., J. Letowski, and T. Barkay, *mer-mediated resistance and Volatilization of Hg(II) under anaerobic conditions.* Geomicrobiology Journal, 2002. **19**(1): p. 87-102.

41. Ehrlich, H.L., *Geomicrobiology*. 1981, New York: Marcel Dekker, Inc.

42. Holley, E.A., et al., *Mercury mobilization by oxidative dissolution of cinnabar (alpha-HgS) and metacinnabar (beta-HgS).* Chemical Geology, 2007. **240**(3-4): p. 313-325.

43. Rytuba, J.J., *Mercury from mineral deposits and potential environmental impact.* Environmental Geology, 2003. **43**(3): p. 326-338.

44. Ravichandran, M., et al., *Inhibition of precipitation and aggregation of metacinnabar (mercuric sulfide) by dissolved organic matter isolated from the Florida Everglades.* Environmental Science & Technology, 1999. **33**(9): p. 1418-1423.

45. Barnett, M.O., et al., *Formation of mercuric sulfide in soil.* Environmental Science & Technology, 1997. **31**(11): p. 3037-3043.

46. Dyrssen, D., *Biogenic Sulfur in 2 DIfferent Marine Environments.* Marine Chemistry, 1989. **28**(1-3): p. 241-249.

47. Kim, C.S., J. Rytuba, and G.E. Brown, *EXAFS study of mercury(II) sorption to Fe- and Al-(hydr)oxides - II. Effects of chloride and sulfate.* Journal of Colloid and Interface Science, 2004. **270**(1): p. 9-20.

48. Kim, C.S., J.J. Rytuba, and G.E. Brown, *EXAFS study of mercury(II) sorption to Fe- and Al-(hydr)oxides I. Effects of pH.* Journal of Colloid and Interface Science, 2004. **271**(1): p. 1-15.

49. Sarkar, D., M.E. Essington, and K.C. Misra, *Adsorption of mercury(II) by kaolinite.* Soil Science Society of America Journal, 2000. **64**(6): p. 1968-1975.

50. Han, F.X., et al., *Binding, distribution, and plant uptake of mercury in a soil from Oak Ridge, Tennessee, USA.* Science of the Total Environment, 2006. **368**(2-3): p. 753-768.

51. Kim, C.S., G.E. Brown, and J.J. Rytuba, *Characterization and speciation of mercury-bearing mine wastes using X-ray absorption spectroscopy.* Science of the Total Environment, 2000. **261**(1-3): p. 157-168.

52. Kim, C.S., J.J. Rytuba, and G.E. Brown, *Geological and anthropogenic factors influencing mercury speciation in mine wastes: an EXAFS spectroscopy study.* Applied Geochemistry, 2004. **19**(3): p. 379-393.

53. Wang, W. and C.T. Driscoll, *Patterns of Total Mercury Concentrations in Onondaga Lake, New-York.* Environmental Science & Technology, 1995. **29**(9): p. 2261-2266.

54. Buffle, J., *Complexation Reactions in Aquatic Systems: An Analytical Approach*. 1988, Chichester, England: Ellis Horwood Limited.

55. Ravichandran, M., et al., *Enhanced dissolution of cinnabar (mercuric sulfide) by dissolved organic matter isolated from the Florida Everglades.* Environmental Science & Technology, 1998. **32**(21): p. 3305-3311.

56. Waples, J.S., et al., *Dissolution of cinnabar (HgS) in the presence of natural organic matter.* Geochimica et Cosmochimica Acta, 2005. **69**(6): p. 1575-1588.

57. Swartz, C.H. and P.M. Gschwend, *Mechanisms controlling release of colloids to groundwater in a Southeastern Coastal Plain aquifer sand.* Environmental Science & Technology, 1998. **32**(12): p. 1779-1785.

58. Lowry, G.V., et al., *Macroscopic and microscopic observations of particle-facilitated mercury transport from new idria and sulphur bank mercury mine tailings.* Environmental Science & Technology, 2004. **38**(19): p. 5101-5111.

59. Slowey, A.J., et al., *Role of organic acids in promoting colloidal transport of mercury from mine tailings.* Environmental Science & Technology, 2005. **39**(20): p. 7869-7874.

60. Slowey, A.J., J.J. Rytuba, and G.E. Brown, *Speciation of mercury and mode of transport from placer gold mine tailings.* Environmental Science & Technology, 2005. **39**(6): p. 1547-1554.

61. Tossell, J.A., *Theoretical studies on the formation of mercury complexes in solution and the dissolution and reactions of cinnabar.* American Mineralogist, 1999. **84**(5-6): p. 877-883.

62. Jay, J.A., F.M.M. Morel, and H.F. Hemond, *Mercury speciation in the presence of polysulfides.* Environmental Science & Technology, 2000. **34**(11): p. 2196-2200.

63. Paquette, K.E. and G.R. Helz, *Inorganic speciation of mercury in sulfidic waters: The importance of zero-valent sulfur.* Environmental Science & Technology, 1997. **31**(7): p. 2148-2153.

64. Baldi, F. and G.J. Olson, *Effects of Cinnabar on Pyrite Oxidation by Thiobacillus ferrooxidans and Cinnabar Mobilization by a Mercury-Resistant Strain.* Applied and Environmental Microbiology, 1987. **53**(4): p. 772-776.

65. Schippers, A. and W. Sand, *Bacterial leaching of metal sulfides proceeds by two indirect mechanisms via thiosulfate or via polysulfides and sulfur.* Applied and Environmental Microbiology, 1999. **65**(1): p. 319-321.

66. Bosecker, K., *Bioleaching: Metal solubilization by microorganisms*. FEMS Microbiology Reviews, 1997. **20**(3-4): p. 591-604.

67. Boulton, A.J., et al., *The functional significance of the hyporheic zone in streams and rivers.* Annual Review of Ecology and Systematics, 1998. **29**: p. 59-81.

68. Alley, W.M., et al., *Hydrology - Flow and storage in groundwater systems.* Science, 2002. **296**(5575): p. 1985-1990.

Page intentionally left blank

CHAPTER 2

BACTERIAL COLONIZATION OF SULFIDE MINERALS IN NEUTRAL FRESHWATER CREEK SEDIMENTS

Corresponding supplementary information is included in Appendix A

Abstract

Numerous microorganisms are involved in the transformation of minerals and can contribute to mineral weathering. Mineral-associated bacterial communities are potential key players in effecting chemical changes that can impact mineral alteration due to their proximity and ability to induce a number of physical and chemical mineral transformations. Chemooautotrophic bacteria, for example, can use sulfide minerals as energy sources in oxic environments thereby promoting mineral oxidation and dissolution. However, little work has been conducted investigating the *in situ* bacterial colonization of sulfide minerals in neutral freshwater systems. Further, while mercury sulfide minerals (HgS) are not considered energy sources for chemoautotropic bacteria, the metabolic activity of HgS-associated communities within the environment is unknown. We examined the distribution, relative abundance and diversity of mineral-associated bacteria colonizing primary and secondary HgS phases (eg. cinnabar and metacinnabar), ZnS (sphalerite), and FeS_2 (pyrite) incubated within the Hg-contaminated hyporrheic zone sediments of the bank and channel of the East Fork Poplar Creek (EFPC) in Oak Ridge, TN. Phylogenetic analysis of targeted-amplicon pyrosequencing data reveal that in shallow sediments, the sequence community of field-incubated metacinnabar, pyrite, and sphalerite was dominated by sulfur-oxidizing bacteria, while in deeper incubations *Geobacter*, a genus comprising obligately anaerobic bacteria, was abundant. Operational taxonomic unit-based statistical tools applied to pyrosequencing data show that the sequence communities on the various sulfide minerals cluster primarily by incubation depth and incubation location within the sediment. To a lesser extent, however, the host mineral also has an effect on the bacterial community, with cinnabar-associated communities clustering together regardless of location. The ecological differences in the bacterial communities colonizing the polymorphs

cinnabar and metacinnabar further highlight the importance of mineral structure, and may have profound effects on differential weathering of these mineral phases by bacteria. This study underlines the importance of understanding the mineral-associated microbial ecology, rather than bulk soil ecology, to elucidate the potential for microorganisms to effect chemical changes on a given mineral.

Introduction

It is widely recognized that microorganisms are involved in the transformation of minerals and can contribute to mineral weathering. For instance, minerals can serve as electron donors to chemoautotrophic bacteria providing energy for metabolic growth and the formation of cellular material from inorganic carbon. By catalyzing redox reactions that are in disequilibrium in the environment, chemoautotrophs promote oxidative reactions on the mineral for energy gain. Sulfide minerals such as pyrite (FeS_2), sphalerite (ZnS), cinnabar (α-HgS), and metacinnabar (β-HgS), which contain sulfide as the major anion, are therefore potential sources of energy to bacteria in oxic and/or suboxic environments.

Oxidation of reduced sulfur compounds through chemolithotrophic processes is one of the most prevalent energy yielding reactions in environments such as deep ocean hydrothermal vents [1-3], and has been proposed as one of the earliest self-sustaining metabolisms [4-7]. The majority (> 95%) of the energy available from oxidation of metal sulfides is derived from the sulfide, rather than the host metal [8-10]. Yet, studies on the interaction between microorganisms and minerals have shown that the mineralogical structure and host metal strongly influence the composition of the mineral-associated microbial community [11].

Much research has been devoted to investigating the microbial colonization and

microbially mediated oxidation of iron sulfides and other metal sulfides in the deep sea ocean [9, 11-13] and acidic freshwater environments [14-16]. However, little work has been done investigating the bacterial colonization of sulfides in neutral freshwater systems. Although chemoautotrophic microorganisms are ubiquitous on the Earth, these organisms are thought to represent only a small fraction of the microbial community abundance and diversity in most environments but may have a disproportionately large influence on sulfide mineral weathering [17].

Further, little is known about the bacterial colonization of mercury sulfide minerals (HgS) in the environment. Sediments, where mercury (Hg) can exist as HgS, represent a major reservoir of Hg in aquatic environments. Although HgS minerals have historically been considered insignificant sources of soluble Hg(II) to the environment due to their low solubility, sulfide-oxidizing bacteria may also be able to oxidize and subsequently dissolve HgS. For instance, under acidic pH conditions (pH~3), HgS dissolution can be enhanced in the presence of mine tailing derived microbial cultures [18]. Also under these acidic conditions, an *Acidithiobacillus* bacterium has been implicated in inducing the volatilization of Hg released from cinnabar [19]. Yet under non-acidic conditions (pH > 4), both HgS phases are considered to be unreactive and stable due to their low solubility and very slow abiotic dissolution kinetics [20-22]. Nevertheless, little is known about the composition of HgS mineral-associated communities and their potential for inducing HgS dissolution within the environment.

HgS-associated bacterial communities may promote HgS dissolution and Hg mobility through a number of mechanisms including but not limited to: Hg reduction, Hg methylation, production of extracellular compounds such as organic acids, increasing the concentration of dissolved organic matter in the environment, and through S^{2-} oxidation by chemolithotrophic

bacteria. Bacteria may interact directly with the solid mineral or through aqueous intermediates. Regardless of the nature of the interaction, mineral-associated communities are potential key players in effecting chemical changes that can impact dissolution.

To this end, we assessed the mineral-associated bacterial community composition and diversity on cinnabar, metacinnabar, pyrite, and sphalerite along a redox gradient of the East Fork Poplar Creek (EFPC) in the Y-12 National Security Facility in Oak Ridge. Identifying this epilithic and endolithic community, rather than the entire sediment community is critical, as microenvironments formed directly on and within the mineral are likely to make this community significantly different from that of the surrounding soil. To our knowledge this is the first study exploring the *in situ* resident bacterial community on various metal sulfides in neutral freshwater sediments.

Materials and methods

Field Sampling

Cinnabar, metacinnabar, pyrite, and sphalerite specimens were obtained from the Harvard Museum of Natural History (HMNH) Mineralogical Collection. Specimens were analyzed using XRD (Scintag XDS2000) to confirm sample composition. Further, microscopy observations revealed pyrite inclusions within the metacinnabar mineral. Iron impurities are known to stabilize the metacinnabar structure against evolution to cinnabar in the ambient environment [23].

Minerals were cut into sections approximately 2 cm by 2cm by 1 mm, and polished. Sections were mounted on glass slides (2 cm by 2.5 cm) using super glue. The glass slides with the mounted minerals were then secured into two rows of precut holes in a 15 cm wide by 30 cm

tall polycarbonate sampler and covered in mesh to prevent large organisms from interfering with the slabs during incubation (***Figure 2.1a***). This sampler was inserted directly into sediments within the East Fork Poplar Creek, Oak Ridge, Tennessee, USA. Depending upon their position within the polycarbonate sampler, mineral sections were incubated at a shallow and deep location, 3.8 cm (~2-5 cm) and 26.7 cm (~25-28 cm) below the water sediment interface, respectively, for 6 weeks between September and October 2010. The sites of sampler deployment within the creek channel (N 36° 00.101', W 084° 15.011', ± 18 ft) and creek bank (N 36° 00.102', W 084° 15.015', ± 16 ft) were located approximately 70m upstream from sampling site EFK 22 (***Figure 2.1b***). Mineral incubations were assigned names based upon their incubation location (CC for creek channel and CB for creek bank), incubation depth ("1" for shallow incubations and "3" for deep incubations), and host mineral (C for cinnabar, M for metacinnabar, P for pyrite, and S for sphalerite) (***Figure 2.1b***). For example, sample CC3-P refers to the deep creek channel pyrite incubation.

Once retrieved, mineral samplers were transported on ice to our laboratory where they were preserved within 24 hours. Mineral slabs used for DNA extraction and sequencing were stored at -80°C. Mineral slabs for FISH were fixed using 4% paraformaldehyde, rinsed twice in PBS solution, and stored at -20°C in a storage buffer consisting of a 1:1 (vol/vol) mixture of PBS and 96% ethanol until further processing. Near the creek bank incubation location, surface sediments were collected aseptically and transported on ice to our laboratory where they were stored at 4°C until further processing (***Figure 2.1b***). Surface sediments were dried and sieved using a 250 μm sieve. Creek bank sediment cores were also collected at EFK 22, located 70m downstream of the mineral incubation site (***Figure 2.1b***). Sediment cores were transported on ice to the lab, and stored at 4°C until further processing. Within 1 week of sampling, sediment cores

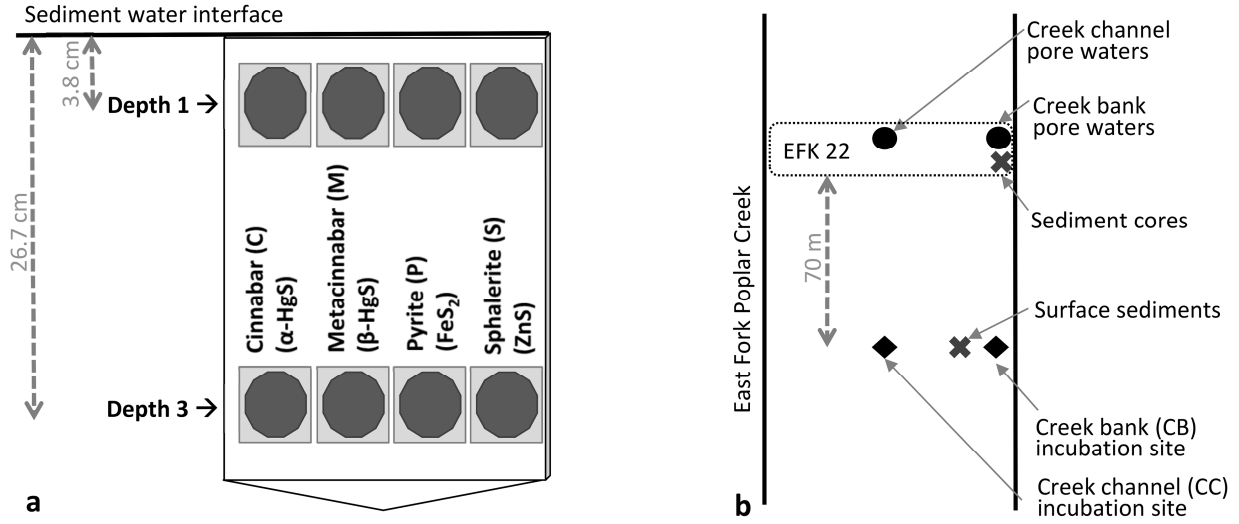

Figure 2.1. (a) Samplers used for mineral incubations, and (b) bird's eye view of the East Fork Poplar Creek showing mineral incubation sites in relation to neighboring sediment and pore water sampling sites. Mineral incubations were assigned names based upon their incubation location (CC for creek channel and CB for creek bank), incubation depth ("1" for shallow incubations and "3" for deep incubations), and host mineral (C for cinnabar, M for metacinnabar, P for pyrite, and S for sphalerite).

were processed under an oxygen-free atmosphere, where the rind was removed and the core was divided into slices corresponding to different depths. Following processing, sediments were stored at -20°C.

Field Site Background and Geochemistry

A history of nuclear weapons production has resulted in elevated Hg levels within sediments of the Y-12 National Security Facility in Oak Ridge, where elemental Hg was used to enrich lithium between the 1950s and 1960s. The plant is located at the headwaters of the EFPC to which process water containing Hg was discharged. Between 108,000 and 212,000 kg of Hg are estimated to have been released into the watershed [24]. A significant fraction of the Hg continues to be deposited in the flood plain [24, 25], a large portion of which has been converted

to HgS [26]. The fraction of Hg found as HgS in the EFPC flood plain ranges from 45 to 90% in the buried, most-contaminated soils [24]. Hg concentrations in the Upper EFPC watershed soils range from 0.01 to 7700 mg/kg [27]. The majority of the contamination is accumulated in the upper 3 meters of floodplain soils and the sediments of the EFPC [28].

The geochemistry of the EFPC pore water at EFK 22, 70 m downstream of the mineral incubation sites, has been extensively monitored. Chemical and physical parameters of creek channel and creek bank pore waters collected in October 2010, on the day of mineral sampler retrieval, are summarized in ***Table 2.1*** and ***Table 2.2***. Because creek channel and creek bank incubation sites were characterized by sand, gravel and cobble deposits through the top 30 cm of sediment, both mineral incubation sites are more similar to the creek channel pore water sampling location at EFK 22 which has similar sediment texture rather than the creek bank pore water sampling location at EFK 22 which is characterized by fine grained silt material with evidence of buried leaf litter. As a result of this sediment texture, there is little change in water quality parameters with depth in the EFK 22 creek channel (***Table 2.1***). Similar geochemistry is expected for both the creek bank and creek channel mineral incubation sites. Measured pH in the creek channel in EFK 22 ranged from 7.8 to 8.1, while temperature ranged from 14.7 to 16.7°C (***Table 2.1***). At depths 0 to 23 cm below the water sediment interphase, dissolved Hg in EFK 22 creek channel pore water was between 7 and 19 ng/L, and ORP ranged from 69 to 118 mV (***Table 2.1***). At a 30 cm sediment depth, pore water was not extractable from the sediments, and hence no pore water data are available regarding the ORP of the deep incubation site (depth = 27 cm). However, following the removal of mineral samplers, thick oxidation rinds were observed on shallow metacinnabar incubations and sparser oxidation patches in deep metacinnabar incubations, suggesting there was less oxygen available in deep than in shallow incubations.

Chemical and physical parameters of the creek channel pore waters at EFK 22 October 2010

Parameter	Depth (cm)			
	0.0	7.6	15.2	22.9
Temperature (°C)	14.7	16.5	16.1	16.7
pH	8.0	8.1	8.0	7.8
Conductivity (µS/cm)	354	356	355	316
ORP (mV)	85	69	118	115
Element Concentration (mg/L)				
Ca	41.5 ± 1.2	39.9 ± 1.2	40.7 ± 1.2	32.1 ± 1.2
Mg	12.9 ± 1.1	12.4 ± 1.1	12.6 ± 1.1	14.7 ± 1.1
Na	9.7 ± 1.1	9.2 ± 1.1	9.1 ± 1.1	5.7 ± 1.1
Dissolved Hg (ng/L)	19.05 ± 4.8	12.8 ± 0.4	12.1 ± 0.4	7.1 ± 0.4
Ion Concentration				
NH_4^+ (ug/L)	82.7 ± 0.8	26.8 ± 0.7	5.9 ± 0.8	15.9 ± 0.7
SRP (ug/L)	26.9 ± 0.5	37.4 ± 0.5	46.9 ± 0.5	30.4 ± 0.5
Sulfide (ug/L)	ND	ND	ND	ND
Cl^- (mg/L)	10.6 ± 0.1	10.7 ± 0.1	10.6 ± 0.1	4.2 ± 0.1
Br^- (mg/L)	ND	ND	ND	ND
NO_3^- (mg/L)	7.3 ± 0.1	7.7 ± 0.1	7.7 ± 0.1	3.3 ± 0.1
SO_4^{3-} (mg/L)	36.8 ± 0.1	36.4 ± 0.1	36.3 ± 0.1	31.2 ± 0.1

Table 2.1. Chemical and physical parameters of the creek channel pore waters at EFK 22 October 2010. ND denotes values below instrument detection limit. Uncertainty in the measurement is reported as ± 1 standard error.

Chemical and physical parameters of the creek bank pore waters at EFK 22 October 2010

Parameter	Depth (cm)			
	0.0	7.6	15.2	22.9
Temperature (°C)	16.8	17	18	18.1
pH	8.2	7.7	7.5	7.4
Conductivity (µS/cm)	354	367	369	391
ORP (mV)	126	105	-9	-148
Element Concentration (mg/L)				
Ca	40.7 ± 1.2	42.8 ± 1.2	44.6 ± 1.2	48.3 ± 1.2
Mg	12.5 ± 1.1	11.8 ± 1.1	10.0 ± 1.1	9.9 ± 1.1
Na	8.3 ± 1.1	9.5 ± 1.1	9.3 ± 1.1	9.0 ± 1.1
Dissolved Hg (ng/L)	11.5 ± 0.4	15.2 ± 0.4	18.9 ± 0.4	12.1 ± 0.4
Ion Concentration				
NH_4^+ (ug/L)	11.3 ± 0.7	17 ± 0.7	339.2 ± 1.9	734.4 ± 4.1
SRP (ug/L)	35.13 ± 0.5	18.46 ± 0.5	24.94 ± 0.5	29.76 ± 0.5
Sulfide (ug/L)	ND	ND	ND	37 ± 5.4
Cl^- (mg/L)	10.2 ± 0.1	11.0 ± 0.1	11.2 ± 0.1	11.0 ± 0.1
Br^- (mg/L)	ND	ND	ND	ND
NO_3^- (mg/L)	5.8 ± 0.2	ND ± 0.2	ND ± 0.2	ND ± 0.2
SO_4^{3-} (mg/L)	33.8 ± 0.2	38.4 ± 0.1	36.8 ± 0.2	29.9 ± 0.2

Table 2.2. Chemical and physical parameters of the creek bank pore waters at EFK 22 October 2010. ND denotes values below instrument detection limit. Uncertainty in the measurement is reported as ± 1 standard error.

During sampler retrieval, sediment cores were collected from a creek bank location 70m downstream of the mineral incubation site at site EFK 22 (***Figure 2.1b***). Aqua regia digestion followed by ICP-AES total metals analysis was conducted for sediment aliquots from different depths. Hg concentrations within the sediments at sampling location decrease as a function of depth (***Figure 2.2***).

Surface sediments collected from the EFPC near the creek bank mineral incubation site were dried and sieved to obtain the size fraction <250μm (***Figure 2.1b***). Mercury L_{III}-edge Extended X-ray absorption fine structure spectroscopy (EXAFS) spectra were collected on beamline 11-2 at the Stanford Synchrotron Radiation Lightsource. Hg L_{III} Edge EXAFS spectra collected were best fit with a Hg-S scattering interaction (***Figure 2.3***) The Hg-S interatomic distance and coordination number agree with those in metacinnabar (4 sulfur atoms at 2.53 Å *(4))*, suggesting that Hg exists predominantly as metacinnabar in creek surface sediment. This is in agreement with previous studies which have also reported metacinnabar to be the dominant solid Hg phase in the flood plain sediments of the EFPC [24].

Molecular Methods

Field-incubated minerals were aseptically crushed and total DNA was extracted using the Ultraclean soil DNA kit (Mo Bio Laboratories) using the maximum yield protocol with the following modifications. After minerals were added to the bead solution tubes, tubes were sonicated for 5 minutes. Following addition of IRS solution, tubes were incubated at 70°C for 10 minutes, and 200 μg of polyadenylic acid was added [29, 30], followed by vortexing at maximum speed for 15 minutes. The 16S rRNA gene of environmental DNA was amplified

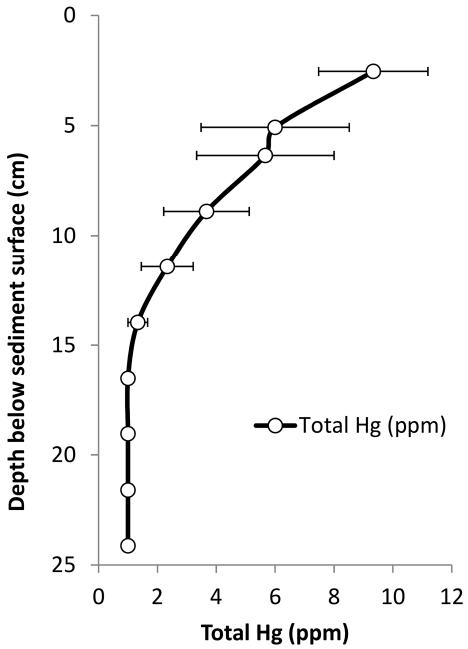

Figure 2.2. Total Hg concentration within EFPC sediments as a function of depth. Error bars represent standard error from 3 separate creek bank sediment cores taken at EFK 22, with the exception of measurements taken at depths 22 and 24 cm which represent values measured in only one sediment core.

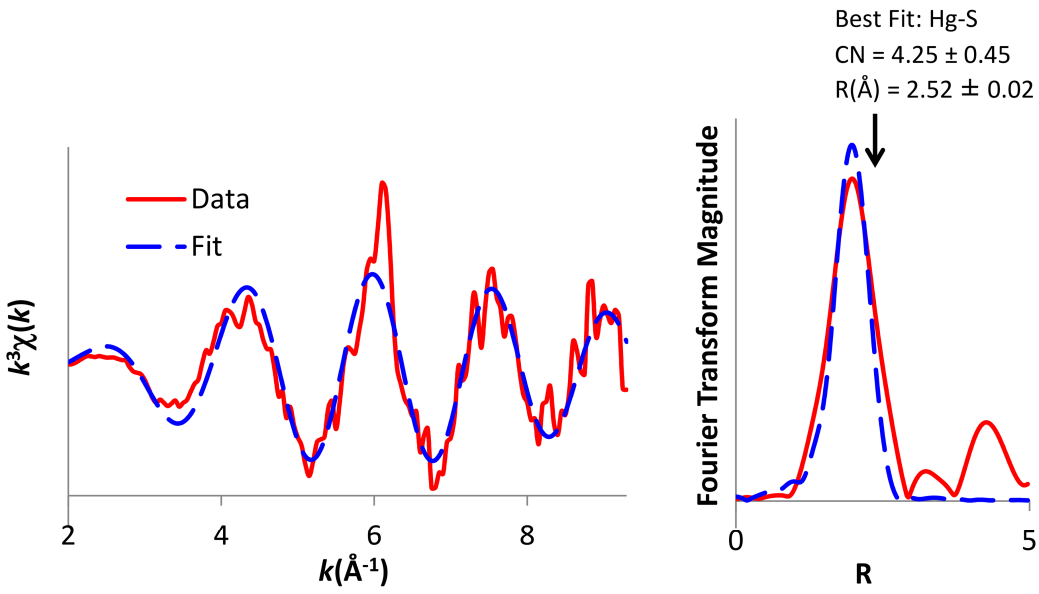

Figure 2.3. k^3 weighted mercury L_{III}-edge bulk EXAFS (right) and Fourier transform (left) showing data and fitting results for collected spectrum for creek surface sediment near the creek bank sieved using a 250µm sieve.

using the 8F and 1492R primer set and conditions used previously [31] in triplicate or quadruplicate to yield sufficient DNA for sequencing. DNA was extractable from all minerals except cinnabar samples incubated in the creek channel (samples CC1-C and CC3-C), where extracted DNA was not sufficiently amplified either due to insufficient DNA quantity or quality. DNA extraction for sample CB1-P was damaged during processing. Amplification products were purified using the QIAquick nucleotide removal kit (Qiagen). Bacterial tag-encoded pyrosequencing (bTEFAP) was conducted by the Research and Testing Laboratory, Lubbock, TX using the GS FLX Titanium sequencing platform (Roche Applied Science). Primers 28F (5′GAGTTTGATCNTGGCTCAG) and 519r (5′GTNTTACNGCGGCKGCTG) were used to sequence variable regions V1-V3 of the 16S rRNA gene.

Sequence Processing

Pyrosequencing reads were denoised using AmpliconNoise, and chimeras removed using Perseus [32]. Resulting sample reads were all longer than 150 bp, had a quality score greater than 20, and no ambiguous reads, therefore no further quality filtering was needed. Sample reads were aligned and clustered using the Ribosomal Database Project (RDP) Pyrosequencing Pipeline [33]. Bacterial 16S rRNA gene sequences were classified using a naïve Bayesian rRNA classifier, version 2.0, with a bootstrap cutoff of 80% [34].

Class-level taxonomical abundances in each sample are presented as percent abundance of sequences falling within that class relative to the total number of sequences, including those that were not classifiable down to the class-level. Classes comprising less than 0.5% of all sequences are not shown in figures. Genus level abundances are presented as percent abundance of sequences falling within that genus relative to the total number of sequences classifiable down

to genus. Unclassifiable sequences were eliminated from this analysis in order not to detract attention from sequences with taxonomic assignments. Genera comprising less than 1.5% of the total classifiable sequences are not shown in figures though they are included in all of the OTU based analyses.

Rarefaction curves and all other OTU based analyses were calculated for each sample, using an OTU cutoff of 0.03 (e.g., 3% dissimilarity threshold) [35]. A Sorensen distance matrix was calculated for all samples with a Chao abundance correction using RDP's Pyrosequencing Pipeline [35]. Distance matrices were imported into the PAST data analysis package for statistical analyses including hierarchical cluster analysis, nonmetric multidimensional scaling (NMDS) analysis, and analysis of similarity (ANOSIM) [36]. NMDS, clustering, and ANOSIM were used to examine how bacterial communities among different minerals across the two depths and locations were related. Because the size of each sample library varied greatly between 1380 reads and 10846 reads, normalized sample libraries containing 1380 reads each were developed to calculate a Sorensen Distance matrix based on an OTU cutoff of 0.03. Hierarchical clustering, NMDS, and ANOSIM analyses were based on this Sorensen Distance matrix.

CARD-FISH

For CARD–FISH analyses, paraformaldehyde-fixed mineral samples were hybridized with horseradish-peroxidase linked oligonucleotide probe *TBD121* [37] with Cy3-tyramides (Biomers.net). This probe targets *Thiobacillus thioparus* and *Thiobacillus denitrificans*. SYBR Green I DNA stain (Invitrogen) was used as a counterstain. Digital images were collected on a LSM510-META laser scanning confocal microscope (Carl Zeiss) at the Marine Biological Laboratory (Woods Hole, MA, USA).

Results

OTU-Based Analyses

After denoising, 64,732 high-quality bacterial sequences with an average read length of 343 bp were obtained from 13 mineral samples. Because sites were unequally sampled, rarefaction rather than absolute OTU numbers or nonparametric estimates, was used to compare sampling effort and richness across all sites at the 3% sequence difference level (***Figure 2.4***). The shallow creek channel pyrite incubation hosted microbial communities exhibiting the highest OTU richness, while the shallow creek channel metacinnabar incubation (CC1-M) exhibited the lowest richness. The 5 richest samples in order of decreasing richness were CC1-P, CC1-S, CC3-P, CB3-P and CB1-C. Due to the denoising algorithm employed, these richness estimates are free from the influence of sequencing errors, PCR mutations, and chimeras [32]. Rarefaction trends were similar at the 5% sequence difference level (data not shown).

A Sorensen distance matrix based on OTU clusters in the pyrosequencing sample data sets at the 3% difference level was used to develop NMDS, hierarchical clustering and ANOSIM analyses. The Sorensen distance is calculated based on the number of total and shared OTUs between two samples. NMDS based on the Sorensen distance yielded the pattern seen in ***Figure 2.5***. Samples group primarily by depth, with shallow samples clustering near the left side of the plot, and deep samples clustering to the right of the plot. Samples also appear to group by their incubation location (e.g. shallow creek bank, shallow creek channel, deep creek bank, and deep creek channel), and polygons are drawn around samples from the same incubation location (***Figure 2.5***). Based on the NMDS plot, samples generally do not group based on host mineral,

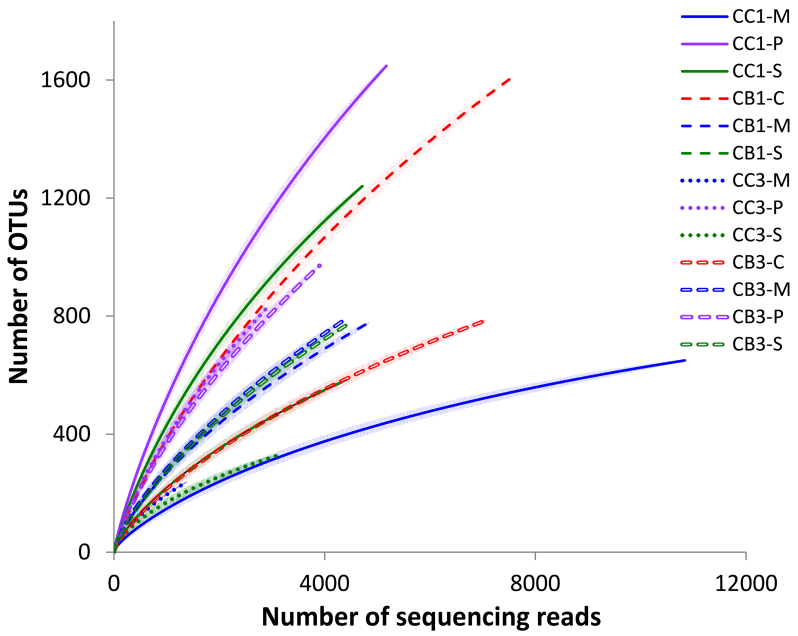

Figure 2.4. Rarefaction curves at the 3% difference level for each of the mineral incubations. Shaded area around line represents the 95% confidence interval.

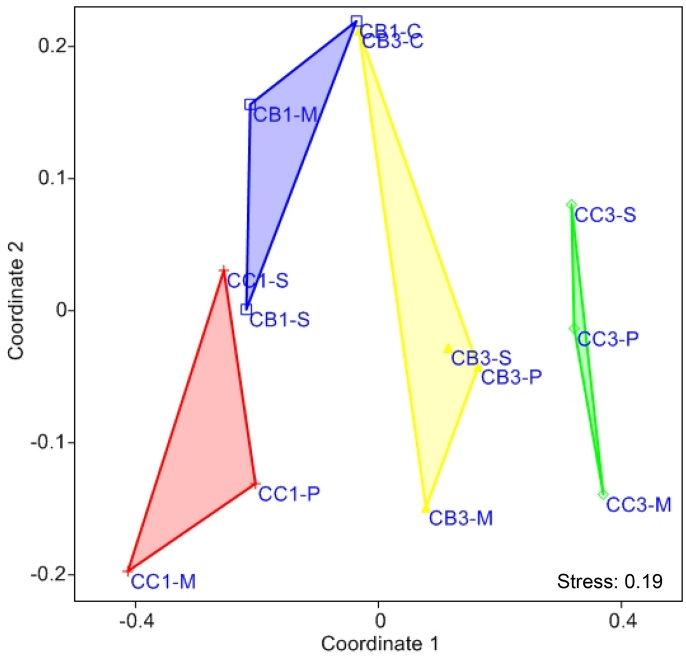

Figure 2.5. nMDS 2D similarity plot based on a Sorensen distance matrix comparing mineral-associated bacterial communities at the 3% difference level. Convex hulls connect points from samples from within the same sampling location and depth.

with the exemption of the cinnabar incubations (CB1-C and CB3-C), which group most closely with each other, and the shallow sphalerite incubations (CC1-S and CB1-S), which also group closely with each other but away from the deep sphalerite incubations (CC3-S and CB3-S).

An UPGMA tree calculated from Sorensen distances also supports grouping primarily by depth as all shallow samples and deep samples fall into two different tree branches, with the exception of sample CB3-C which clusters most closely with the other creek bank cinnabar sample (CB1-C), and outside of the branch with the deep incubations (***Figure 2.6***). The UPGMA tree is color coded with samples from the same sampling location having the same color. This tree supports grouping by incubation location with the exception of samples CB3-C, CB1-C, and CC1-S (***Figure 2.6***). Similar to the findings from the NMDS plot, samples generally do not group based on host mineral, with the exemption of cinnabar incubations (CB1-C and CB3-C) which cluster closely despite differences in incubation depth, and the shallow sphalerite incubations (CC1-S and CB1-S) which also cluster with each other (***Figure 2.6***).

Finally, one-way ANOSIM tests using the Sorensen distance matrix were conducted to determine the statistical significance of grouping samples by depth (shallow vs. deep), location (shallow creek bank, shallow creek channel, deep creek bank, and deep creek channel), and host mineral (cinnabar, metacinnabar, pyrite, sphalerite). ANOSIM tests that grouped samples by depth resulted in a global R value of 0.660 (p=0.0015), indicating that grouping by depth is statistically significant. A one-way ANOSIM test grouping samples by the four location categories resulted in a global R value of 0.657 (p=0.0003), indicating that grouping by location is also statistically significant. However, ANOSIM tests grouping samples by host mineral were inconclusive due to their high p value.

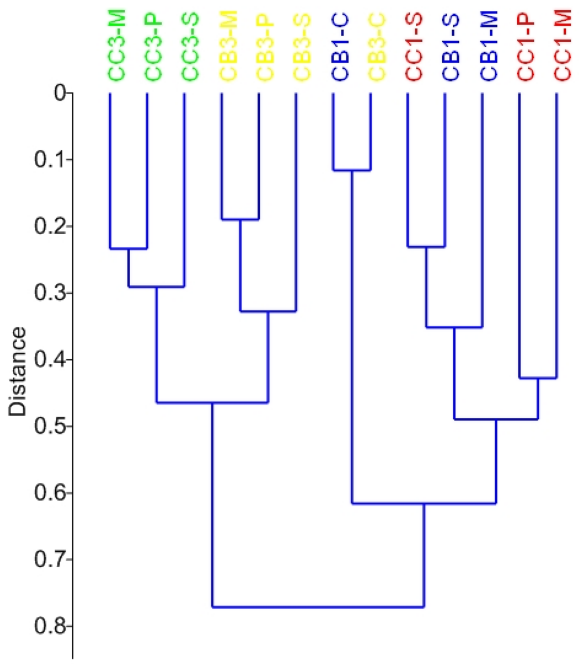

Figure 2.6. UPGMA tree calculated from Sorensen distances between pyrosequencing sample data sets at the 3% difference level.

Taxonomic Profiles

Using a taxonomic approach, between 86% and 100% of sequence reads within each sample could be classified to the phylum level, and between 87% and 99% of sequences within each sample could be classified at the class level. The total classifiable sequences included 48 classes, with only 17 classes each representing >0.5% of the total pyrosequencing reads per sample (***Figure 2.7***). Classes with an abundance below 0.5% represented only 1% to 15% of all sequences within each sample. Dominant classes included the beta-, alpha-, delta, gamma-, and epsilonproteobacteria. (***Figure 2.7***).

Between 23 and 98% of sequence reads within each sample were classifiable at the genus level. The taxonomic breakdown at the genus level for each sample is shown in ***Figure 2.8.*** The

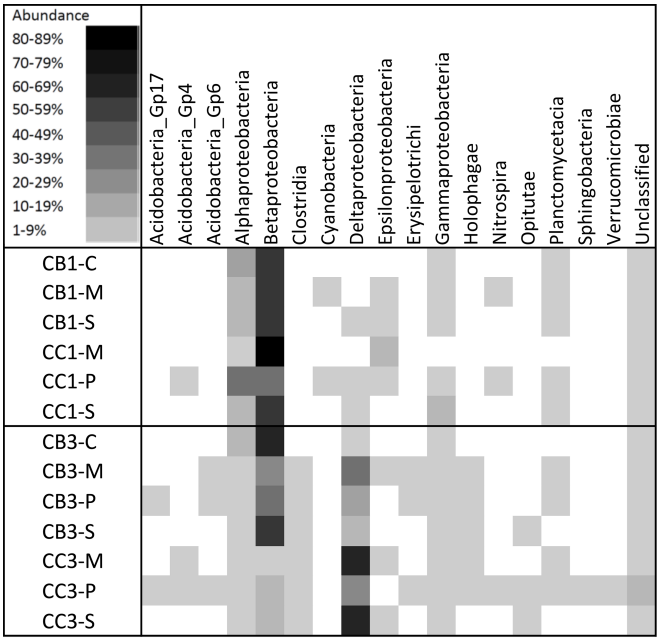

Figure 2.7. Heat map representation of taxonomic abundance at the class level. Abundance is expressed as percent abundance in all sequences including unclassifiable sequences. The 16S rRNA gene sequences were assigned to phylogenetic bacterial taxonomic groups based RDP's naïve Bayesian rRNA classifier with an 80% confidence threshold. Only classes comprising over 0.5% of all sequences per sample are shown.

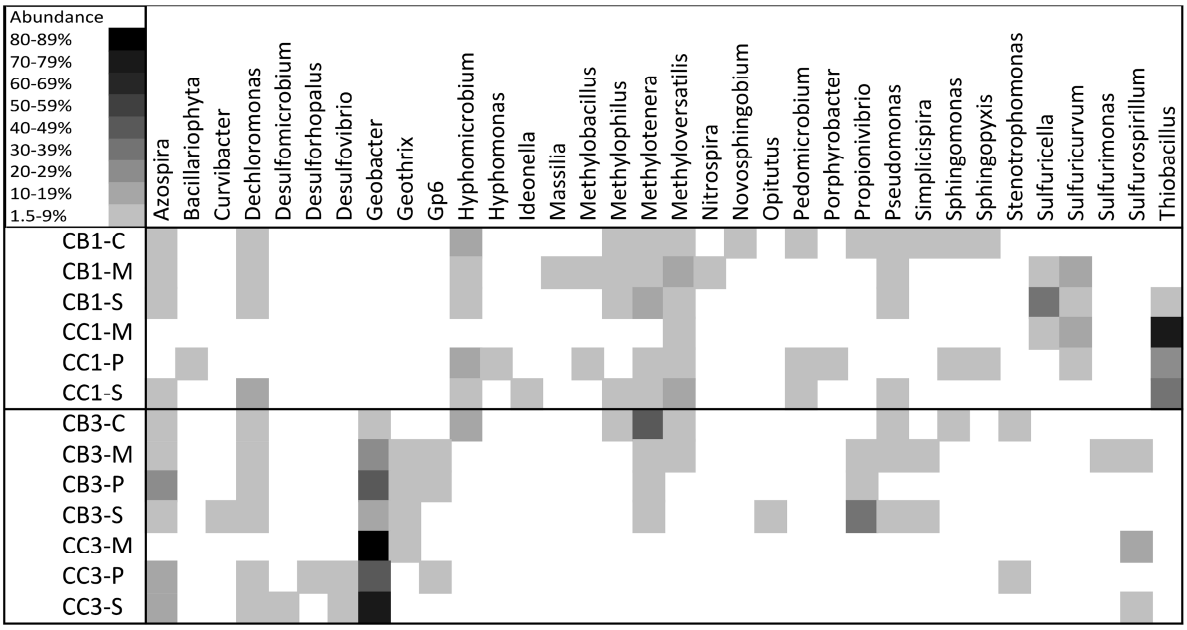

Figure 2.8. Heat map representation of taxonomic abundance at the genus level. Abundance is expressed as percent abundance in classifiable sequences. The 16S rRNA gene sequences were assigned to phylogenetic bacterial taxonomic groups based RDP's naïve Bayesian rRNA classifier with an 80% confidence threshold. Only genera comprising over 1.5% of the total population per sample are shown.

total classifiable sequences included 234 genera, but only 34 genera exceeded 1.5% of the classifiable sample sequence abundance (***Figure 2.8)***. Classes with an abundance below 1.5% represented 6% to 24% of classifiable sequences within each sample.

Shallow Incubation Taxonomy.

In shallow incubations, classifiable sequences with a sample abundance exceeding 0.5% fell within nine distinct classes, with beta- and alphaproteobacteria being among the most abundant (***Figure 2.7***). Together, these two classes represented between 73% and 90% of all sequence reads in shallow incubations. Twenty-three genera were represented within the classifiable sequences with a sample abundance >1.5% in shallow incubations (***Figure 2.8***). *Thiobacillus* was the dominant genus in all shallow creek channel incubations, comprising 71%, 36%, and 26% of the classifiable sequence reads obtained from metacinnabar, sphalerite, and pyrite incubations, respectively. *Thiobacillus* was also present in the shallow creek bank sphalerite incubation where it represented 6% of all classifiable sequences. The genus *Thiobacillus* comprises neutrophilic, obligate chemolithotrophic sulfur-oxidizing bacteria that use reduced sulfur compounds as electron donors during growth [38-43].

Other dominant strict sulfur-oxidizing genera included *Sulfuricurvum* and *Sulfuricella* [44, 45]. *Sulfuricurvum* was present in shallow creek channel metacinnabar and pyrite incubations comprising 13% and 6% of classifiable sequences respectively. *Sulfuricurvum* was also present in creek bank metacinnabar and sphalerite incubations comprising 19% and 9% of classifiable sequences respectively. *Sulfuricella* was identified in shallow creek channel and

creek bank metacinnabar incubations, as well as in the creek bank sphalerite incubation where it represented 8%, 2%, and 35% of the total classifiable sequences respectively.

Added together, genera comprising sulfur-oxidizing bacteria dominated the colonization of all shallow incubations except cinnabar (CB1-C) where genera comprising sulfur-oxidizing were not identified in abundances exceeding 1.5%. In metacinnabar incubations in particular, sulfur-oxidizing bacteria comprised 21% of identified genera in CB1-M, and 92% of genera in CC1-M.

Genera comprising obligate and facultative methylotrophic bacteria were present in all shallow incubations. Genera *Methylobacillus*, *Methylophilus*, *Methyloversatilis*, *Methylotenera*, and *Hyphomicrobium*, identified in these incubations, comprise obligate and facultative methylotrophs [46]. Genus *Methyloversalilis,* comprising facultative methylotrophs, was identified in all shallow incubations with a relative sequence abundance between 3% and 16%. Genus *Hyphomicrobium* was present in all shallow creek bank incubations comprising 18%, 4%, and 3% of the relative abundance on cinnabar, metacinnabar, and sphalerite respectively, and 17% and 3% in creek channel pyrite and sphalerite incubations. *Methylotenera* was identified in all shallow incubations except the creek channel metacinnabar incubations, comprising between 5% and 14% of the relative abundance.

Deep Incubation Taxonomy.

In deep incubations, classifiable sequences with a sample abundance exceeding 0.5% fell within sixteen classes, with delta- and betaproteobacteria being among the most abundant (***Figure 2.7***). Together, these two classes represented between 56% and 87% of all sequence reads in each sample. Twenty-one genera were represented within the classifiable sequences with

a sample abundance >1.5% in deep incubations (***Figure 2.8***). *Geobacter* was detected in all deep incubations, where it was among the top two most abundant genera in all incubations (with abundances between 16% and 81%) except in CB3-C, where it represented only 2% of classifiable sequences. *Geobacter* dominated deep metacinnabar incubations comprising 29% and 81% of classifiable sequences in deep creek bank and creek channel incubations respectively. *Geobacter* is a genus which includes strict anaerobes capable of using various metals, such as Fe(III), Mn(IV), U(VI), and even sulfate, nitrate, and elemental sulfur as electron acceptors while using organic compounds or hydrogen (H_2) as electron donors [47, 48].

Other genera, including species known to be capable of sulfate reduction, were identified in deep incubations, though in much lower abundance relative to *Geobacter*. *Desulfovibrio* comprised 2% and 3% of the sequences in deep creek channel pyrite and sphalerite incubations respectively. *Desulfomicrobium* was identified in the creek channel sphalerite incubation representing 2% of the population, and *Desulforhopalus* represented 3% of the population in the deep creek channel pyrite incubation.

Genus *Sulfurospirillum* was identified in the creek bank and creek channel metacinnabar incubations as well as the creek channel sphalerite incubation comprising 8%, 11%, and 2% of the population respectively. This genus comprises microaerophilic to anaerobic bacteria capable of growth using various substrates and electron acceptors, and is named for its ability to use sulfur compounds, such as elemental sulfur, thiosulfate, and sulfite, but not sulfate, as electron acceptors [49].

Similar to shallow incubations, methylotrophic bacteria including *Hyphomicrobium*, *Methylophilus*, *Methylotenera*, *Methyloversatilis* were also identified in deep creek bank, but not in the deep creek channel incubations. Genus *Methylotenera*, in particular, was detected in all

deep creek bank incubations with abundances ranging between 4% and 44% of the population. The deep creek bank cinnabar incubation in particular appeared to be dominated by methylotrophic bacteria with *Methylotenera* (44%) and *Hyphomicrobium* (19%) being the dominant colonizers.

Thiobacillus Species Level Clustering and CARD-FISH

Based upon species-level clustering of the sequence reads classified as *Thiobacillus* within sample CC1-M, where this genus comprised 71% of sequence reads, only one *Thiobacillus* species was dominant within this sample. Using a phylogenetic tree built using pairwise alignments (ARB), this species was identified as being most closely related to *Thiobacillus thioparus*.

A FISH oligonucleotide probe (TBD121) hybridizing *Thiobacillus thioparus* and *Thiobacillus denitrificans* was used to detect the presence of *Thiobacillus* on the metacinnabar mineral surface [37]. To our knowledge no FISH oligonucleotide probes specific to *T. thioparus* had been developed. CARD-FISH with TBD 121 followed by counterstaining with an unspecific DNA stain (Sybr Green I) confirmed the dominance of *T. thioparus* and/or *T. denitrificans* relative to other cells on the mineral surface ***(Figure 2.9)***.

Discussion

Taxonomic Profiles

In this study, pyrosequencing reads were assigned to taxonomic groups based on

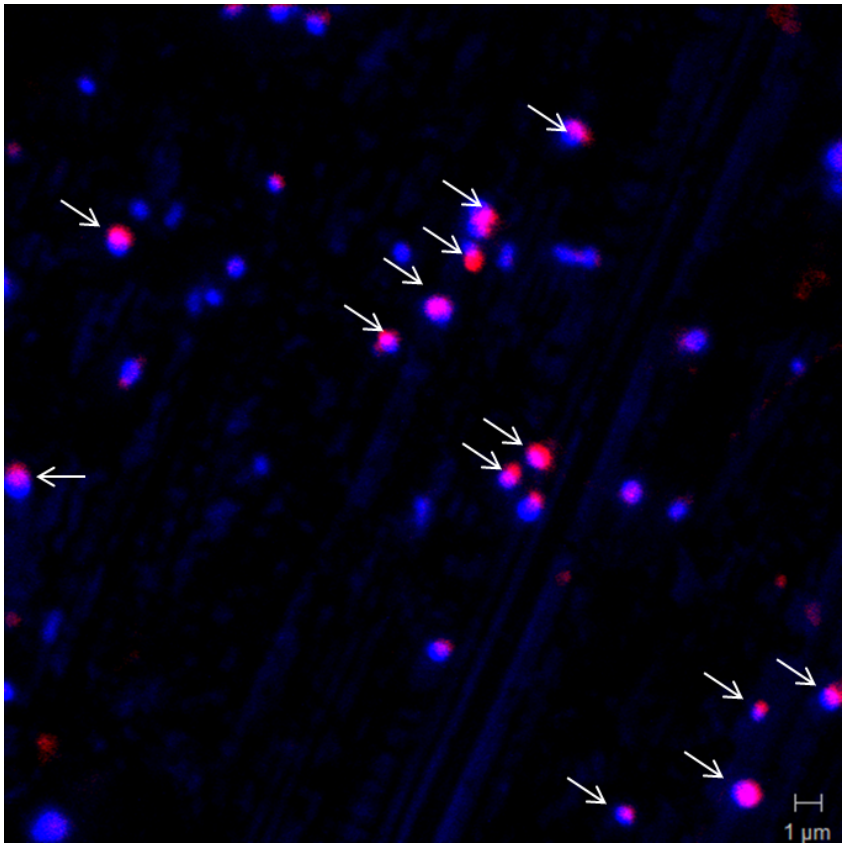

Figure 2.9. Confocal laser scanning micrograph of cells hybridized with a species specific fluorescent probe (via CARD-FISH) on mineral surface CC1-M. *Thiobacillus* cells were identified with probe TBD-121 which targets *T. thioparus and T. denitrificans* (red). Total cells were identified with the general DNA stain SYBR Green (shown in blue). Both stains bind to *Thiobacillus* cells, which show up as pink and are marked by arrows.

sequence similarity. Only 23 to 98% of all the sequence reads within each sample were taxonomically classifiable at the genus level, this is in part due to the short pyrosequencing reads which averaged 343 bp. Meanwhile a far greater proportion of the reads (87% to 99%) were classifiable at the class level. However, because the class level taxonomic abundance in all samples was largely dominated by alpha-, beta-, and gamma proteobacteria, comprising between 62 and 94%, of all sequence reads, we chose to discuss taxonomic profiles based on genus level classifications which better characterize taxonomic variability among the samples. Although it is not possible to infer the metabolism of uncultured microbes from this culture-independent

method, these genus level phylogenetic relationships do shed light on the preferential colonization of particular functional groups and thus likely metabolic processes occurring within the incubated minerals.

Genera comprising sulfur-oxidizing bacteria (i.e., *Thiobacillus*, *Sulfuricella*, *Sulfuricurvum*) dominated the colonization of all shallow incubations except cinnabar. The sulfur-oxidizing genera identified comprise neutrophilic chemoautotrophs that obligately use reduced or partially reduced sulfur compounds as electron donors during growth. Further, *Thiobacillus thioparus,* a neutrophilic obligately aerobic sulfur-oxidizing bacterium that couples the oxidation of various sulfur species to the reduction of oxygen, was identified as the predominant species colonizing shallow creek channel metacinnabar incubations (CC1-M) [40]. The proliferation of sulfur-oxidizing organisms on the sulfide minerals may have provided access to mineral-hosted sulfur to fuel respiration.

Based on sequence abundance, sulfur-oxidizing bacteria were not dominant community members in deep incubations, however, *Sulfurimonas* was identified in incubation CB3-M, where it comprised 5% of the genus classified sequences. This genus comprises autotrophic species which grow optimally on sulfide, elemental sulfur, thiosulfate and hydrogen as electron donors, and with nitrate, nitrite and oxygen as electron acceptors [50-52].

Genera comprising obligate and facultative methylotrophic bacteria were present in all shallow incubations. Methyltrophic bacteria are able to grow on reduced carbon compounds containing no carbon-carbon bonds, such as methanol or formate, while facultative methylotrophs are also able to grow on a variety of other multicarbon organic compounds [46]. The methylotrophic bacteria identified did not include any known methanotrophs. Interestingly, the genus *Hyphomicrobium* which was identified in all but one shallow incubation includes

species *H. sulfonivorans*, a facultative methylotroph with the peculiar ability to grow using methylated sulfur compounds as electron donors, but cannot grow autotrophically on inorganic sulfur compounds [53].

Similar to shallow incubations, methylotrophic bacteria were also identified in deep creek bank sediments, but not in the deep creek channel incubations. The deep creek bank cinnabar incubation in particular appeared to be dominated by methylotrophic bacteria with *Methylotenera* (44%) and *Hyphomicrobium* (19%) being the dominant colonizers. The field data available does not allow for a clear explanation as to why methylotrophic bacteria were identified in the sequences from deep creek channel, but not creek bank incubations. Perhaps despite being incubated at the same depths, the heterogeneity of field incubation sites allowed for distinct environmental factors to also play a role in shaping the community.

Both the autotrophic sulfur oxidizers and the methylotrophs have the ability to build their own carbon-carbon bonds. The sulfur oxidizers identified use the energy gained through the oxidation of reduced sulfur compounds to fix atmospheric CO_2 into cell material. Methylotrophs, on the other hand, can fix the products arising from the oxidation of reduced carbon substrates with no C-C bonds into cell material, though many are facultative [46]. Both groups are equipped to grow in oligotrophic environments with very low organic carbon concentrations. Because the incubation sites were located in a vegetated terrestrial creek, and not an oligotrophic system, the minerals likely enriched for these taxonomic groups.

Geobacter, a genus comprising strict anaerobes, dominated all but one of the deep incubation communities (CB3-C). *Geobacter* species are known to use organic compounds as electron donors while using a variety of electron acceptors including oxidized metals, nitrate, and sulfate [47, 48]. Though in low abundance, other sulfate reducers (e.g., *Desulfovibrio*,

Desulfomicrobium, and *Desulforhopalus*) were also present. The dominance of anaerobic organisms in most deep incubations suggests anoxic conditions at the mineral incubation sites or at the mineral surface. Oxygen depletion at the deep incubation sites is supported by the fact that following removal of mineral samplers, thick oxidation rinds were observed on shallow metacinnabar incubations and sparser oxidation patches in deep metacinnabar incubations, suggesting there was less oxygen available in the deeper incubations. Incubation CB3-C was the only deep incubation not dominated by strict anaerobes, however some member species of its dominant genera, *Methylotenera* and *Hyphomicrobium* are known to be capable of denitrification in addition to aerobic growth [54-56]. Hence the sequences identified on incubation CB3-C although not dominated by strict anaerobes, would have also been capable of anoxic growth.

The mineral sulfides appear to have enriched for a bacterial community that was taxonomically distinct from that in the surrounding sediments. Previous extensive characterization of shallow creek sediments at a nearby upstream and downstream location within the EFPC (EFK 13 and EFK 23) sheds further light on the sulfide incubation taxonomy [57]. Similar to the data from this present study, only 27% to 65% of sequences within each sediment sample were classifiable at the genus level. Genus *Thiobacillus*, although also detected in surrounding soils, was found in relative abundances of 1% or lower relative to the classifiable sequences sampled in September, October, and November. Similarly, genera *Sulfuricurvum*, *Sulfuricella*, and *Hyphomicrobium*, although detected in some surrounding sediment samples, did not exceeded 1% of classifiable sample sequences. Instead, the dominant genera in shallow sediments at these nearby creek locations were different from those found in shallow mineral incubations (***Supplementary Table S2.1***). Therefore, it is likely that the shallow sulfide incubations enriched for the sulfur-oxidizing and methylotrophic bacteria observed in this study

as a result of conditions at or near the mineral that were evidently geochemically distinct from those of the surrounding sediments.

Clustering Dominated by Depth and Location

Clustering analysis findings suggest that mineral-associated bacterial communities were shaped mainly by the characteristics of the location in which they were incubated. It is worth mentioning that although minerals were incubated in four locations (shallow creek bank, shallow creek channel, deep creek bank, deep creek channel) inherent lateral heterogeneities within the sediments meant that no two minerals were incubated within exactly the same location. However the fact that bacterial communities clustered by location suggests each sampling location was relatively homogeneous. The sulfide host metal had a lesser impact on the bacterial taxonomy than did incubation depth and location (***Figure 2.5 and Figure 2.6***). This secondary impact of the sulfide host metal is illustrated by the close clustering of shallow cinnabar incubations (CB1-C and CB3-C) with each other, and well as that of shallow sphalerite incubations (CC1-S and CB1-S) (***Figure 2.5 and Figure 2.6***).

As mentioned, shallow incubations were dominated by sulfur-oxidizing bacteria and methylotrophic bacteria. So it seems that the bacterial taxonomy on shallow incubations was influenced by the fact that the minerals contained reduced sulfur and the surrounding waters were oxic creating favorable conditions for microbial sulfur oxidation. However, the host metal (e.g., Hg, Fe, Zn) appeared to have merely a secondary effect if any on the colonizing community taxonomy. This may be expected due to the fact that the host metals of the minerals incubated are not typical substrates for growth in these incubation conditions. Hg(II), for example, is not known to be used as a subtrate for growth by any known bacterium. Zn(II) is also

not biologically redox active and hence does not serve as a subtrate for growth. Athough Fe(II) can serve as an electron donor for bacteria even under the circumneutral of this environment, there is very little energy to be gained from this process, particularly when compared to the energy available from sulfur oxidation [58, 59]. Although the effect of the host metal on the bacterial taxonomy appeared to be smaller than the effect of depth and location, these metals likely have an effect on other aspects of the bacterial community. For instance, both Hg and Zn are heavy metals that can be toxic to bacteria. If the mineral is solubilized, then one would expect that the bacterial communities colonizing these minerals would be enriched in Hg- and Zn-resitant organisms.

Differences in Cinnabar and Metacinnabar Colonization

A surprising outcome of this study is that despite cinnabar and metacinnabar being polymorphs, different bacterial populations appeared to colonize these minerals. While the shallow metacinnabar incubations resembled each other in the prevalence of sulfur oxidizers and methylotrophs, sulfur oxidizers were not among the dominant organisms identified on the shallow cinnabar incubations, where methylotrophic bacteria comprised the top 2 most abundant genera. Futher, although *Geobacter* was the most abundant genus in deep metacinnabar incubations in the creek channel and creek bank (81% and 29% of the total classifiable sequences, respectively), *Geobacter* comprised a much smaller portion of the deep cinnabar incubation in the creek bank (2%). One might expect for the bacterial colonization on these two minerals to be nearly identical. However, some reasons for the differences in bacterial communities arising on shallow and deep HgS incubations may include diffferences in mineral 1) solubility, 2) structure, 3) reactivity, 4) surfaces area, and 5) presence of Fe impurities.

Both cinnabar and metacinnabar have very low solubilities. The aqueous solubility of cinnabar is over an order of magnitude lower than that of metacinnabar ($\log K_{so}$ = -39.8, -38.5, respectively) [60]. These differences in solubility and hence potential differences in release of sulfur species as a result of oxidative dissolution may have contributed to the observed ecological differences in cinnabar and metacinnabar shallow incubations. Metacinnabar being more soluble than cinnabar, and therefore releasing more reduced sulfur species into the adjacent pore water is consistent with our finding that sulfur-oxidizing bacteria colonized metacinnabar is greater abundance than they did cinnabar in shallow incubations.

Cinnabar and metacinnabar also have different crystal structures. Cinnabar is hexagonal, while metacinnabar is cubic [20, 55, 61, 62]. These differences in mineral structure could lead to differences in the reactivity of the minerals, which would in turn cause differences in the bacterial colonization of the minerals. However, a previous study exploring the oxidative dissolution of cinnabar and metacinnabar, found cinnabar dissolution rates to be between 2 and 3 times those of metacinnabar under the same conditions [20]. This would not be consistent with our finding that sulfur-oxidizing bacteria colonized metacinnabar is greater abundance than cinnabar.

There were also differences in the surface area of the incubated HgS surfaces. Incubated cinnabar was composed of a single cinnabar crystal. Metacinnabar crystals, on the other hand are typically no more than a few millimeters in diameter therefore the exposed surface was actually composed of many crystals. Although both surfaces were polished, the metacinnabar surface was more porous and therefore had more exposed surface area than the cinnabar surface. Differences in surface area might lead to differences in release of substrates such as sulfur species from the mineral. However, we would predict that this would have a greater impact on the total abundance

of the microbial biomass rather than the composition of the microbial community.

Finally, although cinnabar and metacinnabar are polymorphs, metacinnabar is known to have impurities such as Fe [63], meaning that the two minerals may not be chemically identical. As discussed above, the presence of Fe(II) may have had a destabilizing effect on metacinnabar thereby leading to the enhanced release of reduced sulfur species from the mineral.

While cinnabar is the primary ore of Hg, metacinnabar can form authigenically as a result of precipitation in Hg-contaminated soils and floodplains such as the EFPC [20, 24, 61, 64]. Based upon our analysis of EFPC soils, metacinnabar was the dominant HgS, therefore any bacteria that may have adapted to using reduced sulfur species from a HgS mineral as substrate, would have adapted best to metacinnabar in this environment.

The reason for the differences in cinnabar and metacinnabar colonization is likely a complex one that involves a combination of these structural and chemical factors. Our results demonstrate that the metabolisms of bacteria colonizing these polymorphs are different, and hence the role that bacteria play in accelerating the oxidative weathering of metacinnabar may be greater for metacinnbar than for cinnabar.

Implications

This study is the first to identify bacteria that colonize HgS minerals *in situ*. The proximity of mineral-associated bacterial communities coupled with their ability to induce a number of physical and chemical mineral transformations make them likely key players in effecting chemical changes that can impact dissolution. The finding that sulfur-oxidizing bacteria dominated the colonization of shallow metacinnabar incubations begs the consideration of what role they may be playing in the weathering and the potential subsequent release of Hg from this

mineral which has historically been considered an insignificant source of soluble Hg(II) to the environment.

It is widely recognized that chemolithotrophic bacteria are involved in the oxidation and dissolution of other metal sulfides to soluble metal sulfates and sulfuric acid [65]. Members of the *Thiobacillus* genus have been implicated in pyrite weathering (e.g., *T. denitrificans* and *T. thioparus*) by interacting directly with the solid surface or through aqueous intermediates [66-68]. *T. thioparus* has been found to utilize reduced sulfur compounds formed during the non-biological oxidation of FeS_2 thereby enhancing mineral weathering [68]. Similar to the effect of chemolithotrophs on pyrite weathering, it has been thought that sulfur-oxidizing bacteria might also be able to oxidize HgS(s) [18, 19]. We propose that the presence of chemolithotrophic sulfur-oxidizing bacteria colonizing metacinnabar will lead to chemical changes that will ultimately affect HgS weathering. If our supposition is correct then microbial oxidative dissolution of metacinnabar is an unappreciated and previously unrecognized source of Hg to the environment. Accordingly, in a parallel study (**Chapter 3**) we address the role of *Thiobacillus* in metacinnabar dissolution within neutral aerobic conditions and the ultimate fate of mineral-derived Hg.

Chapter 2 - References Cited

1. Huber, J.A., et al., *Microbial population structures in the deep marine biosphere.* Science, 2007. **318**(5847): p. 97-100.

2. Mattes, T.E., et al., *Sulfur oxidizers dominate carbon fixation at a biogeochemical hot spot in the dark ocean.* ISME Journal, 2013. **7**(12): p. 2349-2360.

3. Jannasch, H.W. and M.J. Mottl, *Geomicrobiology of deep-sea hydrothermal vents.* Science, 1985. **229**(4715): p. 717-725.

4. Russell, M.J. and A.J. Hall, *The emergence of life from iron monosulphide bubbles at a submarine hydrothermal redox and pH front.* Journal of the Geological Society, 1997. **154**: p. 377-402.

5. Philippot, P., et al., *Early Archaean microorganisms preferred elemental sulfur, not sulfate.* Science, 2007. **317**(5844): p. 1534-1537.

6. Fuchs, T., et al., *16S rDNA-based phylogeny of the archaeal order Sulfolobales and reclassification of Desulfurolobus ambivalens as Acidianus ambivalens comb nov.* Systematic and Applied Microbiology, 1996. **19**(1): p. 56-60.

7. Burggraf, S., et al., *A phylogenetic analysis of Aquifex-Pyrophilus.* Systematic and Applied Microbiology, 1992. **15**(3): p. 352-356.

8. McCollom, T.M., *Geochemical constraints on primary productivity in submarine hydrothermal vent plumes.* Deep-Sea Research Part I-Oceanographic Research Papers, 2000. **47**(1): p. 85-101.

9. Toner, B.M., et al., *Mineralogy Drives Bacterial Biogeography of Hydrothermally Inactive Seafloor Sulfide Deposits.* Geomicrobiology Journal, 2013. **30**(4): p. 313-326.

10. Sylvan, J.B., et al., *Low temperature geomicrobiology follows host rock composition along a geochemical gradient in Lau Basin.* Frontiers in Microbiology, 2013. **4**.

11. Edwards, K.J., et al., *Seafloor bioalteration of sulfide minerals: Results from in situ incubation studies.* Geochimica et Cosmochimica Acta, 2003. **67**(15): p. 2843-2856.

12. Suzuki, Y., et al., *Microbial diversity in inactive chimney structures from deep-sea hydrothermal systems.* Microbial Ecology, 2004. **47**(2): p. 186-196.

13. Orcutt, B.N., et al., *Colonization of subsurface microbial observatories deployed in young ocean crust.* ISME Journal, 2011. **5**(4): p. 692-703.

14. Mendez-Garcia, C., et al., *Microbial stratification in low pH oxic and suboxic macroscopic growths along an acid mine drainage.* ISME Journal, 2014. **8**(6): p. 1259-1274.

15. Ziegler, S., et al., *Matrix composition and community structure analysis of a novel bacterial pyrite leaching community.* Environmental Microbiology, 2009. **11**(9): p. 2329-2338.

16. Puente-Sanchez, F., et al., *Deep subsurface sulfate reduction and methanogenesis in the Iberian Pyrite Belt revealed through geochemistry and molecular biomarkers.* Geobiology, 2014. **12**(1): p. 34-47.

17. Edwards, K.J., W. Bach, and T.M. McCollom, *Geomicrobiology in oceanography: microbe-mineral interactions at and below the seafloor.* Trends in Microbiology, 2005. **13**(9): p. 449-456.

18. Jew, A.D., et al., *Microbially enhanced dissolution of HgS in an acid mine drainage system in the California Coast Range.* Geobiology, 2014. **12**(1): p. 20-33.

19. Baldi, F. and G.J. Olson, *Effects of Cinnabar on Pyrite Oxidation by Thiobacillus ferrooxidans and Cinnabar Mobilization by a Mercury-Resistant Strain.* Applied and Environmental Microbiology, 1987. **53**(4): p. 772-776.

20. Holley, E.A., et al., *Mercury mobilization by oxidative dissolution of cinnabar (alpha-HgS) and metacinnabar (beta-HgS).* Chemical Geology, 2007. **240**(3-4): p. 313-325.

21. Dyrssen, D., *Biogenic Sulfur in Two Different Marine Environments.* Marine Chemistry, 1989. **28**(1-3): p. 241-249.

22. Barnett, M.O., R.R. Turner, and P.C. Singer, *Oxidative dissolution of metacinnabar (beta-HgS) by dissolved oxygen.* Applied Geochemistry, 2001. **16**(13): p. 1499-1512.

23. Tauson, V.L. and V.V. Akimov, *Introduction to the theory of forced equilibria: General principles, basic concepts, and definitions.* Geochimica et Cosmochimica Acta, 1997. **61**(23): p. 4935-4943.

24. Barnett, M.O., et al., *Formation of mercuric sulfide in soil.* Environmental Science & Technology, 1997. **31**(11): p. 3037-3043.

25. Barkay, T., S.M. Miller, and A.O. Summers, *Bacterial mercury resistance from atoms to ecosystems.* FEMS Microbiology Reviews, 2003. **27**(2-3): p. 355-384.

26. Revis, N.W., et al., *Distribution of Mercury Species in Soil from a Mercury-Contaminated Site.* Water Air and Soil Pollution, 1989. **45**(1-2): p. 105-113.

27. Phillips, E., *Upper East Fork Poplar Creek Watershed*, in *US Department of Energy Mercury Workshop*. 2004: Oak Ridge, TN.

28. Han, F.X., et al., *Binding, distribution, and plant uptake of mercury in a soil from Oak Ridge, Tennessee, USA.* Science of the Total Environment, 2006. **368**(2-3): p. 753-768.

29. Santelli, C.M., et al., *Abundance and diversity of microbial life in ocean crust.* Nature, 2008. **453**(7195): p. 653-U7.

30. Webster, G., et al., *Assessment of bacterial community structure in the deep sub-seafloor biosphere by 16S rDNA-based techniques: a cautionary tale.* Journal of Microbiological Methods, 2003. **55**(1): p. 155-164.

31. Hansel, C.M., et al., *Changes in bacterial and archaeal community structure and functional diversity along a geochemically variable soil profile.* Applied and Environmental Microbiology, 2008. **74**(5): p. 1620-1633.

32. Quince, C., et al., *Removing Noise From Pyrosequenced Amplicons.* BMC Bioinformatics, 2011. **12**.

33. Nawrocki, E.P., D.L. Kolbe, and S.R. Eddy, *Infernal 1.0: inference of RNA alignments.* Bioinformatics, 2009. **25**(10): p. 1335-1337.

34. Wang, Q., et al., *Naive Bayesian classifier for rapid assignment of rRNA sequences into the new bacterial taxonomy.* Applied and Environmental Microbiology, 2007. **73**(16): p. 5261-5267.

35. Cole, J.R., et al., *Ribosomal Database Project: data and tools for high throughput rRNA analysis.* Nucleic Acids Research, 2014. **42**(D1): p. D633-D642.

36. Hammer, O., D.A.T. Harper, and P.D. Ryan, *PAST: paleontological statistics software package for education and data analysis.* Palaeontologia Electronica, 2001. **4**(1): p. Unpaginated-Unpaginated.

37. Fernandez, N., et al., *Microbial community dynamics in a chemolithotrophic denitrification reactor inoculated with methanogenic granular sludge.* Chemosphere, 2008. **70**(3): p. 462-474.

38. Garrity, G.M., J.A. Bell, and T.G. Lilburn, *Taxonomic Outline of the Prokaryotes, Bergey's Manul of Systematic Bacteriology*. 2004.

39. Beller, H.R., et al., *The genome sequence of the obligately chemolithoautotrophic, facultatively anaerobic bacterium Thiobacillus denitfificans.* Journal of Bacteriology, 2006. **188**(4): p. 1473-1488.

40. Kelly, D.P. and A.P. Wood, *Confirmation of Thiobacillus denitrificans as a species of the genus Thiobacillus, in the beta-subclass of the Proteobacteria, with strain NCIMB 9548 as the type strain.* International Journal of Systematic and Evolutionary Microbiology, 2000. **50**: p. 547-550.

41. Smith, N.A. and D.P. Kelly, *Mechanism of oxidation of dimethyl disulfide by Thiobacillus thioparus Strain E6.* Journal of General Microbiology, 1988. **134**: p. 3031-3039.

42. Smith, N.A. and D.P. Kelly, *Oxidation of Carbon Disulphide as the Sole Source of Energy for the Autotrophic Growth of Thiobacillus thioparus Strain TK-m.* Journal of General Microbiology, 1988. **134**: p. 3041-3048.

43. Wood, A.P. and D.P. Kelly, *Isolation and physiological characterisation of Thiobacillus aquaesulis sp. nov., a novel facultatively autotrophic moderate thermophile.* Archives of Microbiology, 1988. **149**(4): p. 339-343.

44. Kodama, Y. and K. Watanabe, *Sulfuricurvum kujiense gen. nov., sp nov., a facultatively anaerobic, chemolithoautotrophic, sulfur-oxidizing bacterium isolated from an underground crude-oil storage cavity.* International Journal of Systematic and Evolutionary Microbiology, 2004. **54**: p. 2297-2300.

45. Kojima, H. and M. Fukui, *Sulfuricella denitrificans gen. nov., sp nov., a sulfur-oxidizing autotroph isolated from a freshwater lake.* International Journal of Systematic and Evolutionary Microbiology, 2010. **60**: p. 2862-2866.

46. Anthony, C., *The biochemistry of methylotrophs*. 1982, London: Academic Press.

47. Caccavo, F., et al., *Geobacter Sulfurreducens Sp-Nov, a Hydrogen-Oxidizing and Acetate-Oxidizing Dissimilatory Metal-Reducing Microorganism.* Applied and Environmental Microbiology, 1994. **60**(10): p. 3752-3759.

48. Lovley, D.R., et al., *Geobacter-Metallireducens Gen-Nov Sp-Nov, a Microorganism Capable of Coupling the Complete Oxidation of Organic-Compounds to the Reduction of Iron and Other Metals.* Archives of Microbiology, 1993. **159**(4): p. 336-344.

49. Schumacher, W., P.M.H. Kroneck, and N. Pfennig, *Comparative Systematic Study on Spirillum-5175, Campylobacter and Wolinella Species - Description of Spirillum-5175 as Sulfurospirillum-Deleyianum Gen-Nov Spec Nov.* Archives of Microbiology, 1992. **158**(4): p. 287-293.

50. Labrenz, M., et al., *Sulfurimonas gotlandica sp nov., a chemoautotrophic and psychrotolerant epsilonproteobacterium isolated from a pelagic redoxcline, and an emended description of the genus Sulfurimonas.* International Journal of Systematic and Evolutionary Microbiology, 2013. **63**: p. 4141-4148.

51. Inagaki, F., et al., *Sulfurimonas autotrophica gen. nov., sp nov., a novel sulfur-oxidizing epsilon-proteobacterium isolated from hydrothermal sediments in the Mid-Okinawa Trough.* International Journal of Systematic and Evolutionary Microbiology, 2003. **53**: p. 1801-1805.

52. Takai, K., et al., *Sulfurimonas paralvinellae sp nov., a novel mesophilic, hydrogen- and sulfur-oxidizing chemolithoautotroph within the Epsilonproteo-bacteria isolated from a*

deep-sea hydrothermal vent polychaete nest, reclassification of Thiomicrospira denitrificans as Sulfurimonas denitrificans comb. nov and emended description of the genus Sulfurimonas. International Journal of Systematic and Evolutionary Microbiology, 2006. **56**: p. 1725-1733.

53. Borodina, E., et al., *Enzymes of dimethylsulfone metabolism and the phylogenetic characterization of the facultative methylotrophs Arthrobacter sulfonivorans sp nov., Arthrobacter methylotrophus sp nov., and Hyphomicrobium sulfonivorans sp.* Archives of Microbiology, 2002. **177**(2): p. 173-183.

54. Urakami, T., et al., *Characterization and Description of Hyphomicrobium denitrificans sp. nov.* International Journal of Systematic Bacteriology, 1995. **45**(3): p. 528-532.

55. Martineau, C., et al., *Hyphomicrobium nitrativorans sp nov., isolated from the biofilm of a methanol-fed denitrification system treating seawater at the Montreal Biodome.* International Journal of Systematic and Evolutionary Microbiology, 2013. **63**: p. 3777-3781.

56. Mustakhimov, I., et al., *Insights into Denitrification in Methylotenera mobilis from Denitrification Pathway and Methanol Metabolism Mutants.* Journal of Bacteriology, 2013. **195**(10): p. 2207-2211.

57. Vishnivetskaya, T.A., et al., *Mercury and Other Heavy Metals Influence Bacterial Community Structure in Contaminated Tennessee Streams.* Applied and Environmental Microbiology, 2011. **77**(1): p. 302-311.

58. Emerson, D., *Microbial oxidation of Fe(II) and Mn(II) at circumneutral pH*, in *Environmental microbe-metal interactions*, D.R. Lovley, Editor. 2000, American Society for Microbiology: Washington, DC. p. 31-52.

59. Ehrlich, H.L., W.J. Ingledew, and J.C. Salerno, *Iron- and manganese-oxidizing bacteria*, in *Variations in autotrophic life*, J.M. Shively and L.L. Barton, Editors. 1991, Academic Press: San Diego, CA. p. 147-170.

60. Dyrssen, D., *Biogenic Sulfur in 2 DIfferent Marine Environments.* Marine Chemistry, 1989. **28**(1-3): p. 241-249.

61. Ehrlich, H.L., *Geomicrobiology*. 1981, New York: Marcel Dekker, Inc.

62. Rytuba, J.J., *Mercury from mineral deposits and potential environmental impact.* Environmental Geology, 2003. **43**(3): p. 326-338.

63. Boctor, N.Z., Y.N. Shieh, and G. Kullerud, *Mercury Ores from the New Idria Mining District, California - Geochemical and Stable Isotope Studies.* Geochimica et Cosmochimica Acta, 1987. **51**(6): p. 1705-1715.

64. Ravichandran, M., et al., *Inhibition of precipitation and aggregation of metacinnabar (mercuric sulfide) by dissolved organic matter isolated from the Florida Everglades.* Environmental Science & Technology, 1999. **33**(9): p. 1418-1423.

65. Schippers, A. and W. Sand, *Bacterial leaching of metal sulfides proceeds by two indirect mechanisms via thiosulfate or via polysulfides and sulfur.* Applied and Environmental Microbiology, 1999. **65**(1): p. 319-321.

66. Torrento, C., et al., *Denitrification of groundwater with pyrite and Thiobacillus denitrificans.* Chemical Geology, 2010. **278**(1-2): p. 80-91.

67. Bosch, J., et al., *Anaerobic, Nitrate-Dependent Oxidation of Pyrite Nanoparticles by Thiobacillus denitrificans.* Environmental Science & Technology, 2012. **46**(4): p. 2095-2101.

68. Arkesteyn, G.J.M.W., *Pyrite Oxidation in Acid Sulfate Soils - Role of Microorganisms.* Plant and Soil, 1980. **54**(1): p. 119-134.

Page intentionally left blank

CHAPTER 3

MERCURY SULFIDE MINERALS AS A SOURCE OF MERCURY TO THE ATMOSPHERE

Submitted as: A.I. Vázquez-Rodríguez[1], C.M. Hansel[2]*, T. Zhang[2], C.H. Lamborg[2], C.M. Santelli[3], S.M. Webb[4], S.C. Brooks[5], Nature Geoscience

Corresponding supplementary information is included in Appendix B

Abstract & Introduction

Mercury (Hg) is a toxic heavy metal that poses significant human and environmental health risks [1, 2]. Because gaseous elemental Hg travels over hemispheric scales, it is now an internationally recognized priority pollutant in need of global regulation [3]. Mineral-associated Hg is the largest Hg reservoir in the environment where it can account for nearly 60% of the total Hg mass inventory [4]. A large fraction of this pool is comprised of mercury sulfide minerals (HgS). These minerals have long been considered a virtual sink for Hg in all but severely acidic environments and thus disregarded as potential source of Hg back to aqueous or atmospheric pools. Here we show that the abundant and widespread sulfur-oxidizing bacterium *Thiobacillus* can extensively colonize metacinnabar within aerobic, near neutral pH creek sediments and induces the release and volatilization of metacinnabar-hosted Hg. These findings reveal a new pathway for metacinnabar dissolution and point to mineral-hosted Hg as an underappreciated source of elemental Hg that may contribute to atmospheric Hg budgets.

In many soils and sediments Hg is predominantly found as mineral precipitates and (ad)sorbed complexes to mineral or organic matrices [5]. The dominant Hg minerals are the two HgS polymorphs cinnabar (α-HgS) and metacinnabar (β-HgS). Metacinnabar is the dominant authigenic phase, where it forms under sulfidic conditions within soils and sediments [6, 7]. Under acidic pH conditions (pH~3), HgS dissolution can be enhanced in the presence of mine tailing-derived microbial cultures [8]. Under these acidic conditions, an *Acidithiobacillus* bacterium has been implicated in inducing volatilization of cinnabar-hosted Hg [9]. Yet under non-acidic conditions (pH > 4), both HgS phases are considered to be unreactive and stable due to their low solubility (e.g., $\log K_{so} \sim -39$) [10] and very slow abiotic dissolution kinetics [11, 12]. There is a growing appreciation, however, for the role of dissolved organic matter in increasing

HgS dissolution and inhibiting HgS precipitation and aggregation in the absence and presence of bacterial activity [13, 14]. Nevertheless, HgS minerals are still largely considered stable Hg phases and microbial-assisted dissolution of HgS at near neutral pH conditions is assumed negligible.

Observations of substantial Hg fluxes from unknown sources within terrestrial and marine sulfidic sediments, however, have called into question the validity of this assumption. For instance, HgS minerals have recently been implicated as a source of high dissolved Hg concentrations originating from sulfide-rich deep-sea vent sediments, raising the possibility that chemosynthetic microorganisms mobilize Hg from these low solubility phases [15]. Despite the widespread presence of HgS minerals in both terrestrial and marine sediments, we lack a clear understanding of the extent and mechanisms of HgS dissolution in these systems. Here we address this critical knowledge gap by conducting a combination of field and laboratory incubations to identify the potential for metacinnabar as a source of dissolved Hg within near neutral pH environments and the underpinning mechanisms at play.

Results & Discussion

We first characterized the microbial colonization and mineralogical transformations of metacinnabar mineral sections that were emplaced below the sediment-water interface (2.5 to 5 cm) within the aerobic hyporheic zone of a Hg-contaminated creek. Culture-independent analysis of the microbial communities showed that the metacinnabar surfaces were extensively colonized by chemosynthetic bacteria, which accounted for a striking majority (>92%) of the total microbial community (***Figure 3.1a***). This chemosynthetic population was composed predominantly of *Sulfuricuvum* (13%), *Sulfuricella* (8%), and *Thiobacillus* (71%), genera that

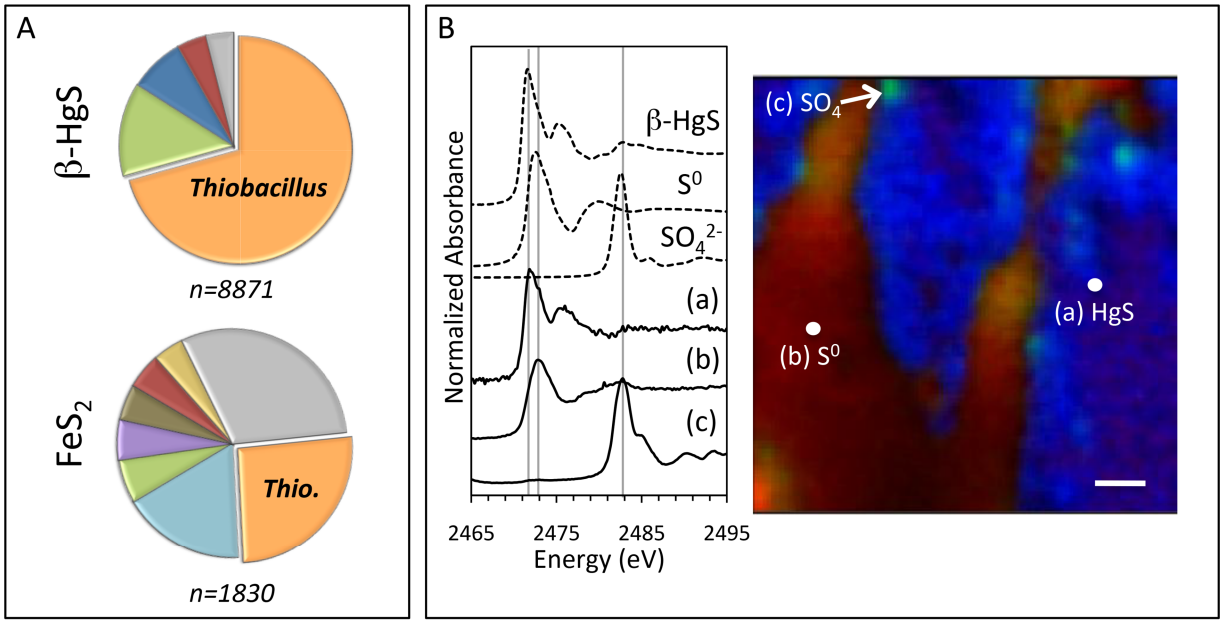

Figure 3.1. Microbial and mineral composition of incubated mineral sections. Sections were incubated within aerobic hyporheic sediments of the East Fork Poplar Creek for 6 weeks 2.5 to 5 cm below the sediment-water interface. (A) Genus-level classification of 16S rRNA sequences obtained from bacteria colonizing the metacinnabar (top) and pyrite (bottom) surface. Pie chart percentages represent the number of sequences assigned to each genus divided by the total number of classified sequences, which include the known sulfur-oxidizing organisms *Thiobacillus* (orange), *Sulfuricurvum* (green), and *Sulfuricella* (dark blue), and also the bacterial genera *Methyloversatilis* (red), *Hyphomicrobium* (light blue), *Sphingomonas* (purple), *Methylotenera* (brown), and *Sphingopyxis* (yellow). The remainder (gray) represents genera that each comprise less than 4% of the total population. (B) Distribution and composition of sulfur (S) in cross sections obtained from the incubated metacinnabar mineral slabs. (left) PCA analysis of the 7 energy S K-edge maps indicate that three components account for the S speciation whose XANES spectra match unreacted metacinnabar (a = β-HgS), elemental sulfur (b = S^0) and sulfate (c = SO_4^{2-}). (right) μ-XRF map illustrating the presence of the oxidation product S^0 (red) and isolated spots of sulfate (green) on the HgS surface (blue) (spot size = 5 μm). Scale bar = 60 μm.

have the demonstrated ability to oxidize reduced sulfur compounds. Pyrite surfaces similarly enriched for these organisms, but to a lower relative magnitude (***Figure 3.1a***). The metacinnabar surface evidently enriched for these sulfur-oxidizing organisms as previous characterization of these creek sediments revealed a microbial community that was taxonomically distinct from those found on the mineral incubations [16]. Further, the *Thiobacillus* population on the metacinnabar surface was comprised of a single species, *Thiobacillus thioparus*. *T. thioparus* is a common neutrophilic obligate aerobic sulfur-oxidizing bacterium that couples the oxidation of

various sulfur species (*e.g.*, sulfur, thiosulfate, sulfide) to the reduction of oxygen [17]. Thus, the proliferation of these organisms on the metacinnabar surface may have ensued due to enhanced access to mineral-hosted sulfur to fuel respiration.

In fact, metacinnabar oxidation is implicated by observations of sulfide oxidation products on the surface of the same metacinnabar sections incubated in the creek sediments (***Figure 3.1b***). Principal component analysis (PCA) of X-ray fluorescence maps (XRF) collected at seven different energies around the sulfur K-edge indicated that three unique components were in the reacted metacinnabar samples. The identity of the three components as HgS, elemental sulfur (S^0) and sulfate (SO_4) was confirmed by comparing spot X-ray absorption near-edge structure (XANES) spectra to model compounds (***Figure 3.1b***). Multiple-energy XRF maps for these three spectral components revealed heterogeneous surface rinds on the incubated metacinnabar surface composed primarily of elemental sulfur with isolated sulfate regions (***Figure 3.1b***). These results indicate that the metacinnabar surface was in fact oxidized leading to the formation of substantial surficial S^0 rinds. This oxidation may be a direct or indirect consequence of the activity of the sulfur-oxidizing bacterial communities that had extensively colonized the mineral surface.

Indeed, incubation of *T. thioparus* axenic cultures with metacinnabar at varying thiosulfate concentrations points to microbially induced metacinnabar oxidation. In incubations containing an environmentally relevant thiosulfate concentration (initially ~100 μM), thiosulfate was consumed within the first 5 days (***Figure 3.2a***) with the dominant oxidation product being sulfate (***Figure 3.2b***), formed through a S^0 intermediate (***Supplementary Figure S3.1***). Following thiosulfate consumption, sulfate concentrations in the presence of metacinnabar

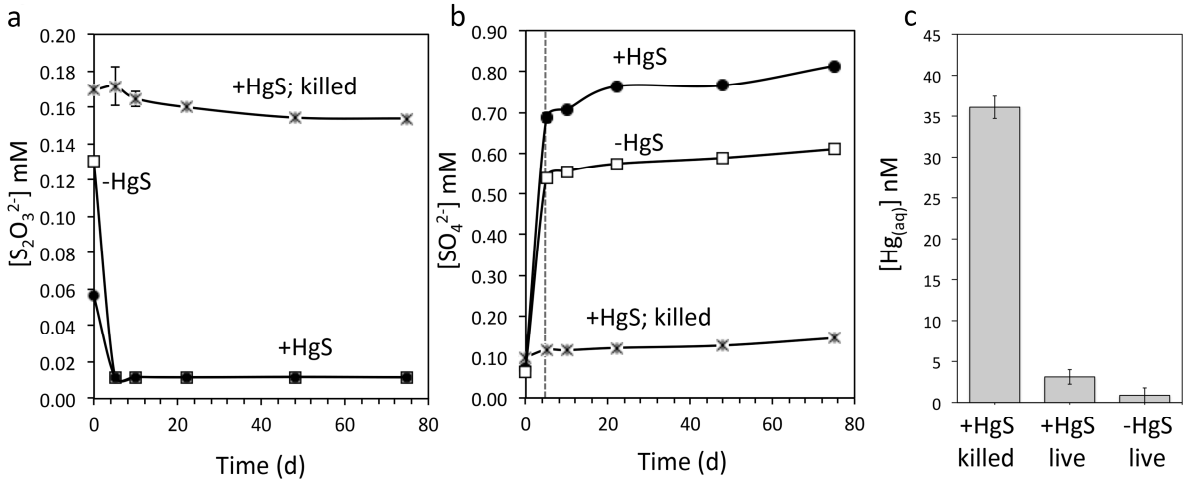

Figure 3.2. Aqueous sulfur and mercury dynamics in *Thiobacillus* incubations with metacinnabar. Aqueous thiosulfate (a), sulfate (b), and Hg (c) concentrations within *Thiobacillus* incubations initiated with ~100 µM thiosulfate and metacinnabar. Thiosulfate concentrations are below detection following 5 days of reaction (a) corresponding with an increase in the oxidation product sulfate (b). Dashed vertical line in (b) indicates time point following which thiosulfate is no longer detected. In the absence of metacinnabar, sulfate production in excess of the stoichiometric amount of sulfate produced from thiosulfate oxidation (2 moles of sulfate produced per mole of thiosulfate), originates from the oxidation of residual elemental sulfur introduced from the inoculum. Minimal abiotic thiosulfate oxidation and sulfate production are observed in killed controls. A background sulfate level of ~10 µM is observed accounting for any sulfate carryover from the killed inoculum as well as abiotic oxidative dissolution and release of surface sorbed sulfate (see Supplementary Table S1). Error bars for most time points are smaller than the symbol. (c) Aqueous Hg concentrations in killed incubations are significantly higher (36 nM) than concentrations in the presence of live *Thiobacillus* cells (3nM) after 10 days of reaction. Error bars are the standard deviation of method duplicates.

continued to increase at a faster rate than in its absence (17 and 10 µM day^{-1} sulfate production respectively, ***Figure 3.2b***). Further, a substantially higher sulfate concentration was observed in the presence of metacinnabar relative to its absence (***Figure 3.2b***) and was formed in excess of that supported solely by oxidation of added thiosulfate and residual elemental sulfur in the inoculum (see ***Supplementary Table S3.1***). In incubations with initial thiosulfate concentrations of 0 and 60 µM, 48-60% of the excess sulfate production, could be solely attributed to microbial-enhanced HgS dissolution (see ***Supplementary Table S3.1*** and ***Supplementary Figure S3.2***). Moreover, after 11 weeks of incubation, the viable cell population was 5 to 15 times greater in incubations with metacinnabar than in its absence (4 x 10^5 and 1 x 10^5 cells mL^{-1} for 100 µM

initial thiosulfate in the presence and absence of metacinnabar respectively, and 7 x 10^7 cells mL^{-1} and 4 x 10^6 cells mL^{-1} for 20 mM initial thiosulfate in the presence and absence of metacinnabar respectively). Together, these results suggest that metacinnabar is in fact fueling sulfur respiration and thereby undergoing microbially mediated oxidative dissolution.

Mercury released during metacinnabar dissolution was rapidly volatilized as gaseous Hg^0 in the presence of viable *Thiobacillus,* precluding the accumulation of dissolved Hg. Dissolved Hg^{2+} was observed in incubations containing killed (formaldehyde-treated or autoclaved) *T. thioparus* cells, with concentrations ranging from 36 nM (***Figure 3.2***) to more than 500 nM within 10 days (***Supplementary Figure S3.3***). In contrast, aqueous Hg was below 3 nM in equivalent incubations containing viable cells regardless of thiosulfate level (***Figure 3.2*** and ***Supplementary Figure S3.3***) and even after extended periods of time (> 11 weeks). Instead, a substantial amount of gaseous Hg^0 was observed in metacinnabar incubations with viable cells (***Figure 3.3***). The cumulative gaseous Hg^0 released in the presence of *Thiobacillus* varied with reaction time, cell density and initial thiosulfate concentration and ranged from ~100 to greater than 8000 ng Hg^0 per liter of culture (***Figure 3.3a,b***). Even in the absence of any exogenous thiosulfate, Hg^0 formation was still occurring after 40 days amounting to nearly 400 ng of Hg(0) per liter of culture (***Figure 3.3c***) and further hinting at microbially sustained oxidative respiration of metacinnabar-derived sulfur. Meanwhile, minimal volatilization was observed in incubations with killed cells, and with viable cells in the absence of metacinnabar (*i.e.*, background Hg levels in air). The non-metabolic contribution in the killed cell controls is likely due to abiotic Hg(II) reduction by Fe(II) [18, 19] impurities within the metacinnabar structure (see Supplementary Methods). Elevated Hg^0 production in the presence of live cells demonstrates that Hg was in fact

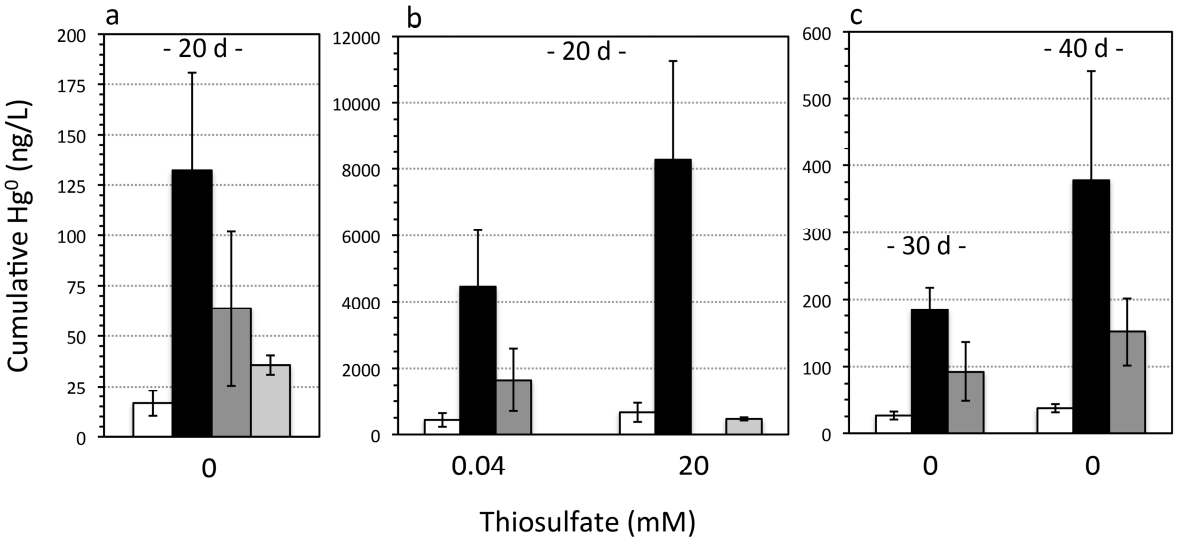

Figure 3.3. Gaseous mercury (Hg^0) measured in *Thiobacillus* incubations. Concentrations are presented as ng Hg^0 per liter of culture volume. (a) Gaseous Hg within incubations after 20 days containing no HgS (white bars), HgS plus live *Thiobacillus* (black bars), HgS plus live *Thiobacillus* at a lower cell density (~10x fewer cells) (dark gray bars), and HgS plus killed *Thiobacillus* cells (light gray bars) and with an initial thiosulfate concentration of (a) zero and (b) 0.04 or 20 mM thiosulfate. (b) Gaseous Hg produced in the zero thiosulfate incubations after 30 and 40 days. Error bars are the standard deviation for two to four biological replicates.

released from metacinnabar and then volatilized to Hg^0 by *Thiobacillus*. Many sulfur-oxidizing organisms possess the enzyme mercuric reductase [20], MerA, which reduces Hg^{2+} to Hg^0 [21]. Indeed, PCR amplification using *mer*-specific primers confirmed that *T. thioparus* possesses the *merA* gene (***Supplementary Figure S3.4***) and hence the genetic potential to reduce Hg^{2+} as observed in our incubations here.

The extent of Hg volatilization was enhanced by the presence of thiosulfate. In the absence of microbial activity (e.g., killed cells), aqueous Hg^{2+} levels increased with increasing initial thiosulfate concentration (***Supplementary Figure S3.3***), indicating that thiosulfate stimulated metacinnabar dissolution. Thiosulfate is a strong Hg^{2+} complexing ligand [15] and MINTEQ modeling indicated that under the experimental conditions tested, nearly all aqueous Hg^{2+} was complexed to thiosulfate, predominantly as $Hg(S_2O_3)_2^{-2}$ (98%) under low (100 μM)

thiosulfate conditions and $Hg(S_2O_3)_3^{-4}$ (77%) under high (20 mM) thiosulfate concentrations. In the presence of live *Thiobacillus*, higher thiosulfate concentrations also led to higher cell densities (see ***Supplementary Figure S3.5***) ultimately resulting in a greater mass of Hg volatilized over a given time period (***Figure 3.3***). The Hg volatilization rate (~100-500 ng L^{-1} d^{-1}) after 11 to 30 days of incubation, when most thiosulfate had been consumed by cells (concentration remaining 0-5 μM), however is similar when normalized to cell abundance (~50 ag Hg $cell^{-1}$ d^{-1}) for a wide range of initial thiosulfate concentrations (40 μM to 20 mM) (***Supplementary Figure S3.6***). Thus, thiosulfate concentration had a dual effect on HgS dissolution, by acting as both a complexing ligand inducing abiotic metacinnabar dissolution before it was consumed through cell respiration and by thereby supporting higher cell densities to stimulate microbially induced dissolution. Thiosulfate is a major intermediate sulfur species in environmental systems formed through both oxidative and reductive legs of the sulfur cycle, leading to high thiosulfate fluxes despite variable steady-state concentrations (typically low- to mid- micromolar concentrations, but as high as 3 mM in estuarine and marine waters and sediments) [22-26]. Our findings demonstrate that at environmentally relevant concentrations, even a small increase in initial thiosulfate abundance (from <4 to 40 μM) resulted in a large enhancement of Hg volatilization (~35 times, ***Figure 3.3***).

Here we show that authigenic mercury sulfide minerals are not merely a sink for Hg within non-acidic natural environments and instead are a source of gaseous Hg (***Figure 3.3***). Volatilization of metacinnabar-hosted Hg is a coupled process involving metacinnabar dissolution and microbial reduction of released Hg. Both microbial activity and thiosulfate enhance Hg release through presumably oxidative and ligand-promoted dissolution processes, respectively. Surprisingly, it appears that metacinnabar could serve as a respiratory source of

sulfur for *Thiobacillus* (***Figure 3.2***) and likely other sulfur-oxidizing bacteria explaining their extensive colonization on metacinnabar in sediments (***Figure 3.1***). Metacinnabar dissolution by thiosulfate (***Supplementary Figure S3.3***) or other Hg complexing ligands will also provide sulfide or other S intermediates (e.g., formed via abiotic oxidation of sulfide) further fueling the metabolism of sulfur-oxidizing organisms. Within aerobic systems, as explored here, this volatilized Hg may evade to the atmosphere. Under fluctuating redox conditions, however, methylation may compete for the released Hg from metacinnabar. The ultimate fate of released Hg from metacinnabar will undoubtedly be a function of the system geochemistry and resident microbial community. Regardless of the dissolution mechanisms and fate of Hg, these complex dynamics challenge the notion that metacinnabar serves as a static Hg host.

These findings point to mercury sulfide minerals as an underappreciated source of Hg to the environment. Based on these Hg volatilization rates, this process could account for a significant amount of Hg release from sediments and soils into the atmosphere. The microbially enhanced dissolution rates observed here, excluding any abiotic contribution, are 9 to 1000 times higher than known oxidative dissolution rates [11, 12] (see ***Supplementary Table S3.1***). A reasonable extrapolation for the environmentally relevant Hg volatilization rate from the processes observed in this study is 69 ng Hg m^{-2} h^{-1} (see ***Supplementary Table S3.2***), which falls within the range of observed emissions from mineral mercury enriched areas (2-440 ng Hg m^{-2} h^{-1}) [27]. Our findings may provide a mechanistic understanding, at least in part, for these field observations. Further extrapolating this area normalized rate to an area roughly equivalent to that of all wetlands yields a Hg release rate of 2 Mmoles yr^{-1}. For scale, total Hg emissions from terrestrial soils are estimated at 15 Mmoles yr^{-1} [5] with the contribution from geologically enriched soils estimated at 2.5-7.5 M yr^{-1} [27]. With that being said, the HgS loadings used in

this study were employed to mimic Hg contaminated systems that are common worldwide [6], and thus the application of this process to regional and global scale budgets that take into account also lower HgS environments requires further exploration and validation.

Methods

Field Incubations

Metacinnabar and pyrite specimens were obtained from the Harvard Museum of Natural History (HMNH) Mineralogical Collection (specimen #122749) (see Supplementary Methods). For in-situ creek incubations, minerals were cut into sections approximately 2 cm by 2 cm by 1 mm, polished, mounted on polycarbonate samplers and then incubated at a depth of 2.5 - 5 cm within the aerobic sediments of the creek channel of the East Fork Poplar Creek (EFPC), Oak Ridge, Tennessee, USA for 6 weeks between September and October 2010 (see Supplementary Methods). The geochemistry of the EFPC pore water near sampler deployment location (EFK 22) has been extensively monitored, and ***Supplementary Table S3.3*** includes geochemical parameters collected on the day of sampler retrieval. Once retrieved, samples were preserved until further processing (see Supplementary Methods).

DNA was extracted from field-incubated minerals followed by pyrosequencing of the 16S rRNA gene. Sequences were denoised, chimeras were removed, and high quality sequences (>150 bp) were aligned and classified (see Supplementary Methods for further details).

Field-incubated metacinnabar slabs were examined by synchrotron-based X-ray spectroscopy. Micro- and bulk-spectroscopic measurements were conducted at beamlines 14-3 and 4-3 at the Stanford Synchrotron Radiation Lightsource (SSRL), respectively. Fluorescence

maps were analyzed using the Microanalysis Toolkit in SMAK [28] as described in the Supplemental Methods.

Pure Culture Incubations

Thiobacillus thioparus (ATCC 8158) was incubated aerobically at room temperature in 100 mL glass serum vials in the dark for all experiments in the presence and absence of ground natural metacinnabar. Metacinnabar obtained from the HMNH Mineralogical Collection was sieved (< 250 μm) prior to use in incubations, and surface area of processed minerals was determined using the BET Kr adsorption technique (0.1321 ± 0.0007 m^2 g^{-1}). Glass serum vials were soaked in 10% Instra-Analyzed HCl (J.T. Baker), and rinsed 4x in nanopure water. Vials were not reused following contact with Hg.

Thiobacillus cultures were pre-grown in a pH 7 buffered basal freshwater medium containing 20 mM $Na_2S_2O_3$, 29 mM KH_2PO_4, 23 mM K_2HPO_4, 3.8 mM Na_2CO_3, 7.5 mM NH_4Cl, 1.0 mM $MgCl_2 \cdot 6H_2O$, 0.3% vitamin solution [29], and 0.1% Trace Element Solution [29] at 30°C for 5 days (see Supplementary Methods for additional details). These cells were then centrifuged (5,000 x g for 10 minutes at 4°C) and concentrated approximately 30x by re-suspending in spent medium, and a 1:100 inoculation of these cells was used for 40 μM, 60 μM, and 20 mM initial thiosulfate experiments. For 20 mM initial thiosulfate experiments, a stock solution of sterile Na_2S_2O was prepared and added into incubations. For 40 μM and 60 μM initial thiosulfate experiments, no additional thiosulfate is added and any thiosulfate present is carryover from the inoculum. For zero thiosulfate experiments, centrifuged cells were re-suspended in thiosulfate-free medium, centrifuged again and then concentrated approximately 30x in the thiosulfate-free medium. A 1:100 or 1:50 inoculation of these cell suspensions was

then performed. Killed controls consisted of autoclaved (121°C, 30 min) concentrated cells or 6-day old pre-grown cultures that were killed with 4% formaldehyde, frozen overnight, thawed, centrifuged down, and re-suspended in thiosulfate-free medium. Similar to the processing for live cells, for killed cell preparations, the washing step was performed once for 40 μM and 20 mM initial thiosulfate experiments, and twice for zero thiosulfate experiments. Experimental inoculum contained elemental sulfur resulting from pre-growth in thiosulfate medium, and was homogenized to minimize differences in this carryover in the experiments. HgS used in experiments was sterilized by autoclaving under an oxygen-free N_2 atmosphere to prevent mineral oxidation. Mineral loading used in all incubations with metacinnabar was 2 g L^{-1}. Cultures were grown without shaking although vials were swirled prior to aseptically drawing samples for aqueous analyses.

Hg volatilization rates were determined by pumping air into *Thiobacillus* incubations at a rate of 1.60 ± 0.2 mL $minute^{-1}$, and then capturing volatile Hg in outflow using gold-coated quartz sand traps. Incoming air was Hg-stripped using an upstream gold-coated sand trap and filtered through a 0.22 μm cellulose filter. Similarly, outflow was filtered upstream of the gold-coated quartz trap. The mass of Hg on traps was subsequently quantified by dual-stage gold amalgamation and the Tekran-2600 cold vapor atomic fluorescence spectrophotometer following previously established modifications [30]. Hg emissions from incubations were sampled in intervals of minutes to hours to collect a Hg mass within the instrument detection range. Total Hg emissions from incubations were then estimated based upon volatilization rates obtained at time intervals throughout the experiment assuming a constant rate of change in volatilization rates.

Samples to be used for sulfate and thiosulfate quantification were filtered through a 0.22 μm cellulose filter and stored at -20°C until analysis. Sulfate and thiosulfate concentrations were quantified via suppressed anion chromatography with conductivity detection using a Dionex ICS-2000 (AS11 Column) with a KOH eluent generator. Samples for total dissolved Hg analysis were filtered using a 0.22 μm cellulose filter, oxidized with bromine monochloride, and analyzed on a DMA-80 direct Hg Analyzer (Milestone Inc.) by thermal decomposition of the sample, catalytic conversion to elemental Hg, amalgamation, and atomic absorption. Cell abundances were determined in parallel with incubations. (See Supplementary Methods for further details).

Acknowledgements

This work was supported by the National Science Foundation Graduate Research Fellowship under Grant No. DGE-0644491 awarded to A.V.R. The authors thank R. Perdigão-Henriques and W.D. Leavitt for assistance in processing field samples; C.S. Kim, C.J. Lentini, and J.P. Shine for helpful conversations regarding this study; G. Swarr for assistance with Tekran operation; and N. Lupoli and Z. Dong for assistance with the DMA-80.

Author contributions

A.V.R and C.M.H jointly conceived of the study and designed the experiments. A.V.R. performed the experiments; A.V.R., T.Z., and C.M.H. collected the data; C.M.S., S.M.W., and C.H.L. assisted in data analysis; S.C.B. assisted with fieldwork. A.V.R. and C.M.H. wrote the manuscript with input from T.Z., C.H.L., C.M.S., S.M.W., and S.C.B.

Chapter 3 - References Cited

1. Clarkson, T.W. and L. Magos, *The toxicology of mercury and its chemical compounds.* Critical Reviews in Toxicology, 2006. **36**(8): p. 609-662.

2. Wiener, J.G., et al., *Ecotoxicology of Mercury*, in *Handbook of Ecotoxicology*. 2002, CRC Press: Boca Raton.

3. McNutt, M., *Mercury and Health*, in *Science*. 2013. p. 1430-1430.

4. Mason, R.P., et al., *Mercury biogeochemical cycling in the ocean and policy implications.* Environmental Research, 2012. **119**: p. 101-117.

5. Smith-Downey, N.V., E.M. Sunderland, and D.J. Jacob, *Anthropogenic impacts on global storage and emissions of mercury from terrestrial soils: Insights from a new global model.* Journal of Geophysical Research, 2010. **115**(G03008).

6. Barnett, M.O., et al., *Formation of mercuric sulfide in soil.* Environmental Science & Technology, 1997. **31**(11): p. 3037-3043.

7. Ravichandran, M., et al., *Inhibition of precipitation and aggregation of metacinnabar (mercuric sulfide) by dissolved organic matter isolated from the Florida Everglades.* Environmental Science & Technology, 1999. **33**(9): p. 1418-1423.

8. Jew, A.D., et al., *Microbially enhanced dissolution of HgS in an acid mine drainage system in the California Coast Range.* Geobiology, 2014. **12**(1): p. 20-33.

9. Baldi, F. and G.J. Olson, *Effects of Cinnabar on Pyrite Oxidation by Thiobacillus ferrooxidans and Cinnabar Mobilization by a Mercury-Resistant Strain.* Applied and Environmental Microbiology, 1987. **53**(4): p. 772-776.

10. Dyrssen, D., *Biogenic Sulfur in Two Different Marine Environments.* Marine Chemistry, 1989. **28**(1-3): p. 241-249.

11. Holley, E.A., et al., *Mercury mobilization by oxidative dissolution of cinnabar (alpha-HgS) and metacinnabar (beta-HgS).* Chemical Geology, 2007. **240**(3-4): p. 313-325.

12. Barnett, M.O., R.R. Turner, and P.C. Singer, *Oxidative dissolution of metacinnabar (beta-HgS) by dissolved oxygen.* Applied Geochemistry, 2001. **16**(13): p. 1499-1512.

13. Ravichandran, M., *Interactions between mercury and dissolved organic matter - a review.* Chemosphere, 2004. **55**(3): p. 319-331.

14. Graham, A.M., G.R. Aiken, and C.C. Gilmour, *Dissolved Organic Matter Enhances Microbial Mercury Methylation Under Sulfidic Conditions.* Environmental Science & Technology, 2012. **46**(5): p. 2715-2723.

15. Crespo-Medina, M., et al., *Adaptation of chemosynthetic microorganisms to elevated mercury concentrations in deep-sea hydrothermal vents.* Limnology and Oceanography, 2009. **54**(1): p. 41-49.

16. Vishnivetskaya, T.A., et al., *Mercury and Other Heavy Metals Influence Bacterial Community Structure in Contaminated Tennessee Streams.* Applied and Environmental Microbiology, 2011. **77**(1): p. 302-311.

17. Kelly, D.P. and A.P. Wood, *Confirmation of Thiobacillus denitrificans as a species of the genus Thiobacillus, in the beta-subclass of the Proteobacteria, with strain NCIMB 9548 as the type strain.* International Journal of Systematic and Evolutionary Microbiology, 2000. **50**: p. 547-550.

18. Amirbahman, A., et al., *Kinetics of Homogeneous and Surface-Catalyzed Mercury(II) Reduction by Iron(II).* Environmental Science & Technology, 2013. **47**(13): p. 7204-7213.

19. Wiatrowski, H.A., et al., *Reduction of Hg(II) to Hg(0) by Magnetite.* Environmental Science & Technology, 2009. **43**(14): p. 5307-5313.

20. Benson, D.A., et al., *GenBank.* Nucleic Acids Research, 2009. **37**: p. D26-D31.

21. Barkay, T., S.M. Miller, and A.O. Summers, *Bacterial mercury resistance from atoms to ecosystems.* FEMS Microbiology Reviews, 2003. **27**(2-3): p. 355-384.

22. Jorgensen, B.B., *A Thiosulfate Shunt in the Sulfur Cycle of Marine Sediments.* Science, 1990. **249**(4965): p. 152-154.

23. Jorgensen, B.B., *The Sulfur cycle of freshwater sediments: Role of thiosulfate.* Limnology and Oceanography, 1990. **35**(6): p. 1329-1342.

24. Zopfi, J., T.G. Ferdelman, and H. Fossing, *Distribution and fate of sulfur intermediates—sulfite, tetrathionate, thiosulfate, and elemental sulfur—in marine sediments.* Geological Society of America Special Papers, 2004. **379**: p. 97-116.

25. Luther, G.W., et al., *Inorganic and Organic Sulfur Cycling in Salt-Marsh Pore Waters.* Science, 1986. **232**(4751): p. 746-749.

26. Mullaugh, K.M., et al., *Voltammetric (micro)electrodes for the in situ study of Fe2+ oxidation kinetics in hot springs and S2O32- production at hydrothermal vents.* Electroanalysis, 2008. **20**(3): p. 280-290.

27. Gustin, M.S., *Exchange of Mercury between the Atmosphere and Terrestrial Ecosystems*, in *Environmental Chemistry and Toxicology of Mercury*. 2011, John Wiley & Sons, Inc.: Hoboken. p. 423-451.

28. Webb, S.M., *SMAK: Sam's Microprobe Analysis Kit*. 2006, Stanford Synchrotron Radiation Laboratory.

29. Widdel, F. and F. Bak, *Gram-negative mesophilic sulfate-reducing bacteria*, in *The Prokaryotes*, A. Balows, et al., Editors. 1992, Springer: New York. p. 3352-3378.

30. Lamborg, C.H., et al., *An intercomparison of procedures for the determination of total mercury in seawater and recommendations regarding mercury speciation during GEOTRACES cruises.* Limnology and Oceanography-Methods, 2012. **10**: p. 90-100.

Page intentionally left blank

CHAPTER 4

DISSOLUTION AND VOLATILIZATION OF METACINNABAR-HOSTED MERCURY IN *THIOBACILLUS THIOPARUS* CULTURES

Corresponding supplementary information is included in Appendix C

Abstract

Mineral-associated mercury (Hg) is the largest reservoir of Hg in the environment, and metacinnabar (β-HgS) is one of the dominant Hg mineral phases. Until recently metacinnabar had been considered a sink for dissolved Hg in circumneutral pH environments and thus disregarded as potential source of mobile Hg. Recently however, the abundant and widespread sulfur-oxidizing bacterium *Thiobacillus thioparus* has been shown to extensively colonize natural metacinnabar within aerobic, near neutral pH creek sediments, and induce the release and volatilization of metacinnabar-hosted Hg. In this study, we tested the effect of successive daily thiosulfate additions, mimicking the continuous thiosulfate fluxes in the environment, on the release of soluble Hg(II) and volatile Hg(0) from natural and synthetic metacinnabar incubated with live and killed *T. thioparus* cultures. Daily thiosulfate spikes are quickly oxidized in the presence of live *T. thioparus* with concomitant sulfate production, while thiosulfate is minimally consumed in killed incubations. Dissolved Hg in killed incubations increases over the course of the experiment, presumably due to thiosulfate-induced Hg complexation and dissolution, with a more pronounced increase in natural than in synthetic metacinnabar incubations. Meanwhile, dissolved Hg in live incubations decreases over time likely due to the MerA induced reduction of dissolved Hg by *T. thioparus.* The timing of thiosulfate additions has a substantial effect on the extent of abiotic metacinnabar dissolution, but not on the extent or timing of abiotic volatilization of metacinnabar-hosted Hg. Meanwhile, the dynamics of biotic microbially induced volatilization of mineral-hosted Hg are impacted by the timing of thiosulfate additions, with release of volatile Hg from natural and synthetic metacinnabar occurring rapidly within the first few hours following the thiosulfate spike, and decreasing volatilization after thiosulfate is

consumed by *T. thioparus*. Future targeted investigations should be conducted to reveal the underpinning processes in order to improve our mechanistic understanding of the volatilization of metacinnabar-hosted Hg.

Introduction

Mercury (Hg) is a toxic metal known to interfere with human neurological development [1]. Mineral-associated Hg is the largest environmental Hg reservoir accounting for nearly 60% of the global Hg mass inventory [2]. The dominant Hg minerals are cinnabar (α-HgS) and metacinnabar (β-HgS), with metacinnabar being the dominant authigenic phase, where it forms under sulfidic conditions within soils and sediments [3, 4]. Metacinnabar has long been considered a sink for dissolved Hg in circumneutral pH environments and thus disregarded as a potential source of mobile Hg. However, we recently showed that the abundant and widespread sulfur-oxidizing bacterium *Thiobacillus thioparus* can extensively colonize metacinnabar within aerobic, near neutral pH creek sediments (**Chapter 2)** and induces the release and volatilization of metacinnabar-hosted Hg (**Chapter 3**). The extent of Hg volatilization is enhanced by the presence of thiosulfate, a substrate for *T. thioparus* and a major intermediate sulfur species in environmental systems. Because thiosulfate is formed through both oxidative and reductive legs of the sulfur cycle, environments can experience high thiosulfate fluxes, despite variable steady-state concentrations (typically low- to mid- micromolar concentrations, but as high as 3 mM in estuarine and marine waters and sediments) [5-9]. However, despite the widespread presence of HgS minerals in both terrestrial and marine sediments, we lack a clear mechanistic understanding of the dissolution and volatilization of HgS-hosted Hg in these systems.

While our previous findings revealed a new pathway for metacinnabar dissolution and unveiled mineral-hosted Hg as an underappreciated source of dissolved and volatile Hg, here we address the critical knowledge gap in HgS dissolution and volatilization by conducting laboratory incubations to begin to identify key factors in Hg release from metacinnabar. Because in our previous study, thiosulfate was only added to incubations initially in the course of the experiment, in this study we tested the effect of maintaining a constant thiosulfate flux, mimicking thiosulfate fluxes in the environment, on the release of soluble Hg(II) and volatile Hg(0) from metacinnabar incubated with live and killed *T. thioparus* cultures. Further, we evaluated Hg releases in live *T. thioparus* cultures incubated with natural and synthetic metacinnabar, at two different mineral loadings and two thiosulfate concentrations. We have only begun to scratch at the surface of the underpinning mechanisms at play, and future studies should be considered in order to provide a more accurate understanding of the factors affecting dissolution and volatilization of metacinnabar-hosted Hg in circumneutral environments.

Materials and Methods

Culture Conditions

Thiobacillus thioparus (ATCC 8158) was incubated aerobically at room temperature in 100 mL glass serum vials in the dark for all experiments in the presence of natural and synthetic metacinnabar. New glass serum vials were soaked in 10% Instra-Analyzed HCl (J.T. Baker), and rinsed 4x in nanopure water. Vials were not reused following contact with Hg. *T. thioparus* cultures were pre-grown in a basal freshwater medium containing 20 mM $Na_2S_2O_3$, 29 mM KH_2PO_4, 23 mM K_2HPO_4, 3.8 mM Na_2CO_3, 7.5 mM NH_4Cl, 1.0 mM $MgCl_2 \cdot 6H_2O$, 0.3% vitamin solution [10], and 0.1% Trace Element Solution [10] at 30°C for 5 days. These cells

were then centrifuged (5,000 x g for 10 minutes at 4°C) and concentrated approximately 30x by re-suspending in spent medium, and a 1:100 inoculation of these cells was used for live cell experiments. No additional thiosulfate was spiked at day 0 of the experiment, and any thiosulfate present was carryover from the inoculum. Killed controls consisted of autoclaved (121°C, 30 min) concentrated cells, and a 1:100 inoculation of these cells was also used for killed cell experiments. Experimental inoculum contained elemental sulfur resulting from pre-growth in thiosulfate medium, and was homogenized to minimize differences in this carryover in the experiments. HgS used in experiments was sterilized by autoclaving under an oxygen-free N_2 atmosphere to prevent mineral oxidation. Mineral loading used in all incubations was 2 g L^{-1} or 1 g L^{-1}. Cultures were started with 50 mL of medium and grown without shaking, although vials were swirled following the daily thiosulfate spike and prior to aseptically drawing samples for aqueous analyses. Every 24 hours cultures were spiked with thiosulfate. Low thiosulfate incubations were spiked with 200 µL of a 25 mM thiosulfate stock, while high thiosulfate incubations were spiked with 200 µL of a 125 mM thiosulfate stock. The resulting thiosulfate concentration following the spike was 125-132 µM and 621-654 µM for low and high thiosulfate incubations respectively, with the range in thiosulfate concentration resulting from the volume change throughout the incubation. Sampling for aqueous components occurred at two timepoints, one initial timepoint was taken 15 hours (h) after inoculation, and another 11.6 days after inoculation (henceforth referred to as the 12 day timepoint).

Hg Volatilization Measurements

Hg volatilization rates were determined by pumping air into *T. thioparus* incubations at a rate of 1.60 ± 0.2 mL $minute^{-1}$, and then capturing volatile Hg in outflow using gold-coated

quartz sand traps. Incoming air was Hg-stripped using an upstream gold-coated sand trap and filtered through a 0.22 μm cellulose filter. Similarly, outflow was filtered upstream of the gold-coated quartz trap. The mass of Hg on traps was subsequently quantified by dual-stage gold amalgamation and the Tekran-2600 cold vapor atomic fluorescence spectrophotometer. Hg emissions from incubations were sampled in intervals of minutes to hours to collect a Hg mass within the instrument detection range. Hg volatilization rates was calculated by dividing the measured Hg mass by the sampling interval.

Metacinnabar Specimens

Natural metacinnabar specimens were obtained from the Harvard Museum of Natural History (HMNH) Mineralogical Collection (specimen #122749). The metacinnabar specimen was analyzed using XRF to confirm that the sample was composed predominantly of Hg and S. In line with a minor Fe XRF contribution, microscopy observations revealed minor pyrite inclusions within the mineral; iron is a common co-precipitate within metacinnabar and iron impurities are known to stabilize the metacinnabar structure in the ambient environment against ripening to cinnabar [11]. Metacinnabar obtained from the HMNH Mineralogical Collection was sieved (< 250 μm) prior to use in incubations. Surface area of processed minerals was determined using the BET Kr adsorption technique to be 0.1321 ± 0.0007 m^2 g^{-1}. A commercial metacinnabar was used for synthetic metacinnabar incubations (black HgS, Alfa Aesar). The surface area of this synthetic metacinnabar was similarly determined using the BET Kr adsorption technique to be 1.2804 ± 0.0045 m^2 g^{-1}. Specimens were analyzed using XRD (Scintag XDS2000) to confirm sample composition was predominantly metacinnabar for both the natural and synthetic specimens.

Ion Chromatography

Samples to be used for sulfate and thiosulfate quantification were filtered through a 0.22 μm cellulose filter and stored at -20°C until analysis. Sulfate and thiosulfate concentrations were quantified via suppressed anion chromatography with conductivity detection using a Dionex ICS-2000 (AS11 Column) with a KOH eluent generator. An eluent gradient method was employed (flow rate 1.5 mL min^{-1}): beginning for 8 min at 1 mM, followed by a linear ramp to 15 mM over 4 min, another linear ramp to 60 mM over 8 min, followed by a sustained 60 mM for 2 minutes, and 1 mM for 13 minutes. A blank was run between all samples and standards to prevent carryover between samples.

Dissolved Hg Quantification

Samples for total dissolved Hg analysis were filtered using a 0.22 μm cellulose filter or a 0.02 μm Anotop-10 alumina filter (Whatman). Filtered samples were oxidized with 1 % (v/v) bromine monochloride (BrCl) per EPA Method 1631. Samples for total dissolved Hg analysis were refrigerated between collection and analysis except during the BrCl oxidation step. Samples were analyzed on a DMA-80 direct Hg Analyzer (Milestone Inc.) by thermal decomposition of the sample, catalytic conversion to elemental Hg, amalgamation, and atomic absorption. Minutes prior to running samples on the DMA-80, 0.2% (v/v) hydroxylamine hydrochloride (HAH) was added to samples per EPA Method 1631. Calibration of the DMA-80 direct Hg analyzer was performed with a series of dissolved Hg(II) standards and the calibration was regularly verified using reference material from the Quebec National Institute for Public Health (INSPQ)

Interlaboratory Comparison Program for Metals in Biological Matrices. It was confirmed that the starting incubation medium, live inoculum, and killed inoculum were Hg-free, with Hg concentrations lower than the method detection limit of 3.8 nM Hg).

Results

Thiosulfate Consumption

Over the course of 12 days, 5 μmoles or 25 μmoles thiosulfate were added daily to low and high thiosulfate incubations respectively. Eleven thiosulfate spikes resulted in a total of 51 μmoles and 273 μmoles thiosulfate added to low and high thiosulfate incubations.

Thiosulfate is quickly oxidized in the presence of *T. thioparus* with concomitant sulfate production (***Figure 4.1***). Low and high thiosulfate spikes are consumed at a rate of 1.9 μM min^{-1}, with thiosulfate being mostly depleted within 1 and 5 hours for low and high spikes respectively (data not shown). Further, nearly all thiosulfate added to live incubations after 11 daily spikes is consumed. Thiosulfate present in all incubations at the 15 h time point (3 μM) is carryover from the inoculum as this measurement precedes the addition of any thiosulfate spikes. Low and high thiosulfate live incubations with 2000 ppm natural metacinnabar are hence replicates of each other at this 15 h time point. The thiosulfate remaining on day 12, approximately 20 hours following the previous thiosulfate spike is 5 μM for low thiosulfate incubations and 17 μM in high thiosulfate incubations, a trivial amount considering the daily spikes would have resulted in a thiosulfate concentrations of 1.3 and 6.4 mM at day 12 had it not been consumed (***Figure 4.1a***). No significant differences in thiosulfate consumption are observed in incubations with natural vs. synthetic metacinnabar. Further, differences in metacinnabar loading (1000 vs 2000 ppm) also do not appear to affect thiosulfate consumption.

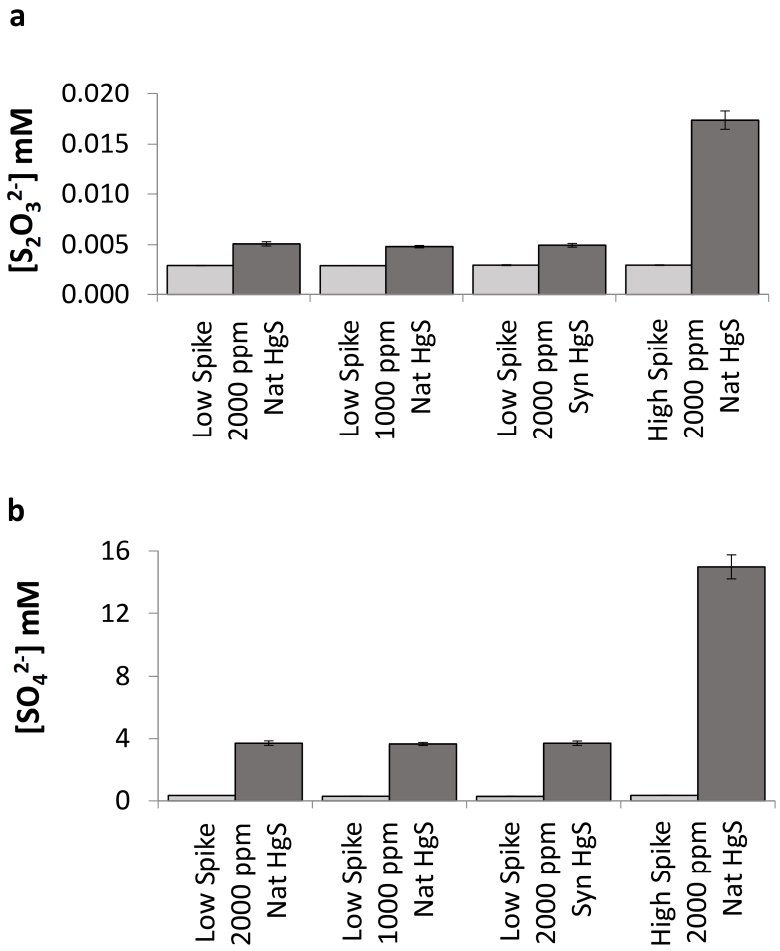

Figure 4.1. Thiosulfate (a) and sulfate (b) concentrations in live incubations. Light grey and dark grey bars indicate measurements taken 15 hours and 12 days after inoculation respectively. Low spike and high spike labels refer to low and high thiosulfate incubations. 1000 ppm and 2000 ppm labels refer to the metacinnabar loading used in incubations. Nat HgS and Syn HgS labels refer to incubations conducted with natural and synthetic metacinnabar respectively. Error bars indicate the standard deviation of three replicate incubations.

On the other hand, little thiosulfate is consumed in killed incubations in the presence of both natural and synthetic metacinnabar (***Figure 4.2a***). The thiosulfate concentration measured at the end of the 12 day incubation in killed controls (~1.5 mM) is 100 μM lower than the expected thiosulfate concentration based on the daily thiosulfate additions and the thiosulfate carryover in the inoculum signaling that some dissolved thiosulfate is lost in these incubation (***Figure 4.2a***).

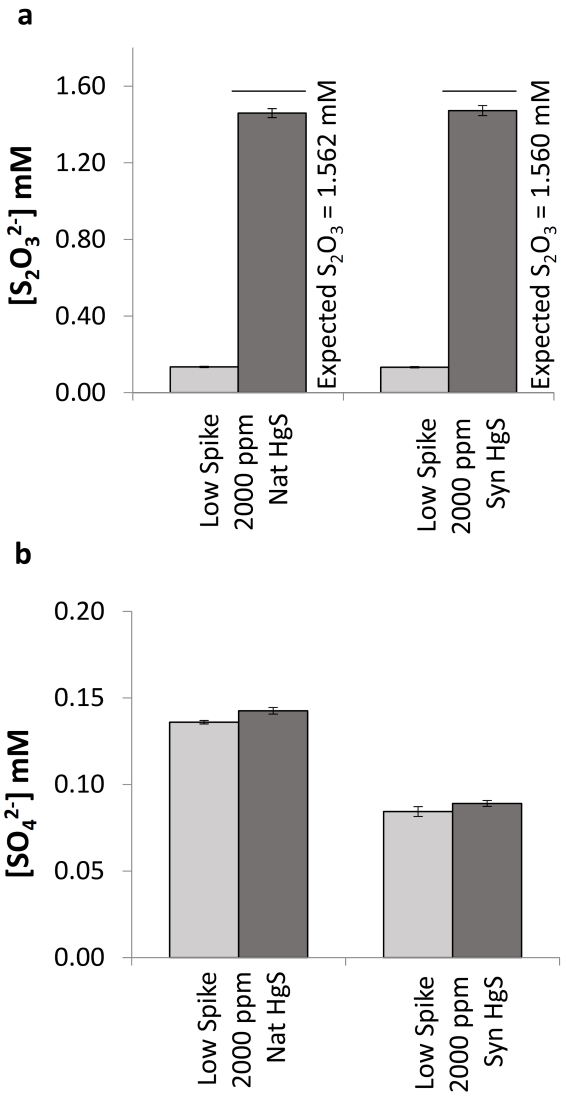

Figure 4.2. Thiosulfate (a) and sulfate (b) concentrations in killed incubations. Light grey and dark grey bars indicate measurements taken 15 hours and 12 days after inoculation respectively. Nat HgS and Syn HgS labels refer to incubations conducted with natural and synthetic metacinnabar respectively. Error bars indicate the standard deviation of three replicate incubations.

Sulfate Production

In all live incubations, sulfate accumulates over the course of 12 days as a result of thiosulfate oxidation by *T. thioparus* (***Figure 4.1b***). No significant differences in sulfate production are observed in incubations with natural vs. synthetic metacinnabar. Further, differences in metacinnabar loading (1000 vs 2000 ppm) also do not appear to affect sulfate

production. As expected, high thiosulfate incubations produce more sulfate than low thiosulfate incubations. The expected sulfate concentration on day 12 in low thiosulfate incubations based on the daily thiosulfate additions, initial sulfate carryover from inoculation, and minor sulfate carryover in thiosulfate spikes, assuming all thiosulfate is converted to sulfate, is 3.173 mM (***Supplementary Table S4.1***). This expected sulfate concentration is slightly lower than the observed sulfate concentration at day 12 in low thiosulfate incubations, which ranges from 3.663 to 3.715 mM (***Figure 4.1b***). In the case of the high thiosulfate incubation, the expected dissolved sulfate concentration on day 12 of the incubation is 14.336 mM, which agrees with the observed sulfate concentration (***Figure 4.1b***).

On the other hand, sulfate concentrations in killed controls remain fairly constant through the 12 days of incubation with only a slight increase of 5 μM over the incubation period (***Figure 4.2b***). This slight increase in sulfate observed in killed controls with both natural and synthetic metacinnabar agrees with the sulfate that is added as a result of trace sulfate in thiosulfate spikes, and does not suggest metacinnabar dissolution in killed controls or conversion of the lost thiosulfate to sulfate. After 15 h of incubation, more sulfate is observed in incubations with natural metacinnabar than in those with synthetic metacinnabar, however we do not see greater dissolved Hg in the same incubations at this same time point (9 nM and 13 nM dissolved mercury for killed incubations with natural and synthetic metacinnabar respectively) (***Figure 4.3***). These results suggest that the initial enhanced sulfate release in natural metacinnabar is due to sorbed sulfate or sulfate impurities in the mineral rather than increased mineral dissolution.

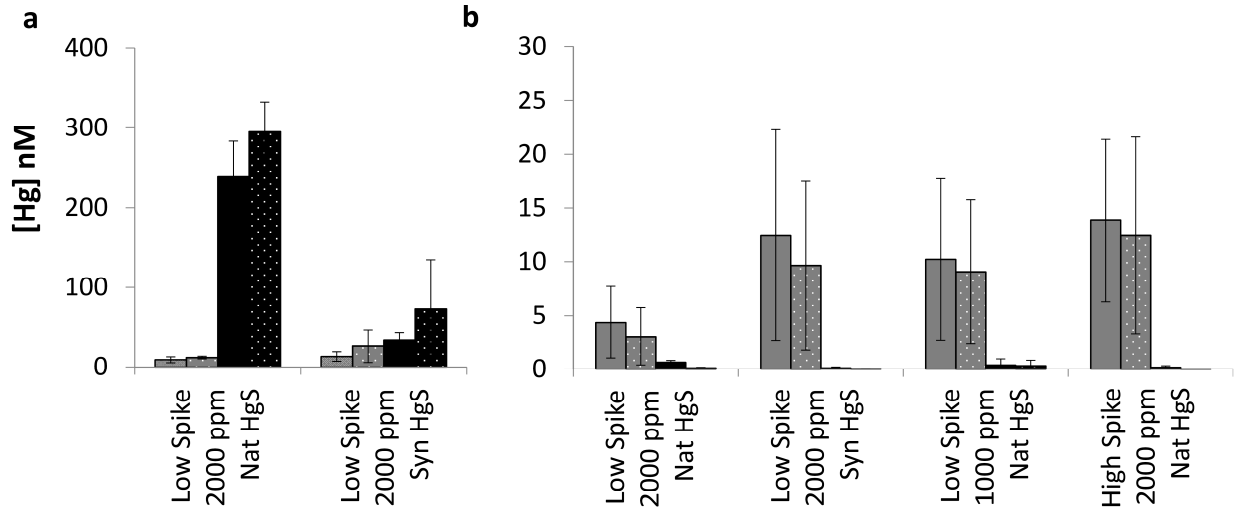

Figure 4.3. Dissolved Hg concentrations in killed (a) and live (b) incubations. Grey and black bars indicate measurements taken 15 hours and 12 days after inoculation respectively. Nat HgS and Syn HgS labels refer to incubations conducted with natural and synthetic metacinnabar respectively. Solid bars represent samples filtered through a 0.2µm filter prior to quantification, while dotted bars represent samples filtered through a 0.02µm filter prior to quantification. Error bars indicate the standard deviation of three replicate incubations. The measurement taken at 12 days passing through a 0.2 µM filter contains only 2 replicates for the "High Spike" sample.

Dissolved and Volatile Hg Production

Dissolved Hg concentrations in killed controls increases from the first measurement taken 15 h after the start to the experiment (6-18 nM) to day 12 of the incubation, with similar trends observed for the two filtration methods used (***Figure 4.3a***). The increase in dissolved Hg is more pronounced for natural than for synthetic metacinnabar killed incubations. After 11 days, dissolved Hg in killed incubations with natural metacinnabar is ~7x higher than it is in incubations with synthetic metacinnabar. This agrees with slightly greater rates of volatilization coming from natural metacinnabar as compared to synthetic metacinnabar killed controls during all but one measurement where significant differences were observed between the two treatments (***Table 4.1***, ***Figure 4.4***).

In live incubations, however, dissolved Hg decreases over time (***Figure 4.3b***). 15 h after

		Avg Hg^0 (ng) emission rate during sampling (ng day^{-1} L^{-1})			
		Live Cell Incubations		Killed Cell Incubations	
Sampling period relative to spike	Day	Natual HgS	Synthetic HgS	Natual HgS	Synthetic HgS
2h - 2.25h	1	3237 ± 2819	105 ± 64	232 ± 95	1452 ± 452
2h - 2.25h	2	353 ± 238	150 ± 46	286 ± 279	150 ± 49
8.5h - 9h	2	117 ± 97	119 ± 71	84 ± 10	81 ± 42
2h - 3h	3	224 ± 220	268 ± 346	92 ± 31	39 ± 15
2h - 3.5h	4	242 ± 276	381 ± 348	61 ± 14	38 ± 10
15h - 16h	4	70 ± 33	62 ± 26	96 ± 14	46 ± 5
0h - 2.25h	6	109 ± 14	na	109 ± 14	316 ± 81
0h - 4h	7	204 ± 48	1104 ± 771	103 ± 6	205 ± 220
0h - 4h	9	134 ± 51	956 ± 1161	124 ± 89	759 ± 794

Table 4.1. Gaseous Hg emission rates from live and killed *T. Thioparus* incubations. Average Hg(0) emission rate from replicate incubations of natural and synthetic metacinnabar in the presence of live and killed *T. Thioparus*. All incubations shown had a mineral loading of 2000 ppm HgS, and a low thiosulfate spike was added daily. Error represents the standard deviation in measurements from two to three replicate incubations.

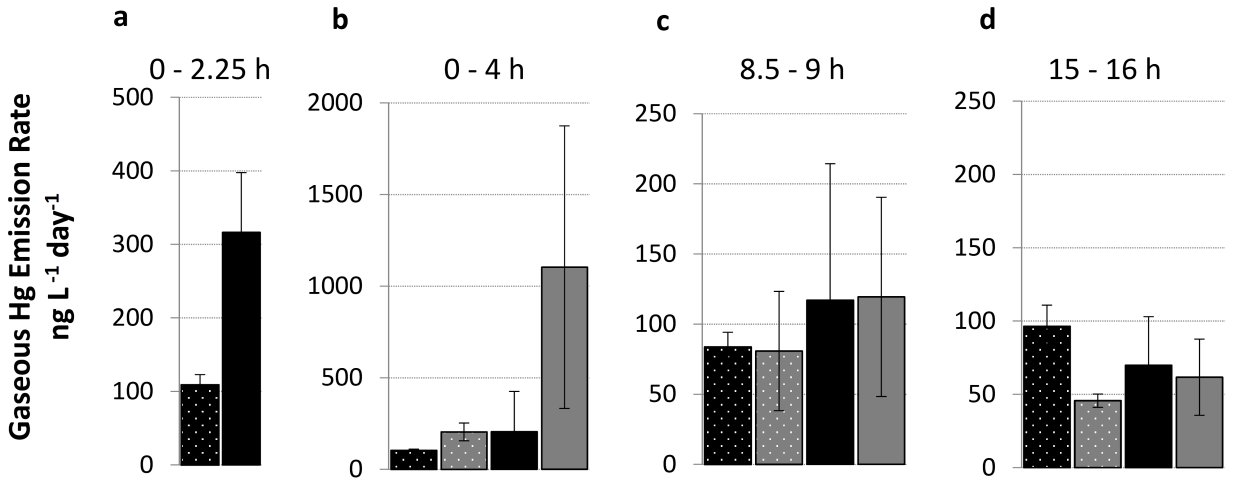

Figure 4.4. Average gaseous Hg emission rates within incubations containing killed cells and natural metacinnabar (black dotted bars), killed cells and synthetic metacinnabar (grey dotted bars), live cells and natural metacinnabar (black bars), live cells and synthetic metacinnabar (grey bars). Metacinnabar loading was the same for all incubations shown (2000 ppm) and a low thiosulfate spike was added daily. Hg emission rates are presented as ng Hg per liter of culture volume per day. Emission rates displayed on each panel were taken during 4 different days at various time periods relative to the thiosulfate spike: (a) Day 6, 0 - 2.25 h following the spike; (b) Day 9, 0 - 4 h following the spike, (c) Day 2, 8.5 – 9 h following the spike; and (d) Day 4, 15-16 h following the spike. Error bars indicate the standard deviation of measurements taken from three replicate incubations.

inoculation Hg concentrations in live incubations range from 3-22 nM, and decrease to 0-1 nM (with a method detection limit of 3.8 nM) after 12 days of incubation. No significant differences in dissolved Hg concentrations are observed between low thiosulfate incubations with natural and synthetic metacinnabar. Similarly, loading 1000 ppm vs. 2000 ppm natural metacinnabar in low thiosulfate incubations does not have a measurable effect on dissolved Hg concentrations. Low and high spikes of thiosulfate in 2000 ppm natural metacinnabar incubations also do not appear to have an effect on dissolved Hg concentrations after 12 days of incubation. The large error bars associated with the dissolved Hg measurements taken 15 h into the experiment obscure any potential differences in the treatments at this time point. The large variability among biological replicates at this time likely results from cells within the replicate incubations being at different metabolic growth stages, with some live incubations exhibiting more activity while others are more latent.

Though dissolved Hg in killed incubations is higher than it is in live incubations, there is an increase in Hg volatilization in live incubations immediately following the thiosulfate spike (***Figure 4.4***). Over the course of the next few hours, volatilization from live incubations decreases until the volatilization rates from live and killed incubations are not significantly different 8 h or 16 h beyond the thiosulfate spike (***Figure 4.4***). Average Hg volatilization rates for live cells in the presence of natural metacinnabar and daily spikes of ~125 μM thiosulfate range from 132 to 353 ng Hg day^{-1} L^{-1} within the 4 hours following a spike, and decrease beyond 8 hours following a spike to 70-117 ng Hg day^{-1} L^{-1} (***Table 4.1***). The exception was a measurement taken 2 hours following the first thiosulfate spike where volatilization was measured at 3237 ng Hg day^{-1} L^{-1}. Similarly, Hg volatilization rates for live cells in the presence of synthetic metacinnabar and daily spikes of ~125 μM thiosulfate found in this study range from

105 to 1104 ng Hg day^{-1} L^{-1} within the 4 hours following a spike, and 61-119 ng Hg day^{-1} L^{-1} Hg beyond the 8 hours following a spike (***Table 4.1***). These rates agree well with those obtained in our previous study, where average volatilization rates for live cell experiments in the presence of natural metacinnabar and a starting thiosulfate concentration of ~40 μM generally range from 132 to 294 ng Hg day^{-1} L^{-1}, with the exception of one measurement which peaks at 551 ng Hg day^{-1} L^{-1} three days following inoculation.

Abiotic Hg emission rates from autoclave killed cells in the presence of natural metacinnabar and daily spikes of ~125 μM thiosulfate range from 60 to 286 ng Hg day^{-1} L^{-1} (***Table 4.1***), and are similar to those in the presence of synthetic metacinnabar which range from 34 to 150 ng Hg day^{-1} L^{-1}, with the exception of day 1 of the experiment when the measured volatilization rate from synthetic metacinnabar killed incubations are 1452 ng Hg day^{-1} L^{-1}. These abiotic Hg emission rates agree well with volatilization rates previously measured for formaldehyde killed cells in the presence of natural metacinnabar and a starting thiosulfate concentration of ~300 μM thiosulfate which range from 44 to 117 ng Hg day^{-1} L^{-1}.

Discussion

This study probes the effects of mineral size/structure, mineral loading, and thiosulfate concentration on metacinnabar dissolution and subsequent Hg volatilization in the presence of *Thiobacillus thioparus*. We have previously shown that the abundant and widespread sulfur-oxidizing bacterium *T. thioparus* can extensively colonize natural metacinnabar within aerobic, near neutral pH creek sediments (**Chapter 2**). In lab incubations initiated with thiosulfate concentrations 0 - 60 μM, *T. thioparus* induces the release and volatilization of natural metacinnabar-hosted Hg (**Chapter 3**). Thiosulfate is a substrate for *T. thioparus* and a major

intermediate sulfur species in environmental systems. The extent of Hg volatilization was enhanced by the presence of thiosulfate (**Chapter 3**). As thiosulfate within natural systems is produced at substantial fluxes, leading to a standing pool of thiosulfate [5-9], metacinnabar and other metal-bearing sulfides will be continuously exposed to this complexing ligand. Further, continuous release of thiosulfate will provide sulfur-oxidizing organisms a more easily metabolized substrate potentially precluding their utilization of metacinnabar-bound sulfur. In this study, we tested the effect of successive daily thiosulfate additions, mimicking more continuous thiosulfate fluxes in the environment, on the release of soluble Hg(II) and volatile Hg(0) from metacinnabar incubated with live and killed *T. thioparus* cultures. Further, the composition and size of metacinnabar greatly varies within natural systems. Here, we compare a natural and synthetic metacinnabar phase to identify the role of mineral size, crystallinity and metal impurities on microbially induced metacinnabar dissolution.

Sulfur Dynamics

Daily thiosulfate spikes are quickly oxidized to sulfate in the presence of live *T. thioparus* with concomitant sulfate production. Over the 12 day incubation period, no significant differences in thiosulfate consumption and sulfate production are observed in incubations with natural vs. synthetic metacinnabar. Differences in metacinnabar loading (1000 vs 2000 ppm) also do not appear to affect thiosulfate consumption or sulfate production. Sulfate production has been previously used as a proxy for metacinnabar dissolution, and differences in sulfate production from the various incubation treatments would suggest differential metacinnabar dissolution under the various conditions [12, 13]. The lack of observed differences in sulfate production from the various treatments suggests that either there were no differences in the

degree of mineral dissolution from the treatments or this quantification method was not sensitive enough to detect differences in sulfate production.

Excess sulfate produced in live incubations cannot be definitively apportioned to elemental sulfur, metacinnabar oxidation, or release of sorbed sulfate. In all live low thiosulfate treatments, the observed sulfate concentration at day 12 is slightly higher (490 - 540 μM) than that expected from the thiosulfate additions and thiosulfate carryover from the inoculum (***Figure 4.1b***). This excess sulfate may be due to the oxidation of elemental sulfur carryover from the inoculum, release of sorbed sulfate from the metacinnabar surface and/or sulfate production from metacinnabar dissolution. We have observed sulfate production from metacinnabar dissolution in the presence of *T. thioparus* in a previous study (**Chapter 3**), however in this case it is difficult to apportion the sources of this excess sulfate. In the case of the high thiosulfate incubation, the expected dissolved sulfate concentration on day 12 of the incubation agrees with the observed sulfate concentration (***Figure 4.1b***).

Thiosulfate consumption in killed incubations likely results from anion sorption onto the mineral surface. The consumption of thiosulfate in killed incubations with natural and synthetic metacinnabar over the 12 day period is slight (~100 μM) though significant (***Figure 4.2a***). The lower than expected thiosulfate concentration in killed incubations, with no corresponding sulfate production (***Figure 4.2b***) suggests sorption of thiosulfate onto the mineral surface. In a parallel purely abiotic study, we saw a similar decrease in dissolved thiosulfate concentration over time in the presence of synthetic metacinnabar (***Supplementary Figure S4.1***).

Release of Aqueous Hg

Dissolved Hg in killed incubations with natural and synthetic metacinnabar increases over the course of the experiment. We have previously shown that in the absence of microbial activity (e.g., killed cells), aqueous Hg(II) levels increase with increasing initial thiosulfate concentration, indicating that thiosulfate**,** a strong Hg-binding ligand, abiotically stimulates metacinnabar dissolution (**Chapter 3**). We also found that after an initial thiosulfate addition on day 0 of the experiment, dissolved Hg concentration continue to increase for at least 22 days following the thiosulfate addition (**Chapter 3**). Differently from our previous study, rather than adding the thiosulfate all at once at the start of the experiment, here we added the thiosulfate to killed incubations in small (~125 μM) daily spikes throughout the course of the experiment. Similar to our previous findings, here we see a rise in dissolved Hg concentrations in the period 15 hours following the start of the experiment to day 12 of the incubation. The increase in dissolved Hg is more pronounced for natural than for synthetic metacinnabar killed incubations, with dissolved Hg concentrations in natural metacinnabar incubations being ~7x higher than it is in incubations with synthetic metacinnabar. This suggests that either more Hg is released from natural metacinnabar than from synthetic or that the greater surface area of synthetic metacinnabar, which was 10x that of natural metacinnabar, allows for more of the dissolved Hg to sorb back on to the mineral surface. Further, the fact that filtering aliquots for dissolved Hg measurements with 0.02 μm filters yields concentrations that are the same or higher than those obtained with the 0.2 μm filters, suggests that released Hg from metacinnabar is in fact dissolved Hg rather than nanoparticulate. The lower dissolved Hg concentrations obtained by filtering with the 0.2 μm filters suggest that some fraction of Hg may be sorbing onto these cellulose filters. Regardless of the filtration method used, dissolved Hg in killed incubations with both natural and

synthetic metacinnabar increases with time. This further validates our previous finding that thiosulfate enhances natural metacinnabar dissolution, and suggests that synthetic metacinnabar dissolution is similarly enhanced.

Making daily thiosulfate additions (i.e., creating a thiosulfate flux) has an enhancing effect on abiotic dissolved Hg release from metacinnabar as compared to adding all the thiosulfate at once. In this experiment, natural metacinnabar killed incubations yielded 240 nM dissolved Hg after 12 days when a total of 1.562 mM thiosulfate had been added. Based on our previous study (**Chapter 3**), adding this amount of thiosulfate all at once at the start of the experiment would have yielded only between 116 and 137 nM dissolved Hg after 12 days of incubations (***Supplementary Calculation S4.1***). Therefore slowly fluxing in the thiosulfate has a 2x enhancing effect on dissolved Hg release from natural metacinnabar. The reason for this enhancement in metacinnabar dissolution from slowly fluxing in the thiosulfate might be related to the percentage of thiosulfate that sorbs onto the mineral surface versus that which complexes Hg and enhances dissolution. As these thiosulfate concentrations are characteristic of many metal sulfide rich environments, thiosulfate may have a substantial influence on metal sulfide dissolution and as in this case, release of mineral-bound metals.

Dissolved Hg in live incubations decreases over time presumably due to the volatilization of dissolved Hg by *T. thioparus*. Many sulfur-oxidizing organisms possess the enzyme mercuric reductase, MerA, which reduces Hg(II) to Hg(II) [14, 15]. Our previous work has shown that this *T. thioparus* strain possesses the *merA* gene and hence the genetic potential to reduce Hg(II) as observed in our incubations here (**Chapter 3**). Fifteen hours after the inoculation, cellular metabolism is likely not active enough to volatilize surrounding dissolved Hg explaining why dissolved Hg concentrations in live and killed incubations are not significantly different initially.

Hg Volatilization

Hg volatilization measurements show a large variance between replicates for both live and killed incubations. No significant difference between abiotic volatilization from natural metacinnabar and synthetic metacinnabar could be quantified on most time points (***Figure 4.4, Table 4.1***). During time points when a significant difference could be discerned, higher Hg volatilization rates were observed for natural metacinnabar, with the exception of a measurement taken on Day 1 when Hg volatilization rates from synthetic metacinnabar were approximately 10x higher than those observed at any other time during the experiment (***Table 4.1***). A slightly higher volatilization from natural metacinnabar might be explained by reduced iron impurities in natural metacinnabar. These iron impurities might enhance mineral dissolution, and Fe(II) might also cause abiotic reduction of the released Hg(II). Abiotic Hg(II) reduction by Fe(II) has been shown previously [16, 17]. An alternative explanation is that as a result of the larger surface area per unit mass in synthetic metacinnabar, Hg released from synthetic metacinnabar is more likely to sorb back onto the mineral surface itself making less dissolved Hg available for abiotic volatilization. The reason for the higher degree of abiotic volatilization in natural metacinnabar incubations might be a combination of these mechanisms, and future targeted investigations should be conducted to elucidate the mechanisms at work.

Further, the reason for the greatly enhanced release of volatile Hg from abiotic synthetic metacinnabar incubations on Day 1 of the experiment, with slightly enhanced release from natural metacinnabar on some subsequent days, and similar release on other days is likely a complex one. Abiotic Hg(II) reduction by Fe cannot be invoked as a potential explanation for the quick release of Hg in killed incubations in Day 1 of the experiment, as XRF measurements

confirmed that any potential Fe impurities in this synthetic mineral were below the instrument limit of detection (0.24% by mass). However, perhaps Fe impurities found at concentrations lower than the instrument limit of detection would have been sufficient to cause abiotic Hg reduction, and the 10x greater surface area of synthetic metacinnabar would have provided a higher number of available reaction sites leading to this quick spurt of volatile mercury release. The information collected in this study is not sufficient to ascertain the reasons for the abiotic volatilization patterns observed in natural and synthetic metacinnabar; future investigations looking at the kinetics of abiotic volatile Hg release from natural and synthetic metacinnabar should be conducted.

Despite the variability in Hg emission rates, abiotic Hg emissions measured from autoclave killed cells in the presence of natural and synthetic metacinnabar and daily spikes of ~125 μM thiosulfate agree well with previously measured volatilization rates for formaldehyde killed cells in the presence of natural metacinnabar and a starting thiosulfate concentration of ~300 μM thiosulfate (***Table 4.1***, **Chapter 3**). This suggests that abiotic Hg volatilization rates observed in autoclave killed cell incubations and formaldehyde killed incubations are similar. Additionally, the differences in the concentration and timing of thiosulfate additions appear to have little measurable effect on abiotic volatilization rates from natural metacinnabar.

Thiosulfate-induced Dissolution Dynamics

Release of volatile Hg from live incubations occurs rapidly within the first few hours following the thiosulfate spike, with decreasing volatilization after thiosulfate is consumed (***Figure 4.4***). The fact that when thiosulfate is fluxed daily, release of volatile Hg from live incubations occurs rapidly within the first few hours following the spike, suggests thiosulfate

stimulates release of Hg from metacinnabar and/or stimulates cell activity and hence activity of the *mer* operon. Once thiosulfate concentrations decrease, Hg volatilization also decreases. Though the average Hg volatilization rates for live cells in the presence of natural and synthetic metacinnabar observed in this study agree well with those measured in our previous study for live cell experiments in the presence of natural metacinnabar and a starting thiosulfate concentration of ~40 μM, the timing of the volatile Hg release is significantly different. We had previously observed that after making only one thiosulfate addition to incubations (the thiosulfate present in the inoculum carryover), live incubations continue to emit more volatile Hg than killed incubations even 30 days after inoculation. In the current study however we observe an increase in Hg volatilization in live incubations immediately following the thiosulfate spike, and a decrease in volatilization over the next few hours until the volatilization rates from live and killed incubations are not significantly different 8 h or 16 h beyond the spike (***Figure 4.4***). This suggests there are two different cellular metabolisms under these two scenarios. When thiosulfate is fluxed in daily, the cells consume predominantly thiosulfate, with their metabolism slowing down after the thiosulfate is consumed, hence a decrease in volatilization. When thiosulfate is not added daily, the cells must switch to other reduced sulfur sources such as HgS as a substrate for metabolism. These differences in cellular metabolism given the availability of reduced sulfur substrates are intriguing and highlight a high degree of temporal and spatial complexity at the mineral-microbe interface. Future exploration of substrate competition in microbial metabolism and metacinnabar dissolution is warranted.

Implications

Other researches have observed Hg volatilization from microbial cultures in the presence of HgS. A Hg-resistant *Acidithiobacillus ferrooxidans* bacterium has been previously implicated in inducing volatilization of cinnabar-hosted Hg [18]. *A. ferrooxidans* was incubated in shake flasks in the presence of cinnabar with observed Hg volatilization rates of 892 ng Hg day^{-1} L^{-1} culture, and no dissolved Hg detected. This volatilization rate is within the range of rates observed in this study in the presence of natural and synthetic metacinnabar, though it is 4-5 times higher than the rates observed during most days. It is problematic to directly compare *A. ferrooxidans* volatilization rates to those obtained in the present study due to the number of variables that are different between the two experimental setups. The Baldi and Olson (1987) study was performed with cinnabar rather than metacinnabar, and it was conducted in acidic conditions where cinnabar is more prone to dissolution. Further, experiments were inoculated with a cell concentration of 10^8 cells mL^{-1} which is two orders of magnitude higher than inoculation cell densities used in our study. Based on these factors, we would expect for the volatilization rates observed with *A. ferrooxidans* to be significantly higher than those we observed in the present study.

Mine tailing-derived microbial cultures dominated by iron- and sulfur-oxidizing bacteria can also enhance HgS dissolution under acidic pH conditions [19]. Incubating an AMD microbial community with metacinnabar resulted in dissolved Hg concentrations up to 2000 nM Hg over a 30-day incubation period, whereas dissolved Hg concentrations in abiotic controls did not exceed 0.5 nM which was the Hg concentration of the acid mine drainage water used as experimental medium. Although volatile Hg was not quantified from the mine tailing-derived microbial cultures, it is evident that a different mechanism for microbial enhancement of

metacinnabar dissolution is at play here: one that induces the release of aqueous Hg in the presence of microorganisms, while not promoting volatilization in quantities that preclude dissolved Hg accumulation in the medium.

The fact that microbially enhanced HgS dissolution can result in high dissolved Hg concentrations and/or volatile Hg production, and the difficulties in comparing Hg volatilization rates from the *A. ferrooxidans* study and ours highlights the fact that volatilization of HgS-hosted Hg is a complex process involving various competing and synergistic mechanisms. A deeper mechanistic understanding of the individual underpinning processes is needed to understand the true mobililty of Hg hosted in this dominant Hg reservoir. Here, we see that a combination of factors are involved in the dissolution of metacinnabar, including thiosulfate flux and mineralogical structure. While synthetic metacinnabar has a higher surface area and thus theoretically higher solubility, enhanced abiotic dissolution of natural metacinnabar here points to more complex controls on metacinnabar dissolution and likely highlights the importance of impurities such as iron. Further, modulation of microbial activity at the mineral surface stimulated by the availability of soluble and alterative electron donors will control the release and volatilization of Hg. Thus, understanding the risk posed by HgS in the environment requires further future targeted investigations to elucidate the range of microbial and geochemical variables dictating the dissolution and volatilization of HgS-hosted Hg.

Chapter 4 - References Cited

1. Clarkson, T.W. and L. Magos, *The toxicology of mercury and its chemical compounds.* Critical Reviews in Toxicology, 2006. **36**(8): p. 609-662.

2. Mason, R.P., et al., *Mercury biogeochemical cycling in the ocean and policy implications.* Environmental Research, 2012. **119**: p. 101-117.

3. Barnett, M.O., et al., *Formation of mercuric sulfide in soil.* Environmental Science & Technology, 1997. **31**(11): p. 3037-3043.

4. Ravichandran, M., et al., *Inhibition of precipitation and aggregation of metacinnabar (mercuric sulfide) by dissolved organic matter isolated from the Florida Everglades.* Environmental Science & Technology, 1999. **33**(9): p. 1418-1423.

5. Jorgensen, B.B., *A Thiosulfate Shunt in the Sulfur Cycle of Marine Sediments.* Science, 1990. **249**(4965): p. 152-154.

6. Jorgensen, B.B., *The Sulfur cycle of freshwater sediments: Role of thiosulfate.* Limnology and Oceanography, 1990. **35**(6): p. 1329-1342.

7. Zopfi, J., T.G. Ferdelman, and H. Fossing, *Distribution and fate of sulfur intermediates—sulfite, tetrathionate, thiosulfate, and elemental sulfur—in marine sediments.* Geological Society of America Special Papers, 2004. **379**: p. 97-116.

8. Luther, G.W., et al., *Inorganic and Organic Sulfur Cycling in Salt-Marsh Pore Waters.* Science, 1986. **232**(4751): p. 746-749.

9. Mullaugh, K.M., et al., *Voltammetric (micro)electrodes for the in situ study of Fe2+ oxidation kinetics in hot springs and S2O32- production at hydrothermal vents.* Electroanalysis, 2008. **20**(3): p. 280-290.

10. Widdel, F. and F. Bak, *Gram-negative mesophilic sulfate-reducing bacteria*, in *The Prokaryotes*, A. Balows, et al., Editors. 1992, Springer: New York. p. 3352-3378.

11. Tauson, V.L. and V.V. Akimov, *Introduction to the theory of forced equilibria: General principles, basic concepts, and definitions.* Geochimica et Cosmochimica Acta, 1997. **61**(23): p. 4935-4943.

12. Barnett, M.O., R.R. Turner, and P.C. Singer, *Oxidative dissolution of metacinnabar (beta-HgS) by dissolved oxygen.* Applied Geochemistry, 2001. **16**(13): p. 1499-1512.

13. Holley, E.A., et al., *Mercury mobilization by oxidative dissolution of cinnabar (alpha-HgS) and metacinnabar (beta-HgS).* Chemical Geology, 2007. **240**(3-4): p. 313-325.

14. Benson, D.A., et al., *GenBank.* Nucleic Acids Research, 2009. **37**: p. D26-D31.

15. Barkay, T., S.M. Miller, and A.O. Summers, *Bacterial mercury resistance from atoms to ecosystems.* FEMS Microbiology Reviews, 2003. **27**(2-3): p. 355-384.

16. Amirbahman, A., et al., *Kinetics of Homogeneous and Surface-Catalyzed Mercury(II) Reduction by Iron(II).* Environmental Science & Technology, 2013. **47**(13): p. 7204-7213.

17. Wiatrowski, H.A., et al., *Reduction of Hg(II) to Hg(0) by Magnetite.* Environmental Science & Technology, 2009. **43**(14): p. 5307-5313.

18. Baldi, F. and G.J. Olson, *Effects of Cinnabar on Pyrite Oxidation by Thiobacillus ferrooxidans and Cinnabar Mobilization by a Mercury-Resistant Strain.* Applied and Environmental Microbiology, 1987. **53**(4): p. 772-776.

19. Jew, A.D., et al., *Microbially enhanced dissolution of HgS in an acid mine drainage system in the California Coast Range.* Geobiology, 2014. **12**(1): p. 20-33.

APPENDIX A

SUPPLEMENTARY INFORMATION FOR CHAPTER 2

		September 2008		October 2007		November 2007	
EFK 13	Creek Bank	Subdivision3_genera_incertae_sedis	18%			Gp6	31%
		Gp6	9%			Subdivision3_genera_incertae_sedis	8%
		Sulfuritalea	6%			Novosphingobium	7%
	Creek Channel	Gp6	16%			Gp6	27%
		Subdivision3_genera_incertae_sedis	13%			Novosphingobium	10%
		Novosphingobium	6%			Subdivision3_genera_incertae_sedis	6%
EFK 23	Creek Bank	Bacillariophyta	18%	Bacillariophyta	28%	Gp6	25%
		Subdivision3_genera_incertae_sedis	13%	Subdivision3_genera_incertae_sedis	27%	Luteolibacter	16%
		Luteolibacter	8%	Luteolibacter	5%	Subdivision3_genera_incertae_sedis	10%
	Creek Channel	Bacillariophyta	26%	Subdivision3_genera_incertae_sedis	27%	Gp6	30%
		Subdivision3_genera_incertae_sedis	23%	Gp6	14%	Subdivision3_genera_incertae_sedis	10%
		Gp6	11%	Gp17	12%	Gp4	7%

Supplementary Table S2.1. Dominant genera in EFPC sediments. The top 3 genera identified in each sediment sample taken at nearby EFPC locations are listed. Percentages indicate the percent abundance of each genus relative to the total number of classifiable reads.

APPENDIX B

SUPPLEMENTARY INFORMATION FOR CHAPTER 3

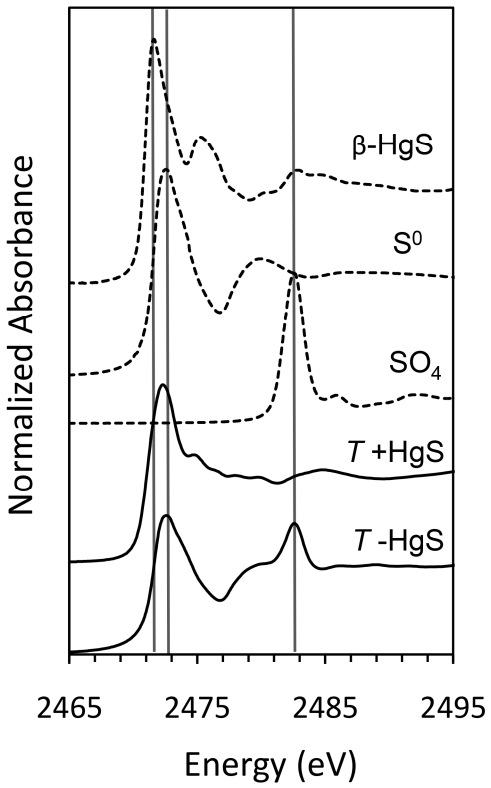

Supplementary Figure S3.1. Sulfur (S) K-edge XANES spectra of bulk S speciation within *Thiobacillus* (T) incubations either in the presence or absence of metacinnabar. In the absence of metacinnabar (T -HgS), the dominant S speciation is elemental sulfur (S^0) and sulfate (SO_4), illustrating these two species as the byproduct of thiosulfate oxidation by *Thiobacillus*. The spectrum is difficult to deconstruct, however, in the presence of the high sulfide signature in the spectrum. Nevertheless, a shift in the white line energy to high oxidation states coincides with the presence of elemental S in these incubations as well (T +HgS). Standard spectra are also provided for reference (dotted lines).

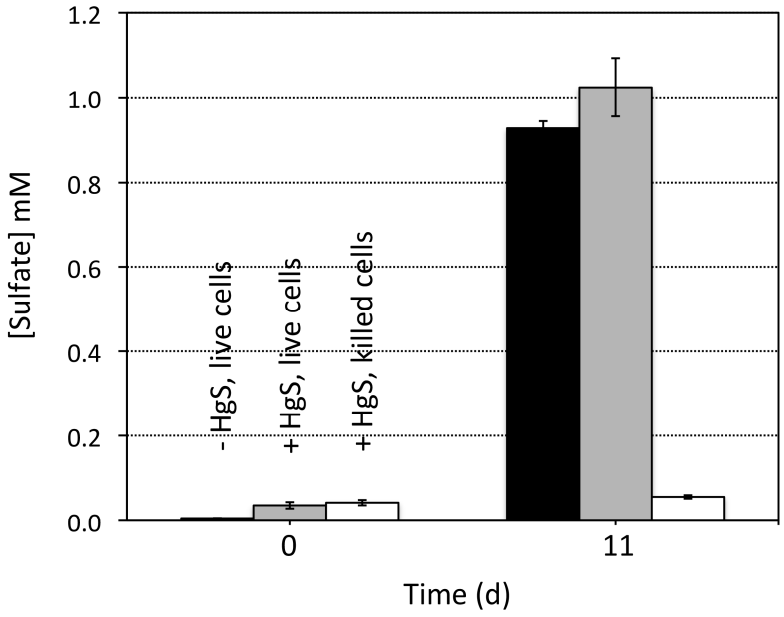

Supplementary Figure S3.2. Aqueous sulfate concentrations within *Thiobacillus* incubations initiated with zero added thiosulfate. In all cultures, elemental S is present within the inoculum, with the concentration equivalent between all samples. In the absence of metacinnabar (-HgS), sulfate production is formed solely via oxidation of this transferred S(0). In the presence of metacinnabar (+HgS), sulfate produced via bacterial oxidation of metacinnabar-derived sulfide is that in excess of the amount produced in the absence of metacinnabar (~100 μM) and the amount produced in the presence of metacinnabar (+HgS) and killed cells (~50 μM) (see Supplementary Table S3.1). The standard deviation of biological triplicates is indicated.

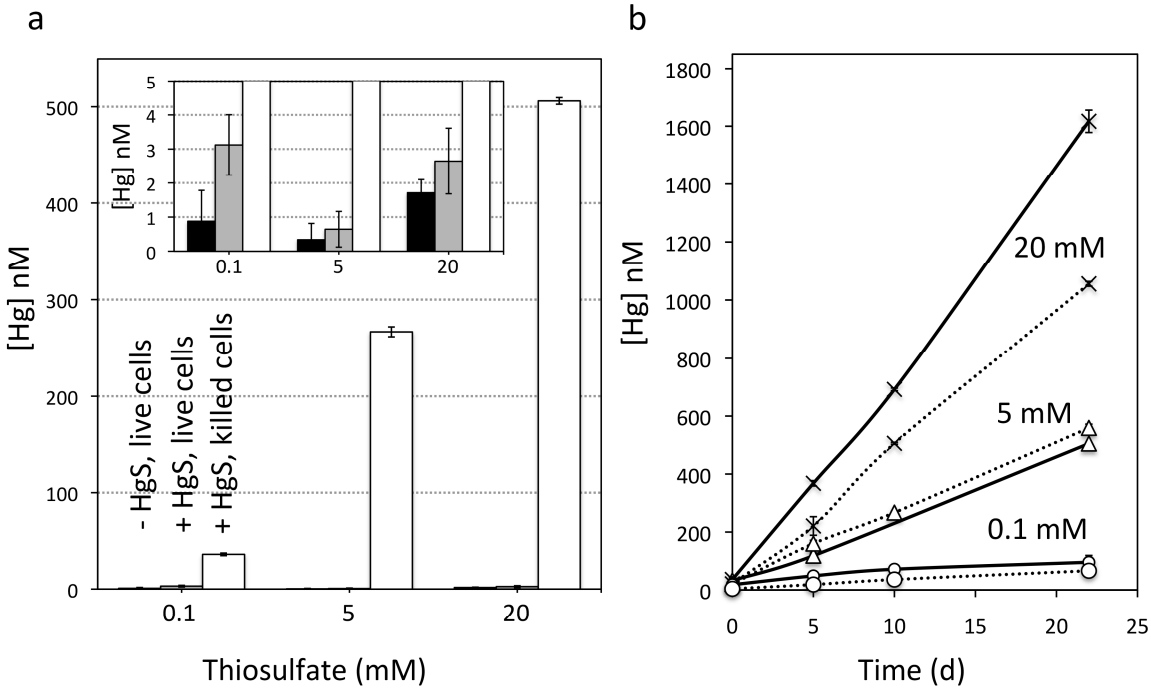

Supplementary Figure S3.3. Aqueous Hg concentrations in incubations. (a) Aqueous Hg concentrations (nM) in incubations containing various concentrations of thiosulfate after 10 days of reaction. The conditions included (black bars) live cells, no metacinnabar; (gray bars) live cells plus metacinnabar, and (white bars) killed cells plus metacinnabar. The inset shows data up to 5 nM Hg to illustrate the differences in the live incubations that are masked in the full range due to the high Hg in the presence of 20 mM thiosulfate in the killed cell incubations. (b) Aqueous Hg concentrations (nM) over time as a function of thiosulfate concentration within incubations containing killed cells and metacinnabar. The solid lines were conducted in a basal freshwater medium containing EDTA, while the dashed lines contained no EDTA. The standard deviation of two method replicates is indicated.

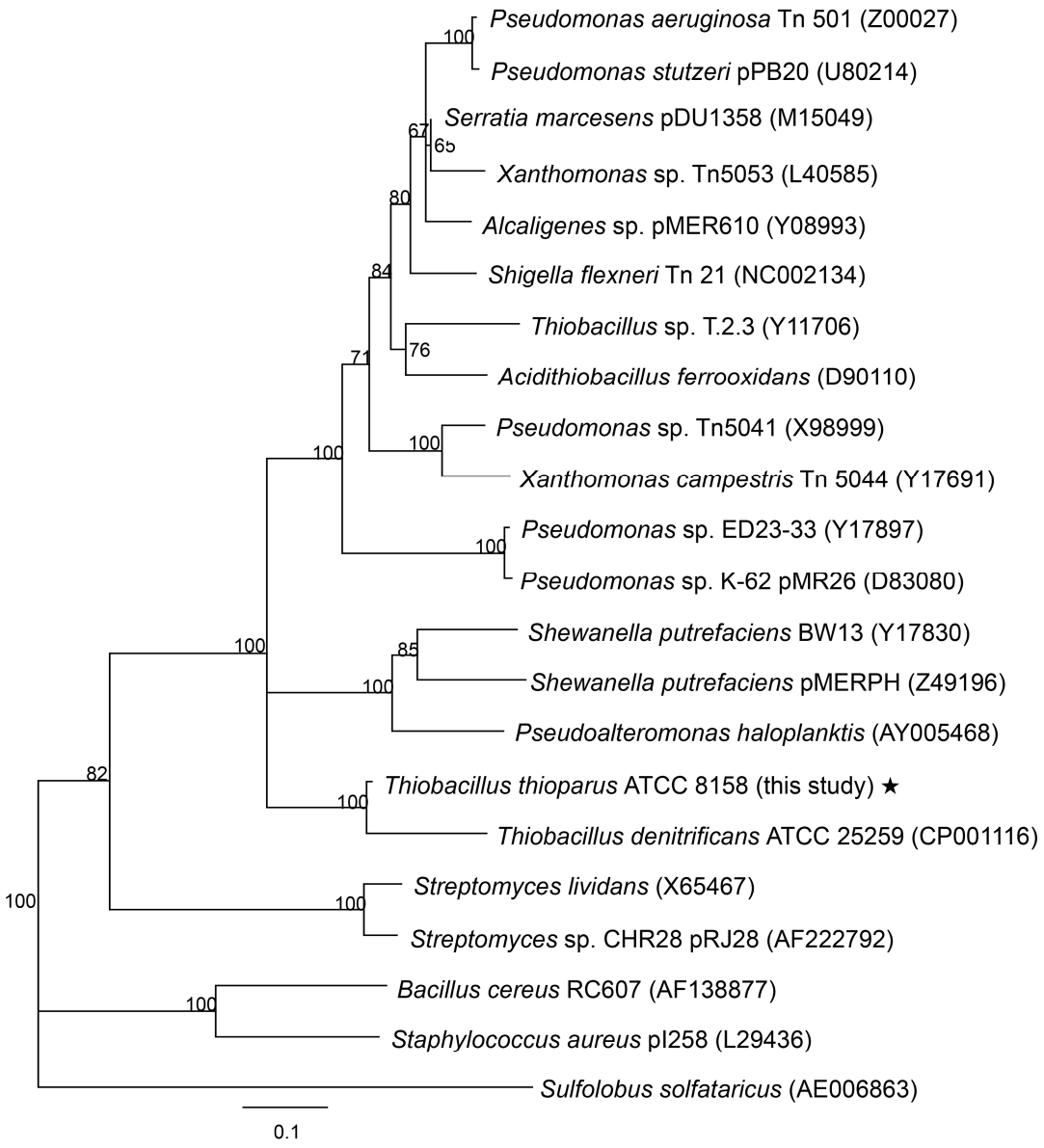

Supplementary Figure S3.4. Neighbor-joining tree showing the phylogenetic relationship between the translated *Thiobacillus thioparus* ATCC 8158 MerA sequence and other prokaryotic MerA sequences obtained from Chadhain *et al.* 2006 [1] and Genbank [2]. Bootstrap values are shown at each branch point. The bar represents 0.1 amino acid substitutions per site. For Genbank sequences, NCBI accession numbers are indicated in parentheses. Archaeal MerA of *Sulfolobus solfataricus* served as an out group. MerA protein sequences were aligned in ClustalX v. 2.1 and the tree created and drawn in Geneious v. 7.0.6 by Biomatters.

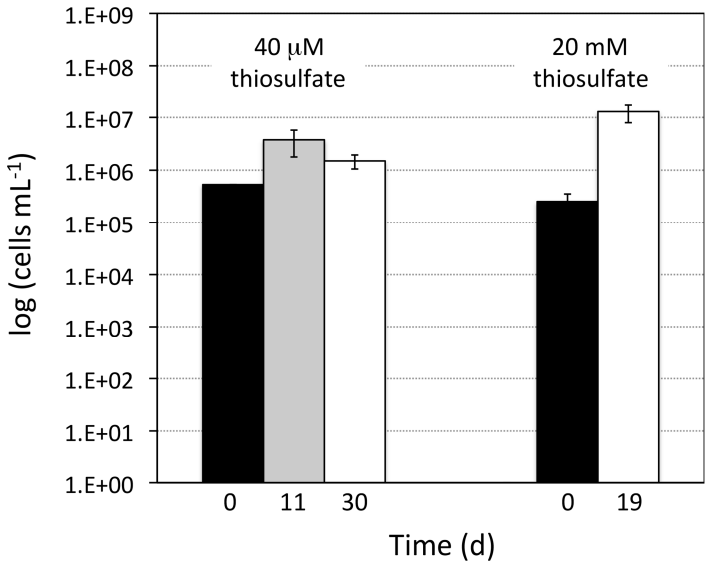

Supplementary Figure S3.5. Bacterial cell counts (cells mL^{-1}) in incubations within the initial inoculum (t=0) and over time, illustrating growth under two initial thiosulfate concentrations and higher cell counts obtained in the presence of higher initial thiosulfate concentrations. The standard deviation of biological triplicates (40 μM) and duplicates (20 mM) is indicated; no standard deviation is shown for the 40 μM inoculum.

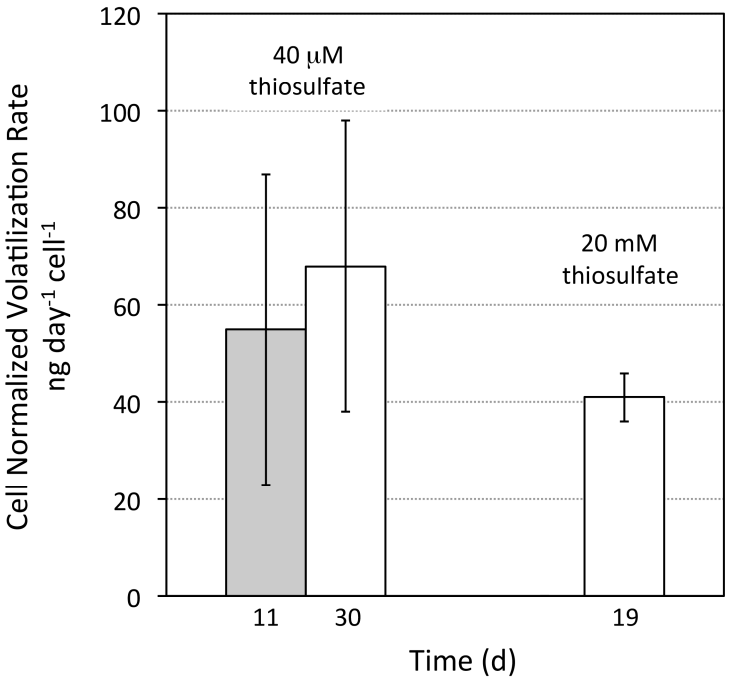

Supplementary Figure S3.6. Cell normalized Hg volatilization rates within *Thiobacillus* incubations (+HgS) initiated with 40 μM and 20 mM thiosulfate. Gaseous Hg emission rates collected on the day indicated are divided by the number of cells present at that timepoint and presented as ng Hg^0 per day per cell. Most of the initial thiosulfate had been consumed at these timepoints (concentration remaining 0 – 5 μM), and the cell normalized Hg volatilization rate is similar for initial thiosulfate concentrations shown here. The standard deviation of biological triplicates (40 μM thiosulfate) and duplicates (20 mM thiosulfate) is indicated.

Initial Thiosulfate Concentration	x days	H_x μM	N_x μM	A_x μM	C_0 μM	M_x μM	Contribution of microbial processes to total HgS dissolution (%)	R μmol (sulfate) m^{-2} d^{-1}
0 μM	11	1024	927	57	7	47	48%	16.2
60 μM	10	710	560	120	60	90	60%	34.1
	22	760	570	120	60	130	68%	22.4
	75	810	610	150	60	110	55%	-

Supplementary Table S3.1. Microbial contribution to metacinnabar dissolution and microbially mediated dissolution rates. The microbial contribution to metacinnabar dissolution observed in our incubations was calculated using sulfate production as a proxy for metacinnabar dissolution as has been reported previously [3, 4] using the following equation:

$$M_x = (H_x - N_x) - (A_x - C_0),$$

where M_x is the microbial contribution to sulfate production x days after inoculation, H_x is the sulfate produced in live *Thiobacillus* incubations in the presence of metacinnabar (+HgS), N_x is sulfate produced in live *Thiobacillus* incubations in the absence of metacinnabar (–HgS), A_x is sulfate produced in killed cell incubations in the presence of metacinnabar (+HgS), and C_0 is the initial sulfate concentration (t = 0) in live *Thiobacillus* incubations in the absence of metacinnabar (–HgS). The term N_x represents sulfate production attributed to thiosulfate and elemental sulfur oxidation, as well as carryover sulfate from the inoculum, and ($H_x - N_x$) represents sulfate release from metacinnabar from biotic and abiotic processes. The term ($A_x - C_0$) represents abiotic oxidative dissolution and release of any sulfate bound to the metacinnabar

(Supplementary Table S3.1 continued)

surface, with C_0 representing carryover sulfate from the inoculum. M_x, H_x, N_x, A_x, *and* C_0 are reported in μM. Microbially mediated metacinnabar dissolution rates (R) are calculated by taking into account mineral loading (2 g metacinnabar L^{-1} incubation) and surface area (0.1321 m^2 g^{-1}) and are presented as μmoles (sulfate) m^{-2} d^{-1}. Reported rates of abiotic metacinnabar dissolution under oxidative conditions using sulfate production as a proxy vary from 3.15 x 10^{-2} to 1.90 μmol (sulfate) m^{-2} d^{-1} [3, 4].

Conditions	Lower Bound	Upper Bound	Reasonable Estimate
For cell-normalized mercury volatilization rate of 41 ag cell $^{-1}$ day $^{-1}$			
Soil Cell Density (cells/g)[a]	6.75E+07	3.62E+09	1.00E+08
Hg resistance (% of total bacterial population)[b]	0.20%	24.60%	1%
Projected Mercury Release Rate (umoles Hg m $^{-2}$ yr $^{-1}$)[c]	*0.30*	*1993*	***2.2***
Projected Global Mercury Release Rate (Mmoles Hg yr $^{-1}$)[d]			***1.4***
For cell-normalized mercury volatilization rate of 55 ag cell $^{-1}$ day $^{-1}$			
Soil Cell Density (cells/g)[a]	6.75E+07	3.62E+09	1.00E+08
Hg resistance (% of total bacterial population)[b]	0.20%	24.60%	1%
Projected Mercury Release Rate (umoles Hg m $^{-2}$ yr $^{-1}$)[c]	*0.41*	*2674*	***3.0***
Projected Global Mercury Release Rate (Mmoles Hg yr $^{-1}$)[d]			***1.9***
For cell-normalized mercury volatilization rate of 68 ag cell $^{-1}$ day $^{-1}$			
Soil Cell Density (cells/g)[a]	6.75E+07	3.62E+09	1.00E+08
Hg resistance (% of total bacterial population)[b]	0.20%	24.60%	1%
Projected Mercury Release Rate (umoles Hg m $^{-2}$ yr $^{-1}$)[c]	*0.50*	*3306*	***3.7***
Projected Global Mercury Release Rate (Mmoles Hg yr $^{-1}$)[d]			***2.3***

[a]Vishnivetskaya et al., 2011

[b]Crespo-Medina et al., 2009

[c]projected for top 2 cm of soil

[d]projected including a global wetland area of 6.3x10^{11} m^2

Supplementary Table S3.2. We extrapolated Hg volatilization rates from metacinnabar assuming bacterial cell density for Hg-contaminated wet soils [5], and a typical wet soil density of 1.5 g/cm^3. We assume a percentage of the bacterial community is Hg resistant based on resistance observed in Hg-contaminated environments [6]. We assume all resistance to result in Hg-volatilization. To constrain our estimate, we take only the top 2 cm of soil into account, where emitted Hg^0 might be expected to diffuse into the atmosphere [7] and conditions might be expected to be aerobic.

Three extrapolations were performed: 1) a lower bound, 2) an upper bound, and 3) a reasonable estimate taking into account low end, high end, and a reasonable estimation of each assumed parameter, respectively. Three cell normalized Hg-volatilization rates were used as observed in

(Supplementary Table S3.2 continued)

our study within lab incubations after (a) 19 days with an initial thiosulfate concentration of 20 μM (41 ag cell^{-1} d^{-1}), (b) 11 days with an initial thiosulfate concentration of 40 μM (55 ag cell^{-1} d^{-1}), and (c) 30 days with an initial thiosulfate concentration of 40 μM (68 ag cell^{-1} d^{-1}). This exercise results in a *Projected Mercury Release Rate* (Mmoles Hg m^{-2} yr^{-1}).

Using the "reasonable estimates", we show further predicted global emissions for the extrapolated land area normalized volatilization rate. Here we take into account the global wetland area only, which is projected as 6.3 x 10^{11} m^2 [8].

Chemical and physical parameters of the East Fork Poplar Creek channel pore waters at EFK 22 October 2010				
Parameter	**Depth (cm)**			
	0.0	7.6	15.2	22.9
Temperature (°C)	14.7	16.5	16.1	16.7
pH	8.0	8.1	8.0	7.8
Conductivity (µS/cm)	354	356	355	316
ORP (mV)	85	69	118	115
Element Concentration (mg/L)				
Ca	41.5 ± 1.2	39.9 ± 1.2	40.7 ± 1.2	32.1 ± 1.2
Mg	12.9 ± 1.1	12.4 ± 1.1	12.6 ± 1.1	14.7 ± 1.1
Na	9.7 ± 1.1	9.2 ± 1.1	9.1 ± 1.1	5.7 ± 1.1
Dissolved Hg (ng/L)	19.05 ± 4.8	12.8 ± 0.4	12.1 ± 0.4	7.1 ± 0.4
Ion Concentration				
NH_4^+ (mg/L)	82.7 ± 0.8	26.8 ± 0.7	5.9 ± 0.8	15.9 ± 0.7
SRP (mg/L)	26.9 ± 0.5	37.4 ± 0.5	46.9 ± 0.5	30.4 ± 0.5
Sulfide (mg/L)	ND	ND	ND	ND
Cl^- (mg/L)	10.6 ± 0.1	10.7 ± 0.1	10.6 ± 0.1	4.2 ± 0.1
Br^- (mg/L)	ND	ND	ND	ND
NO_3^- (mg/L)	7.3 ± 0.1	7.7 ± 0.1	7.7 ± 0.1	3.3 ± 0.1
SO_4^{2-} (mg/L)	36.8 ± 0.1	36.4 ± 0.1	36.3 ± 0.1	31.2 ± 0.1

Supplementary Table S3.3. Chemical and physical parameters of the East Fork Poplar Creek channel pore waters at EFK 22 October 2010. ND denotes values below instrument detection limit. Uncertainty in the measurement is reported as ± 1 standard error.

Supplementary Methods

Metacinnabar Specimen

The metacinnabar specimen was analyzed using XRF to confirm that the sample was composed predominantly of Hg and S. In line with a minor Fe XRF contribution, microscopy observations revealed minor pyrite inclusions within the mineral; iron is a common co-precipitate within metacinnabar in the ambient environment.

In-Situ Incubations Sample Preservation

Mineral sections were incubated in the center of the East Fork Poplar Creek (EFPC) at N 36° 00.101', W 084° 15.011', ± 18 ft. Mineral sections were mounted on glass slides (2 cm by 2.5 cm), which were then secured into precut holes on a polycarbonate sampler, and covered in mesh to prevent large organisms from interfering with the slabs. This sampler was inserted directly into the EFPC sediments. Once retrieved from the creek, mineral samplers were transported on ice to our laboratory where they were preserved within 24 hours. Mineral slabs used for DNA extraction and sequencing were stored aseptically at -80°C. Mineral slabs for thin sections were fixed using 4% paraformaldehyde, rinsed twice in PBS solution, and stored at -20°C in a 1:1 (v/v) mixture of PBS and 96% ethanol until further processing.

Molecular Methods

Field-incubated minerals were aseptically crushed and DNA was extracted using the Ultraclean soil DNA kit (Mo Bio Laboratories) using the maximum yield protocol with the

following modifications. After minerals were added to the bead solution tubes, tubes were sonicated for 5 minutes. Following addition of IRS solution, tubes were incubated at 70°C for 10 minutes, and 200 µg of polyadenylic acid was added [9, 10], followed by vortexing at maximum speed for 15 minutes. The 16S rRNA region of environmental DNA was amplified using the 8F and 1492R primer set and conditions used previously [11] in triplicate or quadruplicate to yield sufficient DNA for pyrosequencing. Amplification products were purified using the QIAquick nucleotide removal kit (Qiagen). Bacterial tag-encoded pyrosequencing (bTEFAP) was conducted by the Research and Testing Laboratory, Lubbock, TX using the GS FLX Titanium sequencing platform (Roche Applied Science). Primers 28F (5′GAGTTTGATCNTGGCTCAG) and 519r (5′GTNTTACNGCGGCKGCTG) were used to sequence variable regions V1-V3 of the 16S rRNA gene.

Sequence Processing

Pyrosequencing reads were denoised using AmpliconNoise, and chimeras were removed using Perseus [12]. Resulting sample reads were all longer than 150 bp, had a quality score greater than 20, and no ambiguous reads, therefore no further quality filtering was needed. Sample reads were aligned and clustered using the Ribosomal Database Project (RDP) Pyrosequencing Pipeline [13]. Bacterial 16S rRNA gene sequences were classified using a naïve Bayesian rRNA classifier, version 2.0, with a bootstrap cutoff of 80% [14].

merA Gene Amplification and Sequencing

Genomic DNA from *T. thioparus* pure cultures was extracted using the Ultraclean soil DNA kit (Mo Bio Laboratories). A 285 bp fragment at the 3′ end of *merA* was amplified using PCR primers A1s-n.F and A5-n.R following previously reported amplification conditions [1]. Gel electrophoresis was used for size separation of the PCR products, and the expected 285 bp *merA* amplification product was confirmed. The gel purified (QIAquick gel extraction kit, Qiagen) 285 bp amplification product was concentrated (DNA Clean & Concentrator-5, Zymo Research), cloned (StrataClone PCR Cloning Kits, Agilent Technologies) and sequenced. The partial *merA* sequence of *T. thioparus* was closest in sequence similarity to that of *Thiobacillus denitrificans* ATCC 25259 (Genbank accession number CP001116). The *T. Thioparus* partial *merA* sequence was translated into a MerA protein sequence (Geneious v. 7.0.6 by Biomatters), and aligned with other published MerA sequences [1] as well as that of *Thiobacillus denitrificans* ATCC 25259 using ClustalX v. 2.1. A neighbor-joining tree showing the phylogenetic relationship between MerA sequences was created using Geneious v. 7.0.6 by Biomatters.

X-ray Absorption Spectroscopy

Fixed field-incubated metacinnabar slabs were air dried and embedded in EpoHeat Epoxy (Buehler). Cross sections (~500 μm) of the embedded minerals were obtained using a diamond saw, subsequently attached to a high-purity fused quartz slide using Hillquist Thin Section Epoxy A-B (Hillquist), and filed and polished down to 50-100 μm thickness using a microtome and 1000 grit silicon carbide paper (Buehler).

Spatially-resolved (μ-scale) X-ray fluorescence (XRF) and X-ray absorption spectroscopy were conducted by collecting spectra at select points of interest or defining and

rastering a defined region. Synchrotron-based μ-XRF on beamline 14-3 at SSRL was used to map the Hg (M-edge) and S (K-edge) spatial distribution within the mineral matrix and oxidation rind. The beam size on the sample was approximately 2 x 2 μm and total Hg and S distributions were collected at 2495 eV. Maps were also collected at several discrete incident energies (2470.7, 2473, 2473.7, 2478.5, 2481.3, and 2483 eV) in continuous raster scanning mode in order to collect the fluorescence at several distinguishing points within the S absorption edge. X-ray absorption near edge structure (XANES) spectra were collected at spots of interest to confirm the oxidation state at discrete locations. Fluorescence maps and XANES spectra were analyzed using the MicroAnalysis Toolkit [15] and SIXPACK [16], respectively.

For bulk S solid-phase speciation, dried samples were mounted onto S-free Lexan. S XANES spectra were collected within a He-purged sample chamber under a continuous He flow with a Lytle detector at beamline 4-3. The spectra were calibrated with a thiosulfate standard. Samples were run in a He-purged anaerobic bag surrounding the sample holder chamber within the beamline hutch. XAS scans were averaged, background-subtracted, normalized, and deglitched if necessary using SIXPACK [16]. The lineshapes (peak position and peak shape) of the XANES spectra were used to compare the relative proportions of different sulfur species within the sample.

Pure Culture Incubations

Basal freshwater medium containing EDTA was used only for one sample series of aqueous Hg measurements as a function of thiosulfate concentration within incubations containing killed cells and metacinnabar (Figure S3 B) . All other experiments are conducted in the absence of EDTA. Basal freshwater medium containing EDTA was identical to the basal

freshwater medium described with the exception that Trace Element Solution was prepared following the T2 Medium for *Thiobacillus* Trace Metals solution [17] using Na_2MoO_4 instead of $(NH_4)_2MoO_4$. This Trace Element Solution contained 5% (w/w) EDTA resulting in 0.005% EDTA in the final medium.

Ion Chromatography

An eluent gradient method was employed (flow rate 1.5 mL min^{-1}): beginning for 8 min at 1 mM, followed by a linear ramp to 15 mM over 4 min, another linear ramp to 60 mM over 8 min, followed by a sustained 60 mM for 2 minutes, and 1mM for 13 minutes. A blank was run between all samples and standards to prevent carryover between samples.

Dissolved Hg Quantification

Samples for total dissolved Hg analysis were oxidized with 1-2% (v/v) bromine monochloride (BrCl) per EPA Method 1631. High thiosulfate samples had greater reducing capacity and were oxidized with either 5 or 10% (v/v) BrCl. Samples for total dissolved Hg analysis were refrigerated between collection and analysis except during the BrCl oxidation step. Calibration of the DMA-80 direct Hg analyzer was performed with a series of dissolved Hg(II) standards and the calibration was regularly verified using reference material from the Quebec National Institute for Public Health (INSPQ) Interlaboratory Comparison Program for Metals in Biological Matrices.

Cell counts

For the determination of total cell abundance, cultures were fixed with a final concentration of 4% formaldehyde and frozen. Prior to enumeration using epifluorescence microscopy, cells were stained using SYBR Green I Nucleic Acid Stain. A 0.1% p-phenylenediamine mounting solution was used to prevent photo bleaching [18]. Cell counts were performed for twenty random fields of view. Viable cell enumeration was conducted by making serial dilutions of the culture in PBS, and then plating onto agar dishes with the same culture medium.

Appendix B - References Cited

1. Chadhain, S.M.N., et al., *Analysis of mercuric reductase (merA) gene diversity in an anaerobic mercury-contaminated sediment enrichment.* Environmental Microbiology, 2006. **8**(10): p. 1746-1752.

2. Benson, D.A., et al., *GenBank.* Nucleic Acids Research, 2009. **37**: p. D26-D31.

3. Barnett, M.O., R.R. Turner, and P.C. Singer, *Oxidative dissolution of metacinnabar (beta-HgS) by dissolved oxygen.* Applied Geochemistry, 2001. **16**(13): p. 1499-1512.

4. Holley, E.A., et al., *Mercury mobilization by oxidative dissolution of cinnabar (alpha-HgS) and metacinnabar (beta-HgS).* Chemical Geology, 2007. **240**(3-4): p. 313-325.

5. Vishnivetskaya, T.A., et al., *Mercury and Other Heavy Metals Influence Bacterial Community Structure in Contaminated Tennessee Streams.* Applied and Environmental Microbiology, 2011. **77**(1): p. 302-311.

6. Crespo-Medina, M., et al., *Adaptation of chemosynthetic microorganisms to elevated mercury concentrations in deep-sea hydrothermal vents.* Limnology and Oceanography, 2009. **54**(1): p. 41-49.

7. Mazur, M., C. Eckley, and C. Mitchell. *Where does the mercury in gaseous fluxes from soil come from? An applied stable isotope experiment*. in *European Geosciences Union General Assembly 2013*. 2013. Vienna, Austria.

8. Schuyt, K. and L. Brander, *The Economic Values of the World's Wetlands*. 2004, WWF-International and Institute for Environmental Studies, Vrije Universiteit: Gland/Amsterdam.

9. Santelli, C.M., et al., *Abundance and diversity of microbial life in ocean crust.* Nature, 2008. **453**(7195): p. 653-U7.

10. Webster, G., et al., *Assessment of bacterial community structure in the deep sub-seafloor biosphere by 16S rDNA-based techniques: a cautionary tale.* Journal of Microbiological Methods, 2003. **55**(1): p. 155-164.

11. Hansel, C.M., et al., *Changes in bacterial and archaeal community structure and functional diversity along a geochemically variable soil profile.* Applied and Environmental Microbiology, 2008. **74**(5): p. 1620-1633.

12. Quince, C., et al., *Removing Noise From Pyrosequenced Amplicons.* BMC Bioinformatics, 2011. **12**.

13. Nawrocki, E.P., D.L. Kolbe, and S.R. Eddy, *Infernal 1.0: inference of RNA alignments.* Bioinformatics, 2009. **25**(10): p. 1335-1337.

14. Wang, Q., et al., *Naive Bayesian classifier for rapid assignment of rRNA sequences into the new bacterial taxonomy.* Applied and Environmental Microbiology, 2007. **73**(16): p. 5261-5267.

15. Webb, S.M., *SMAK: Sam's Microprobe Analysis Kit, v.0.25*. 2006, Stanford Synchrotron Radiation Laboratory.

16. Webb, S.M., *SIXPack a graphical user interface for XAS analysis using IFEFFIT.* Physica Scripta, 2005. **T115**.

17. Atlas, R.M., *Handbook of Media for Environmental Microbiology*. Second ed. 2005, Boca Raton: CRC Press.

18. Noble, R.T. and J.A. Fuhrman, *Use of SYBR Green I for rapid epifluorescence counts of marine viruses and bacteria.* Aquatic Microbial Ecology, 1998. **14**(2): p. 113-118.

APPENDIX C

SUPPLEMENTARY INFORMATION FOR CHAPTER 4

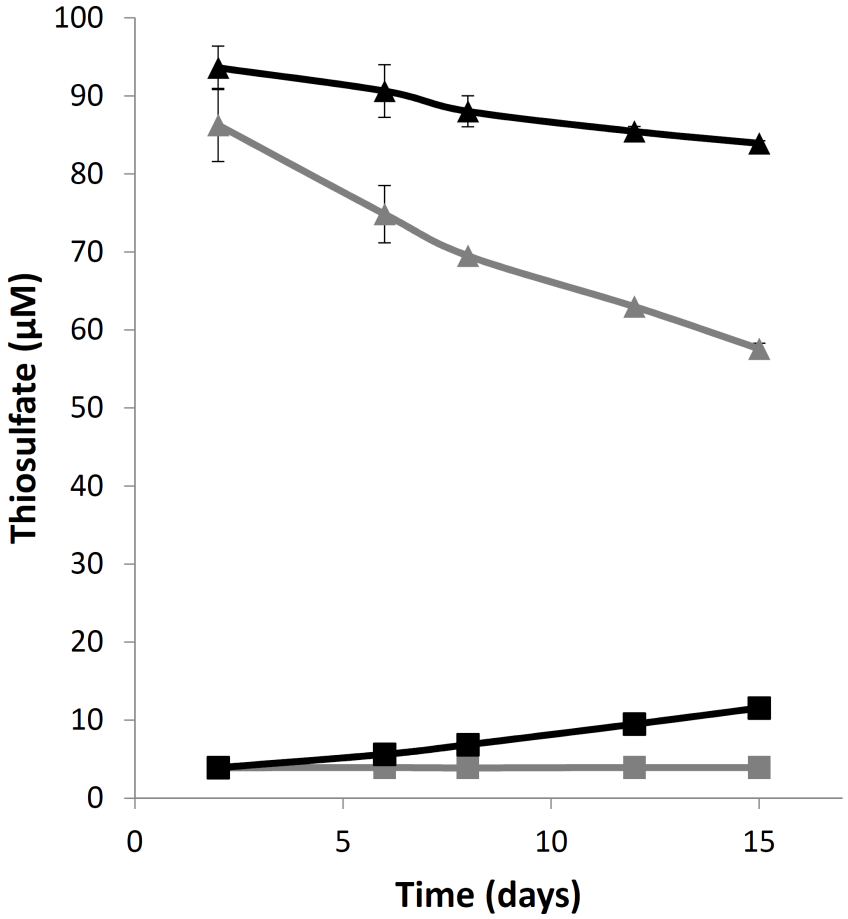

Supplementary Figure S4.1. Thiosulfate concentrations over time for a parallel abiotic experiment. Thiosulfate was added to incubations at Day 0 and concentrations were tracked over the next 15 days. Error bars represent the standard deviation for method duplicates. Black and grey symbols indicate incubations conducted with natural and synthetic metacinnabar respectively. Triangles denote incubations started with 100 µM initial thiosulfate, while squares denote incubations started with no added thiosulfate.

	Incubation vial volume prior to spike (mL)	*Volume 25 mM $S_2O_3^{2-}$ added (µL)*	*Additional [$S_2O_3^{2-}$] added during spike (µM)*
Day 1	37.7	200	133
Day 2	37.9	200	132
Day 3	38.1	200	132
Day 4	38.3	200	131
Day 5	38.5	200	130
Day 6	38.7	200	130
Day 7	38.9	200	129
Day 8	39.1	200	128
Day 9	39.3	200	128
Day 10	39.5	200	127
Day 11	39.7	200	126
Day 12		no spike performed	

Initial thiosulfate for live incubations (based on IC at 15 h)	108 µM
Initial sulfate for live incubations (based on IC at 15 h)	97 µM
Sulfate carryover resulting from sulfate in thiosulfate spikes	5 µM
Expected [SO_4^{2-}] on day 12	***3173 µM***

Supplementary Table S4. 1. Calculations of expected sulfate concentration in live low thiosulfate incubations during aqueous sampling at Day 12 of the incubations based on the daily thiosulfate additions, thiosulfate carryover in the inoculum, sulfate carryover in the inoculum, and sulfate present in thiosulfate stock. Expected sulfate concentration is 3.173 mM whereas measured thiosulfate concentrations range from 3.663 to 3.715 mM.

Supplementary Calculation S4.1. Predicted dissolved Hg concentration at day 12 of killed low thiosulfate incubations in the presence of natural metacinnabar assuming all thiosulfate had been added at once at day 0 of the experiment, rather than being added as a daily thiosulfate spike.

In a previous study, autoclave killed *T. thioparus* and natural metacinnabar were incubated in the presence of varying concentrations of thiosulfate, and a linear increase in dissolved Hg concentration with increasing initial thiosulfate concentration was observed. Interpolating data collected during days 10 and 22, yields the following dissolved Hg concentrations as a function of initial thiosulfate added to the incubation:

Initial $[S_2O_3^{2-}]$ concentration (mM)	Resulting dissolved Hg concentration after 12 days (nM)
0.18	40
5	305
20	580

Two linear regressions of thiosulfate concentration versus dissolved Hg concentration after 12 days of incubation were calculated:

Regression 1 *(based on all 3 $S_2O_3^{2-}$ concentrations)*	
Slope	25.12
Intercept	97.47
R^2	0.9617

Regression 2 *(based on 0.18 and 5 mM $S_2O_3^{2-}$ concentrations)*	
Slope	54.98
Intercept	30.10
R^2	1.0000

(Supplementary Calculation S4.1 continued)

Based on these two linear regressions, we calculated the predicted dissolved Hg concentration at day 12 of the incubation assuming all thiosulfate in low thiosulfate incubations had been added at once at day 0 of the experiment:

	Predicted dissolved Hg concentration (nM) after 12 days incubation assuming an initial $S_2O_3^{2-}$ concentration of 1.562 mM
Regression 1	137
Regression 2	116